Beach representation in morphodynamic predictions

Coupling models to improve beach behavior applied to Anmok beach

D. Caichac

Technische Universiteit Delft

TUDelft

Deltares
Enabling Delta Life

Front cover: Juno Beach Fishing Pier, Florida. © Kim Seng (modified)

Beach representation in morphodynamic predictions

Coupling models to improve beach behavior applied to Anmok beach

By

Daniel Caichac

in partial fulfilment of the requirements for the degree of

Master of Science
in Civil Engineering

at the Delft University of Technology,
to be defended publicly on Wednesday August 09, 2017 at 14:00.

Supervisor:	Prof. dr. ir. S.G.J. Aarninkhof	TU Delft
Thesis committee:	Ir. A. P. Luijendijk	TU Delft, Deltares
	Dr. ir. R.T. McCall	Deltares, TU Delft
	Ir. W.P. de Boer	Deltares, TU Delft
	Ir. J. Reyns	IHE Delft, Deltares

An electronic version of this thesis is available at http://repository.tudelft.nl/.

Você é o criador do seu próprio mérito
Aconteça o que acontecer, você merece
Ezequiel

Preface

This thesis concludes the Master of Science program in Civil Engineering at Delft University of Technology, the Netherlands. This thesis has been carried out at Deltares, in collaboration with TU Delft.

I would like to thank all the committee members for their contributions on this exciting project. I would like to thank Arjen Luijendijk, my daily supervisor, for the continuous support, attention and guidance throughout the development of this work. I deeply believe that it was his optimism what really steered this project from start to finish and eventually made it happen. I thank Stefan Aarninkhof, Robert McCall and Johan Reyns for their experience, academic support and technical suggestions during the constructive meetings we had. I also thank Wiebe de Boer for his support, especially for the always necessary final encouragement by the end of the project.

Apart from my supervisors I would like to thank Bas Hoonhout from Deltares, who took the time and effort to help me during the first stages of my project, when I needed help the most. I would also like to thank Rufus Velhorst, who shared his work and spared me months of coding.

Thank you to my friends and colleagues at Deltares, specially Carlos, Hithaishi, Renan, Panos, Bart, Irene, Ermano and Elly. Without you this thesis would have not been possible. The use of your nodes will not be forgotten. I also thank the opportunity to meet such wonderful friends at TU Delft like Jannek, Maricarmen, Lea, Claudio and Patocarlo among others.

I would like to thank all my previous lecturers/mentors from Chile, Aldo Tamburrino, Christian Ihle and Andrea Gonzalez. Without your initial support and recommendation this whole experience would have not been possible. I also thank the Chilean government and CONICYT's scholarship programme "Becas Chile", which made my stay in the Netherlands possible for the past two years.

To my family, who were always there (through Facetime™ of course) giving me their advice and making me feel like the 12,000 km of distance were nothing at all.

Finally, but most importantly, I want to thank Susan, who quit on everything to follow me in this crazy adventure. This work is for you.

Daniel Caichac
Delft, July 2017

Summary

Numerical process-based morphodynamic models are widespread in coastal engineering practice and have become the new standard when it comes to assessing the impact of natural or man-made structures on coastal environments. The most common practice among engineers is to focus on a single spatial and time scale, which means either neglecting certain processes under the assumption that they will average out, or performing detailed simulations for short time-spans in order to optimize the normally limited computational resources. Despite the efforts from several authors, at the moment there is a lack of a clear methodology which would allow incorporating the relevant physical phenomena only when required, hence optimizing the computational effort.

The above leads to the main research objective of this thesis: to gain insight in what is the added value of coupling process-based morphodynamic models, regarding the morphological impacts near the beach. For this purpose two models that were originally conceived to resolve different timescales are selected; XBeach as a storm model, and the new suite from Deltares, Delft3D-Flexible Mesh (D3D-FM) as a long-term morphodynamic model. The area selected as study site is Anmok beach, located at the east coast of South Korea. The coastal erosion at this location is not yet well understood (mainly due to human interventions and storms) plus the micro-tidal wave-dominated environment makes this location ideal for this study. Recent researches on this site have found that there is a delicate balance between the stormy and calm periods, where the high energy wave events are the main drivers of local morphology.

One of the main findings in this thesis is that the coupling of independently calibrated models does not necessarily provide better morphodynamic results than the results obtained by running each model separately. Including different processes such as infragravity waves or Eulerian mass transport (which enhances the offshore sediment transport in the surf zone) during highly energetic events tend to generate large supratidal beach erosion. However, the post-storm recovery mechanisms present in long-term morphodynamic models are not sufficient to bring the sediment back to the beach. Therefore, it is recommended to include all the relevant physical processes (storm erosion and post-storm recovery mechanisms) when following a coupling approach in order to have a coherent morphodynamic balance. Furthermore, the coupling of models can play an important role in identifying which processes are missing or are not fully represented by the different modelling packages.

The erosive effect of cumulative storms was shown to be relevant in the short-to-medium term and might become a key parameter when defining, for instance, the worst case scenario regarding shoreline retreat. Despite the fact that uncoupled long-term morphodynamic models produce better average results in the case of Anmok beach, the implementation of a coupled scheme was proven to be important when the erosion due to cumulative storm effects cannot be neglected.

Among the advantages of using D3D-FM for this work is the implementation of the Basic Model Interface, which meant an important reduction in bookkeeping efforts and the possibility to seamlessly couple D3D-FM with XBeach. This procedure allowed for the incorporation of more complex phenomena (such as infragravity waves) with an acceptable increase in computational time.

A research version of Delft3D (D3D) with specialized sediment transport equations in the swash zone was tested in an attempt to enhance the post-storm recovery mechanisms. The results obtained are promising in the sense that the accretion of the shoreline and lower dry beach was reasonably enhanced, especially when considering all the limitations involved in modelling the morphodynamics of the swash zone with a stationary wave model. Another important conclusion is that these models were capable of depositing the sediments at the lower backshore at best. Hence, there is still the need of a mechanism/process capable of transporting the sediments farther upslope into the dry beach or dunes, such as aeolian transport.

The decision to undergo with a coupled or uncoupled approach depends on case-by-case basis. For current practice, it is recommended to develop a coupled simulation in the medium-term, where both storms and calm periods have significant effects and where the intra seasonal variation could be a parameter of interest. For short-term simulations, an uncoupled storm model (e.g. XBeach) is recommended as is the most accurate for such a time span. For long-term simulations, the general recommendation is to run an uncoupled long-term model such as D3D. In this case the storm erosion and post-storm recovery processes are expected to average out, being the long-term model the most suitable package to obtain average morphological results.

For future work it is recommended to add an aeolian process-based model and incorporate the swash zone sediment transport module into D3D-FM as this would move us one step closer towards the development of a fully coupled model where all the relevant processes (storm erosion, post-storm recovery and aeolian transport) are included.

List of Symbols

Symbol	Unit	Description
β	rad	Slope of the beach or artificial structure
β_e	rad	Equilibrium slope of the foreshore
Δbl	m	Variation or change in bed level between two models
γ_{max}	$-$	Wave breaker parameter
$\widehat{\eta_{blw}}$	m	Shoaling of bound long waves
$\widehat{\eta_{flw}}$	m	Shoaling of free long waves
ϕ_m	deg	Sand friction angle
ρ	kg/m^3	Water density
A_1	$-$	Empirical coefficient to determine wave momentum flux (Hughes, 2004)
A_0	$-$	Empirical coefficient to determine wave momentum flux (Hughes, 2004)
c_f	$-$	Dimensionless bed roughness coefficient
D_{50}	m	Median grain size
D_{90}	m	Particle diameter larger than 90% of the sample (in weight)
g	m/s^2	Gravitational acceleration
h	m	Water depth
H_s	m	Significant wave height
H_{RMS}	m	Root mean square wave height
H_{sfac}	$-$	Amplification or reduction factor for the maximum wave run-up
K_c	$-$	Cross-shore sediment transport empirical coefficient
K_l	$-$	Longshore sediment transport empirical coefficient
M_{Fmax}	kg/s^2	Maximum wave momentum flux (Hughes, 2004)
$q_{b,c,net}$	m^2/s	Cross-shore net bed load transport rates over a swash cycle
$q_{b,l,net}$	m^2/s	Longshore net bed load transport rates over a swash cycle
$R_{u2\%}$	m	Wave run-up exceeded by 2% of the waves
T	s	Wave period
$\overrightarrow{u^E}$	m/s	Eulerian velocity vector
$\overrightarrow{u^L}$	m/s	General Lagrangian Mean velocity vector
$\overrightarrow{u^S}$	m/s	Stokes drift velocity vector
u	m/s	Flow velocity in cross-shore direction
v	m/s	Flow velocity in longshore direction

List of Acronyms

BMI	Basic model interface (Peckham et al., 2013)
BSS	Brier Skill Score (Sutherland et al., 2004)
CFL	Courant–Friedrichs–Lewy condition
D3D	Delft3D
D3D-FM	Delft3D – Flexible Mesh
EUL	Eulerian
GLM	Generalized Lagrangian Mean
LiDAR	Light Detection And Ranging
m.a.s.l. (m.a.m.s.l.)	Meters above (mean) sea level
MKL	Momentary coastline
morfac	Morphological acceleration factor
SBW	Submerged breakwater

Table of Contents

1. Introduction

In this chapter an introduction to the research topic is presented, as well as the problem definition, the objective and research questions and a general outline of the project phases.

1.1. Background

Numerical models have become the new standard when it comes to assessing and/or designing new coastal protection projects, both in the academic field as well as in the industry. However, it is common practice to focus on a single spatial/time-scale, even for large projects such as the mega nourishment known as the Sand Engine (Stive et al., 2013), where the initial morphodynamic predictions were obtained from a single long-term numerical model (Pekkeriet, 2011). It is possible nowadays to use different modelling packages for assessing different timescales, depending upon the physical phenomena that are relevant for each situation, as depicted in Figure 1.

The new software Delft3D-Flexible Mesh (D3D-FM) (Deltares, 2016c) is used in this thesis as a tool to investigate how model coupling, by means of including different physical phenomena only when required, changes the morphological predictions at Anmok beach with respect to the base case of running a stand-alone simulation.
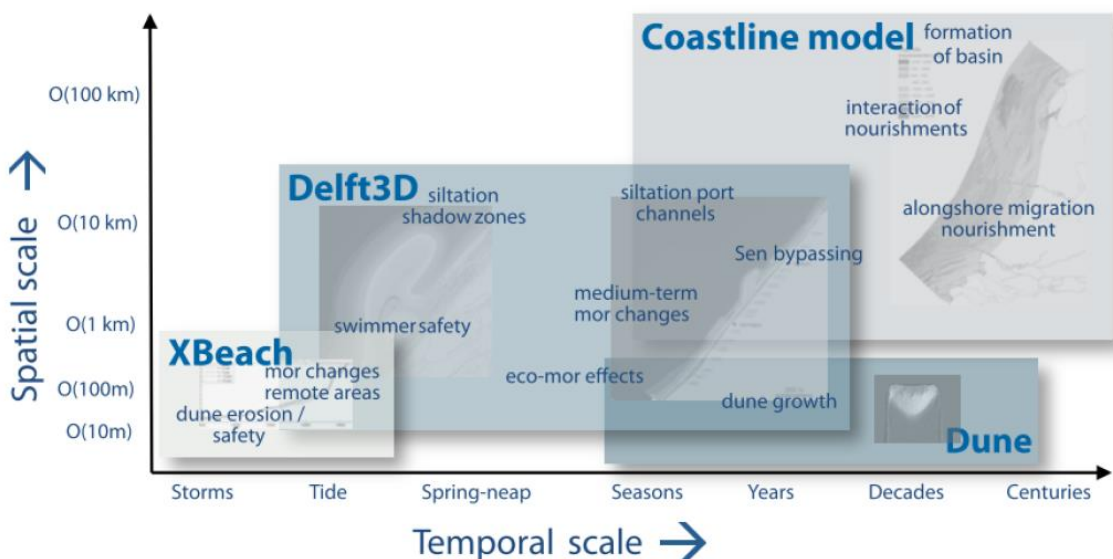
Figure 1: Time and spatial scales for hydro/morphodynamic processes and different simulation suites. From Baart et al. (2012) as cited in Nederhoff (2014).

1.2. Problem definition

Normally different types of models are used for hydro/morphodynamic predictions based on the timescale of the involved processes. Hence, for medium-to-long term simulations, short-term effects are neglected, and at the same time it is computationally inefficient to do detailed simulations in the long run. Thus, at the moment, there is a lack of a clear methodology which would allow running the relevant physical processes only when required, saving processing time without significantly losing accuracy.

Based on recent studies of Anmok beach, located at the east coast of South Korea, new findings or recommendations have been raised which can be interpreted as research questions. In Ton (2017) it was suggested that a better representation of the morphology could be achieved by running an Eulerian mass transport mode only during storms (i.e., advecting the sediment with the average velocity below the wave trough) and a Generalized Lagrangian Mean (GLM) mass transport the rest

1

of the time (i.e., including the stokes drift in the advection of sediment); however this is yet to be proved.

In Koudstaal (2016) and Deltares (2016a) it was stated that the combination of long waves and longshore variation may help distribute the sediments along the Anmok coast, yet this still needs to be verified against measurements and with simulation periods longer than a single storm.

Since D3D-FM, the latest suite from Deltares, implements the BMI interface (Peckham et al., 2013) it should be possible to create a controller (or composite model) that couples two different instances of D3D-FM: (1) One that accounts for processes that are relevant during calmer wave conditions, and; (2) one that is representative of stormy conditions. With the BMI interface it is also possible to couple D3D-FM with different software such as XBeach (Roelvink et al., 2009). The coupled model could then be applied to Anmok beach in order to answer the proposed research questions. The coupling of models is not a straightforward procedure, since some of the assumptions of one model might be in conflict with the other, leading to instabilities or inconsistencies in the final results.

The morphological results obtained from the integration of models are not known beforehand, and the cumulative effects of several storms may have a severe impact near the shoreline, especially if there are man-made structures at the beach, as portrayed in Figure 2.
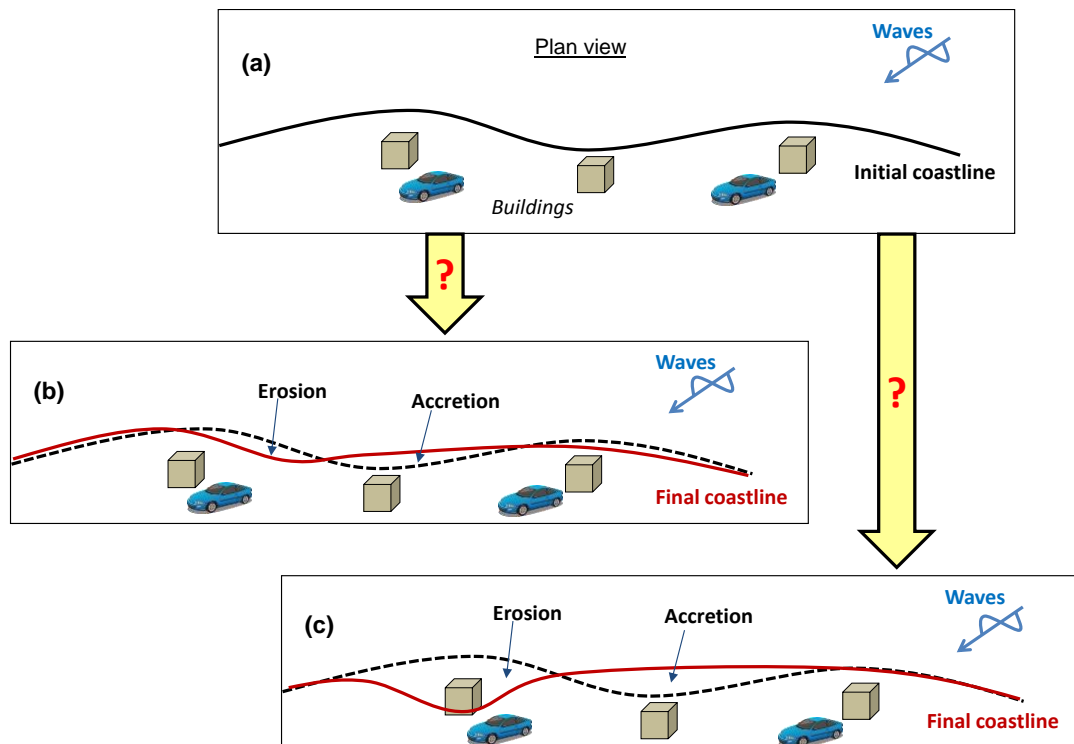
Figure 2: Sketch of the uncertain possible impact of cumulative storms when undertaking a model coupling procedure. (a) Original shoreline and man-made structures at the beach; (b) Small cumulative storm impact without any evident hazard; (c) Large cumulative storm impact posing a hazard on a building.

1.3. Objective and research questions

1.3.1. Objective

The main objective of this thesis project is to assess the added value of coupling the models XBeach and D3D-FM in reproducing medium and short-term morphodynamic processes at Anmok beach.

1.3.2. Research questions

In order to fulfill the project's objective, some research questions are formulated, which are divided in main question and secondary questions.

Main question

1. What are the (dis)advantages of coupling different morphodynamic models regarding the beach evolution predictions at Anmok beach?

Secondary questions

2. What is the morphological impact of including Eulerian mass transport or long (infragravity) waves only during storms at Anmok beach?
3. What are the (dis)advantages of applying D3D-FM over D3D in this particular project?
4. Can the beach recovery processes be enhanced by including specialized swash zone sediment transport formulations in D3D?

1.4. Methodology and outline

In order to fulfill the main objective of this thesis project the research questions must be answered. To do so, a strategy is followed, which divides the tasks in four phases: (1) Literature study; (2) model familiarization and coupling; (3) application to Anmok beach and; (4) discussion and conclusions. These phases are described next:

First phase: In this first phase a literature study is carried out. This focuses on the hydrodynamic and morphodynamic processes that play a role in coastal and dune/beach erosion at Anmok Beach. It also focuses on studying different hydro/morphodynamic models (D3D, D3D-FM and XBeach) that have been primarily used to assess the coastal evolution at this location.

Second phase: The second phase consists of getting familiar with the different models. This involves gaining insight in model inputs, outputs, boundary conditions, syntax, limitations and common errors. It is necessary to get involved in the usage of D3D-Flow, D3D-Wave, D3D-FM and XBeach. At the same time during this phase the development of a coupling procedure takes place, which is done in a Python environment. In this phase it is required to get insight into the BMI interface in order to create an effective coupling controller. This familiarization process will have an increasing order of difficulty which ends in coupling the full 2DH model of Anmok Beach.

Third phase: During the third phase most of the information required to answer the research questions is gathered. It commences by running a D3D model of Anmok Beach, starting from the calibrated results of the model already developed by Ton (2017). Then this model is coupled offline to determine the base case to analyze. Later the same model is set-up in D3D-FM. The results are compared with the ones obtained by Ton (2017), assessing the differences of moving from D3D to D3D-FM. When this is completed, a coupled model is developed which alternates from a GLM mass transport to an Eulerian mass transport during severe storm events. During this stage a threshold for the offshore significant wave height is specified, in order to define for what storms the controller switches between instances or simulations.

The next task is to set-up an XBeach model of the same location starting from the model developed by Koudstaal (2016), and couple it with D3D-FM. The XBeach model is first run in stationary mode

and then in surf beat mode. In the coupled simulations the long wave resolving takes place only during severe storms. The morphodynamic outcome is compared with the uncoupled simulations. During this phase also a new sediment transport module which includes special swash zone formulations is tested in D3D, assessing the morphodynamic changes near the shoreline and its capabilities as a possible post-storm recovery process-based model.

To finalize this phase an XBeach calibration of the stormy season is done with pre-and-post storm data from the year 2016. These settings are later applied to the 2015 simulation assessing the improvement of the results.

Fourth phase: In the last phase of the project, the results are discussed and conclusions and recommendations are drawn.

2. Literature study

In this chapter an introduction to the case study is presented, as well as some relevant hydro and morphodynamic literature research related to this thesis.

2.1. South Korean coast and CoMIDAS program

In the last few decades the east coast of South Korea has been suffering from erosion. The causes of this erosion are believed to be a combination of occasional storms, dynamics of crescentic bars and human interventions which induced a decrease in sediment supply. These interventions are mainly ports, dams, seawalls and breakwaters (Deltares, 2016a; Ton, 2017). Despite efforts supported by the central government, counter measurements have not been effective, leading to unsatisfactory results due to lack of understanding of the associated physical processes.

That is why in the year 2013 a research and development project was started in order to achieve a better understanding and effectively deal with the erosion problems. This South Korean national project, called CoMIDAS (Coastal Modelling, Intelligent Defence and Adaptation based on Scientific understanding), has set up a research cooperation with Deltares in order to strengthen Korean competency in the field of coastal and numerical modelling (Ton, 2017).

2.2. Anmok beach

Anmok beach is located in the east coast of Korea, just North-West of Gangeung port, in the city of Gangneung, as depicted in Figure 3. The east coast is characterized by a micro-tidal environment which is wave dominated, and has severe swell waves attacking the coastline during winter. Most of the time the significant wave height is low ($H_s < 1.5\ m$) and the peak waves period are below 7.5 s (Koudstaal, 2016). However, the coast is occasionally hit by typhoons with maximum offshore significant wave heights higher than 9 m (Deltares, 2016a).
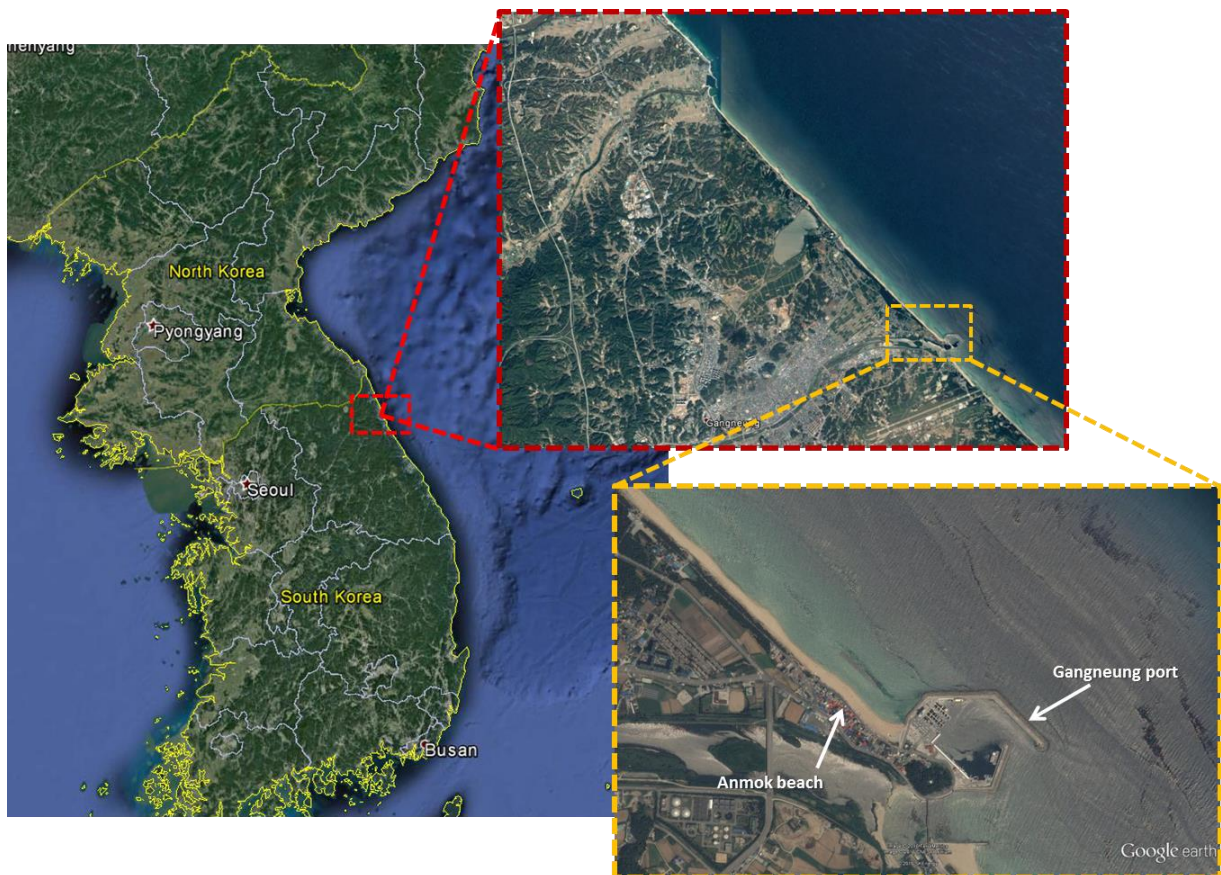
Figure 3: Overview of the South Korean east coast and the location of Anmok Beach and Gangneung port

The nearshore bathymetry shows some alongshore variation and is characterized by crescentic bars, which are rhythmic alongshore perturbations of the sandbars, and are shown in Figure 4.

Anmok beach was chosen as a case study by CoMIDAS because it is believed to be representative for the east coast of South Korea (Deltares, 2016a). This beach is complex from a hydrodynamic point of view since it can be classified as an intermediate beach experiencing both high and low frequency motions (Koudstaal, 2016).
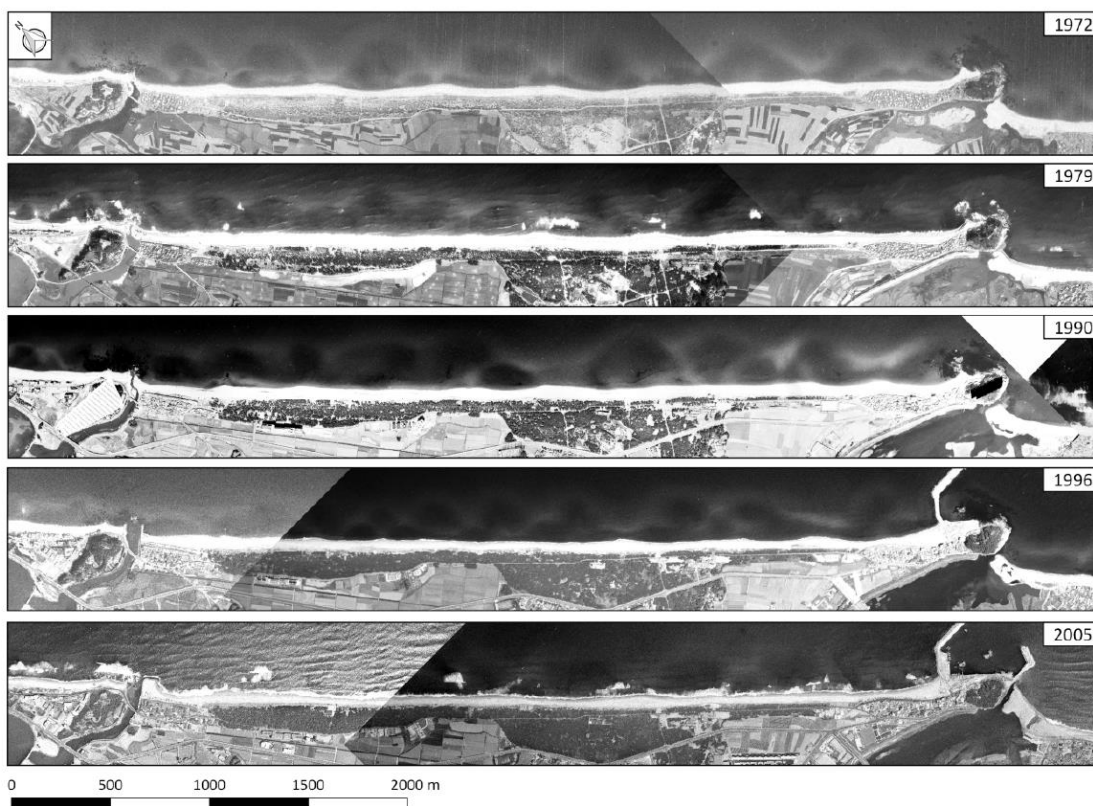
Figure 4: Historical images of Anmok beach depicting the crescentic sandbars. From Deltares (2016a)

2.3. Coastal terminology

In order to discuss about coastal, beach and dune processes, a basic understanding of coastal terminology must be set in place. The terminology from the Coastal Engineering Manual (USACE, 2008) and Shore Protection Manual (USACE, 1984) is used, as shown in Figure 5.

The nearshore extends from the foreshore well beyond the breaker zone, down to a water depth of 20 meters. It defines the area influenced by longshore currents. In the nearshore, waves start to break in the breaker zone, propagate up to the beach in the surf zone and eventually reach the swash zone.

The surf zone is the zone of wave action extending from the water line (which varies with wave conditions, tide, set-up, etc.) up to the most seaward point of the breaker zone. In this context the surf zone contains the breaker zone.

The breaker zone is the zone where waves that are approaching the beach commence breaking. The breaker zone is contained in the surf zone, although the width of the breaker zone might vary with time, depending on variables such as tide level, surge level, waves conditions, etc.

The swash zone is the zone of wave action on the beach, where run-up and run-down can take place.

The beach or shore, which can be divided in foreshore and backshore, is the place where wave action (swash) can take place. It is also defined as "The zone of unconsolidated material that extends

from the mean low water line to the place where there is a marked change in material or physiographic form, or to the line of permanent vegetation" (USACE, 2008).

Dunes are located in between the coastline and the hinterland. They are defined as ridges or moulds of loose, wind-blown sand forming on the backshore. Dunes act as a kind of flexible natural protection against erosion and flooding. The dune face (also called foredune) is sea-facing part of the dune, where wave collisions happen.
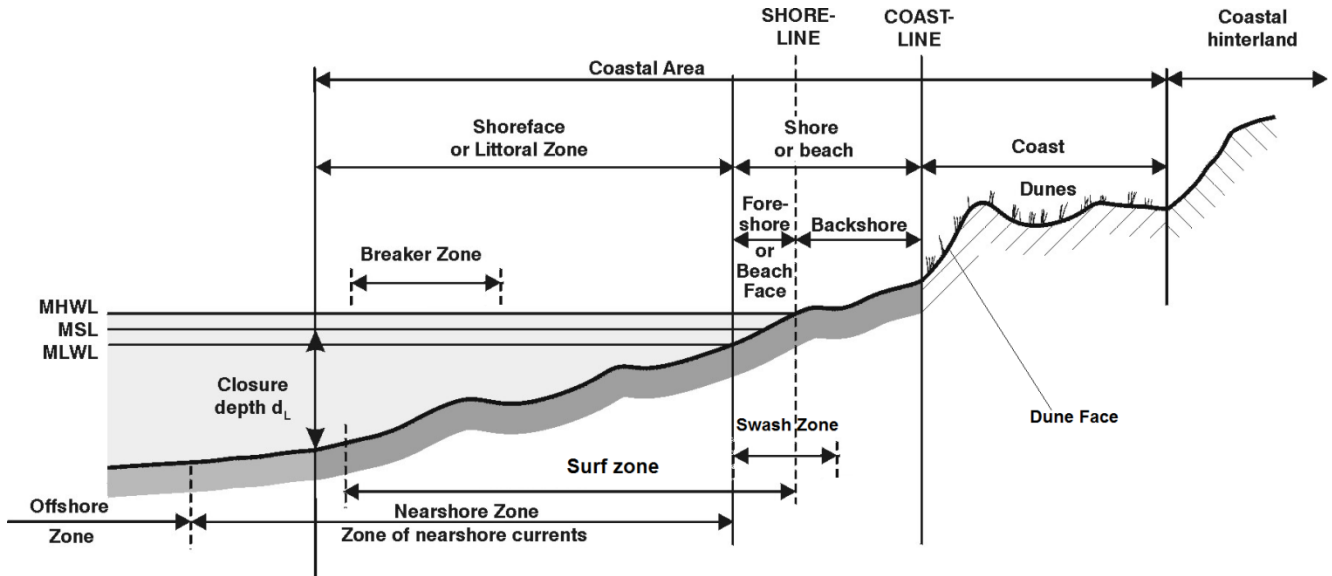
Figure 5: Dune and coastal definitions, adapted from USACE (1984) as cited in Mangor (2008)

Dunes are part of a dynamic system that changes position (and/or volume) in space and time. Dune erosion and accretion are processes that (mainly) arise from natural phenomena: while accretion is usually linked to aeolian sediment transport from the beach towards the dune face during calm conditions, dune erosion is strongly linked to marine processes during storm events. As explained by van Thiel de Vries et al. (2011), storm impacts on sandy dune coasts are usually considered as a 1D cross-shore phenomenon with the following phases:

1. During a severe storm the water level rises and the beach is flooded. Because of this the storm waves can reach the dune face and impact it, which causes episodical slumping of the dune face.
2. The sediment that is released with a slump falls on the beach where it is picked up by long waves that transport the sediment through the swash into the inner surf.
3. In this area a strong undertow is present and the concentration of suspended sediment is high. This is related to the intensity of short wave breaking.
4. Sand that is eroded from the dunes remains in suspension in the inner surf and is transported seaward until the strength of the undertow and the intensity of wave breaking decrease, hence leading to a sediment transport capacity that is not sufficient to keep the sediment in suspension.
5. Finally, the sediment starts to settle down and a new foreshore is developed that is closer to equilibrium with the extreme hydraulic boundary conditions.

Despite that 1D dune erosion analyses are used traditionally for erosion assessments, recent studies by several authors (Roelvink et al., 2009; van Thiel de Vries et al., 2011; Roelvink et al., 2012; van Santen et al., 2012) have concluded that longshore currents and non-uniform transports are important in many cases where 1D models fail to capture these phenomena. It is also indicated by van Thiel de Vries et al. (2011) that longshore variations in bathymetry and topography introduce longshore variations in dune profile evolution.

2.4. Storm regimes of Sallenger

A scale for categorizing the impact of storms on barrier islands (which is also applicable for dunes) was proposed by Sallenger (2000). The main difference with other scales is that he proposed that the final impact of the storm on dune erosion is not only a function of the hydrodynamic forcings, but also of the geometry of the coast. Sallenger proposed that the storm impact regimes are a function of the hydro-morphodynamic variables R_{Low} (minimum run-down), R_{High} (maximum run-up), D_{Low} (dune's foot), D_{High} (dune's crest), as shown in Figure 6.
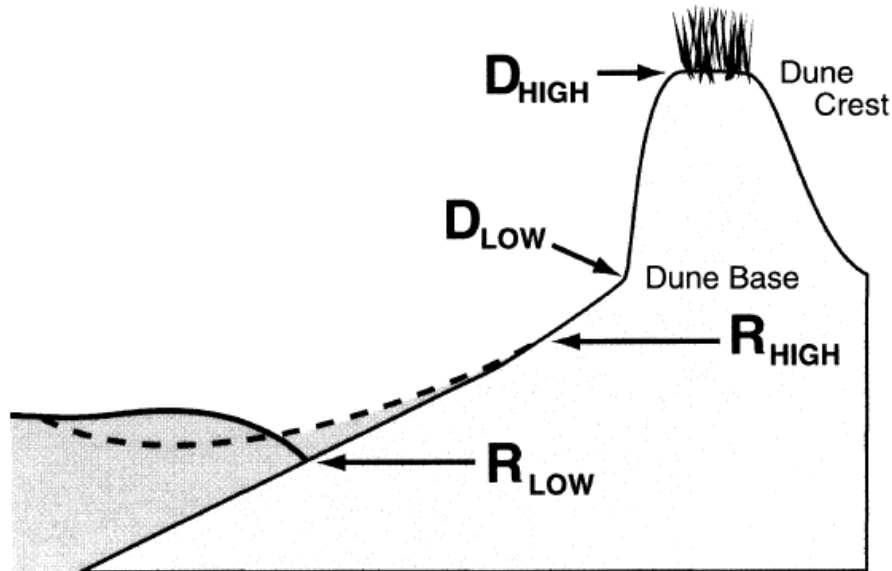
Figure 6: Definition sketch describing variables used in scaling the impact of storms on barrier islands, adapted from Sallenger (2000)

Sallenger identified four different storm impact regimes: swash, collision, overwash and inundation. These can roughly be described as:

1. **Swash**: In this storm regime the wave run-up is confined to the foreshore. Usually the foreshore erodes during a storm, but it recovers itself in the following weeks to months. Thus, the net change in sediment balance is null (this regime is the one shown in Figure 6). In this case $R_{High} < D_{Low}$.

2. **Collision**: The collision regime is defined as the case when the wave run-up exceeds the foot of the dune, hence impacting against the face of the dune ($D_{Low} < R_{High} < D_{High}$). As explained by Nederhoff (2014) following van Thiel de Vries (2009), the collision regime is mostly associated with dune erosion. As stated in the previous section, due to the impact of waves on the dune face, episodical slumping of sediment occurs. This process is called avalanching. Both short and long waves are important for dune morphological development, and long waves are especially effective in triggering the avalanching mechanism of the dune face (van Thiel de Vries, 2009). In this regime there is a net offshore sediment transport (or net erosion).

3. **Overwash**: The overwash regime happens when the wave run-up occasionally overtops the dune's crest ($R_{Low} < D_{High} < R_{High}$). In this case the mean water level is still lower than the dune's crest hence the overtopping is not constant. When overtopping occurs, some sediment might be deposited on the landward side of the dune, hence there is sediment deposition (and erosion) on both sides (face and back) of the dune.

4. **Inundation**: This regime describes storms where the surge level is such that there is a constant overflow/overtopping of the dune, or $D_{High} < R_{Low}$. Sallenger (2000) indicates that there is a landward net transport of sand over the dune, which can take place over large distances. Also, it is believed that the amount of transport is much greater than what occurs during the overwash regime.

It is important to note that not all these regimes have to occur during a storm, yet large storms can undergo through all of these stages, especially if it is taken into consideration that the dune morphology can change. For instance, for a constant wave forcing and surge level, the erosion mechanisms on the dune might lower its crest, changing the regime from overwash to inundation.

2.5. Long waves dynamics

Usually in the surf zone, waves contain a large amount of energy at frequencies lower than the incoming swell or wind waves as explained by Bosboom & Stive (2013). These waves have frequencies ranging from 25 seconds up to several minutes (~250 seconds), and are called infragravity waves, long waves, or surf beat.
The first observations that wave group height (wave group envelope) variations are responsible for the presence of infragravity waves were made by Munk (1949). Afterwards, Longuet-Higgins & Stewart (1964) suggested that these bound waves were released later in the surf zone as free infragravity waves.

Long wave generation: The origin of long waves in deep water as proposed by Longuet-Higgins & Stewart (1964) is funded on the concept of gradients in wave radiation stresses. When waves are travelling towards the coast, wave groups will be generated due to frequency dispersion (Holthuijsen, 2010). Within these wave groups, variation in wave heights (or wave group envelope) will generate variations in wave radiation stresses, which happen to be proportional to the wave height. This gradient in radiation stress, which can be seen as a force, is opposed by a gradient in the water surface, thus the regions with higher (short) wave heights will have lower water surface elevation, and the opposite also holds. This variation in water level is what is known as long waves. These long waves are 180 degrees out of phase with the wave group envelope and travel with the same speed, hence are also called "bound long waves", as they are somewhat "locked" to the wave groups, until they are "released" (Longuet-Higgins & Stewart, 1964) due to short wave breaking, as the mechanism that holds these (short and long) waves together is no longer present. These free waves are also known as free infragravity or leaky waves, as long as they do not become trapped in the surf zone.

Long wave shoaling: It is known that both long and short waves shoal when entering shallower water, yet not in the same way. As the steepness of long waves is lower than short waves, the latter start breaking while the former do not. Also due to non-linear wave-wave interactions the infragravity waves receive energy from the short waves (Holthuijsen, 2010). Another peculiar behaviour of these long waves, as indicated in Reniers et al. (2002), is that according to Longuet-Higgins & Stewart (1962) when bed slope effects can be neglected, the shoaling of the incident bound long waves strongly varies with the water depth ($\widehat{\eta_{blw}} \sim h^{-5/2}$) whereas in leaky free waves there is much less dependency on the same parameter ($\widehat{\eta_{flw}} \sim h^{-1/4}$). More recent studies (van Dongeren et al., 2007) concluded that the actual rate of growth or shoaling varies in between the values indicated by Longuet-Higgins & Stewart (1962), and depends on a normalized (and dimensionless) bed slope parameter β, which is analogous to the Iribarren number or surf similarity parameter (Battjes, 1974). One important behaviour, as stated in Nederhoff (2014), is that the long waves need time (or space) to shoal, hence in steep slopes the growth rate is rather small.

Long wave refraction and dissipation: Reniers et al. (2002) indicated that free infragravity waves will refract stronger than bound long waves, at such degree that the outgoing (reflected) infragravity waves may even become trapped in the shoreline. This happens when the angle of incidence is large enough, in which case these waves are known are "trapped long waves", in contrast with the "leaky free waves". The nonlinear interaction between short waves and trapped long waves might lead to resonance, in which case the energy of the former is transferred to the latter. The waves resulting from these interactions are known as "edge waves" (Gallagher (1971) as cited by Reniers et al. (2002)). There is not a lot of insight into the dissipation (and reflection) of long waves, however van Dongeren et al. (2007) indicated that the ratio between reflection and dissipation is controlled by the parameter β.

Sediment transport and nearshore importance: When approaching very shallow water, short waves commence to break, but long waves due to their low steepness do not. Also in very shallow water, energy is transferred from the short waves to the infragravity waves (Holthuijsen, 2010). The combination of these phenomena leads to a dominance of the long waves (over the short waves) with respect to velocity and water level. These phenomena are very important for processes such as wave run-up and beach/dune erosion (van Thiel de Vries et al., 2008). Investigations regarding the relative importance of the long wave induced sediment transport in the surf zone were carried out by Roelvink (1993) and Roelvink & Stive (1989), who concluded that it represents a significant contribution to the total cross-shore sediment transport when compared with other sediment transport mechanisms.

The nearshore importance of the long waves is sketched in Figure 7:
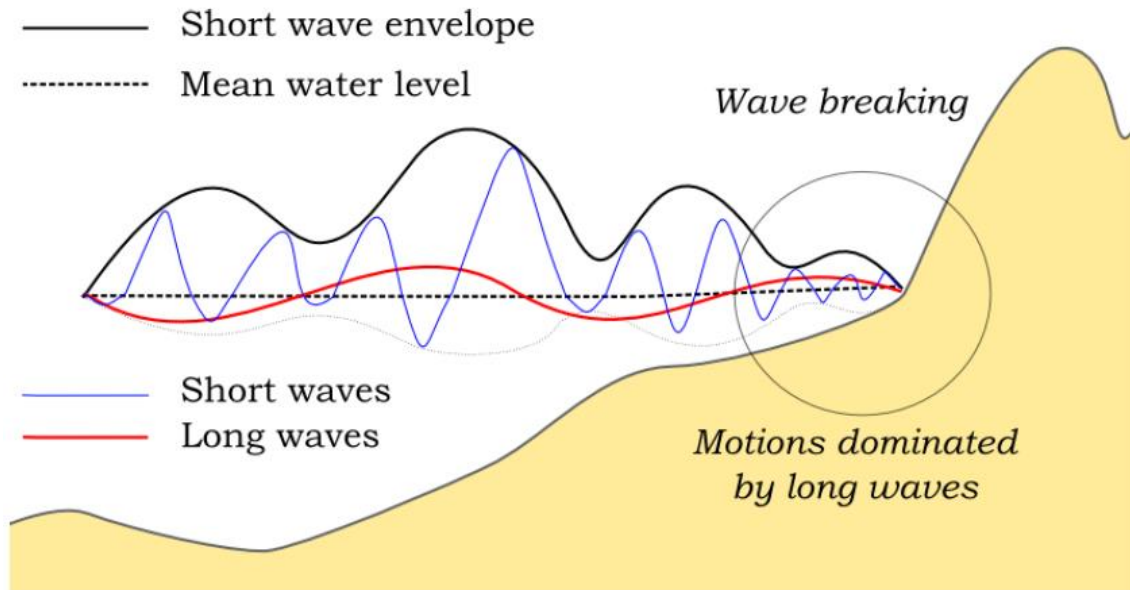
Figure 7: Relevant (wave) processes in the nearshore. Figure from Deltares (2015b).

2.6. Swash zone sediment transport

The swash zone, defined before as the part of the beach where run-up and run-down can take place, is usually a very narrow strip, although it is of great importance for sediment exchange between land and sea (Larson & Wamsley, 2007). The hydrodynamics and sediment transport in the swash zone are highly complex, involving phenomena such as rapid varying flow, nonlinear wave transformation, wave-wave interaction and asymmetrical uprush and backwash among others.

All swash motions combined make up for the wave run-up, which is the maximum elevation of the waves on the beach (or structure) relative to still water level. Over the years there have been several studies to determine or express this value, with a fairly recent one developed by Hughes (2004) for an irregular wave field, shown in eq. [1]:

$$\frac{R_{u2\%}}{h} = 4.4\tan(\beta)^{0.7}\left[\frac{M_F}{\rho g h^2}\right]^{0.5} \qquad \text{for } 1/30 \leq \tan(\alpha) \leq 1/5 \qquad [1]$$

Where $R_{u2\%}$ is the wave run-up exceeded by 2% of the waves, h is the water depth up to the still water level, $\tan(\beta)$ is the slope of the beach or structure, and M_F is the depth-integrated wave momentum flux across a unit width. The gravitational constant and fluid density are g and ρ respectively. The maximum wave momentum flux can be estimated from an empirical fit as shown in eq. [2].

$$M_{F\,max} = A_0 \rho g h^2 \left(\frac{h}{gT^2}\right)^{-A_1} \qquad [2]$$

Where T is the wave period, and A_0 and A_1 are empirical coefficients dependant on the water depth h and the uniform steady wave height H_0, as explained in Hughes (2004).

Predicting the swash motions accurately is required in order to have a good estimation of the coastline, since morphological processes such as erosion during severe storms, post-storm recovery and seasonal variation of the foreshore (among others) are strongly linked to the sediment exchange that happens in the swash zone.

Recently, Larson & Wamsley (2007) developed a formula to estimate the sediment transport in the swash zone both in cross-shore and longshore directions, as shown in equations [3] and [4] respectively:

$$q_{b,c,net} = K_c \frac{\tan \phi_m}{\tan^2 \phi_m - \left(\frac{dh}{dx}\right)^2} \frac{u_0^3}{g} \left(\frac{dh}{dx} - \tan \beta_e\right) \frac{t_0}{T} \qquad [3]$$

$$q_{b,l,net} = K_l \frac{\tan \phi_m}{\tan^2 \phi_m - \left(\frac{dh}{dx}\right)^2} \frac{u_0^2 v_0}{g} \frac{t_0}{T} \qquad [4]$$

Where $q_{b,c,net}$ and $q_{b,c,net}$ are the cross-shore and longshore net bed load transport rates over a swash cycle; K_c and K_l are empirical coefficients; u_0 is the wave front velocity at uprush; t_0 is the duration of the swash at a particular location; v_0 is the alongshore transporting velocity; $tan\beta_e$ is the local equilibrium slope; dh/dx is the local slope; ϕ_m is the friction angle of a sand grain (~30 deg); and T is the wave period.

2.7. Mass transport formulations

Mass transport by waves can be seen in two different ways: from a fixed point in space (Eulerian view) or from a moving reference frame following the particles path (Lagrangian view). The Eulerian velocity averaged over a wave period has a zero value under the trough, and a non-zero value in direction of the wave propagation between wave crest and trough (Bosboom & Stive, 2013), as depicted in Figure 8-a.

When following the path of a single water particle (Lagangrian approach), it is found that due to small differences in wave celerity, the particle move slightly faster under the wave crest (in direction of wave propagation) and somewhat slower under the wave trough (opposite direction). This leads to particle paths that are not closed orbits, and a net movement in wave propagation direction is observed (Figure 9). This residual motion is known as Stokes drift.

The relation between Lagrangian velocities, Eulerian velocities and Stokes drift is shown in eq. [5] (Walstra et al., 2001). This is known as the Generalized Lagrangian Mean (GLM) formulation.

$$u^L = u^E + u^s \qquad [5]$$

In the surf zone, the residual flow located between wave crest and though is balanced by a return current known as the undertow (Figure 8-b), which has a non-zero time-averaged value in the offshore direction. Thus, it is expected that the Eulerian velocity is a good estimate of the velocity at the bottom (as felt by the bed). From a modelling point of view, it can be seen from eq. [5] that if a simulation is run with Eulerian mass transport, a smaller velocity in wave propagation direction would be considered, because the Stokes drift (which is always onshore directed) is not included. In this case, the undertow, which is counteracted by the Stokes drift, would be larger, hence generating a larger offshore mass transport (Ton, 2017).
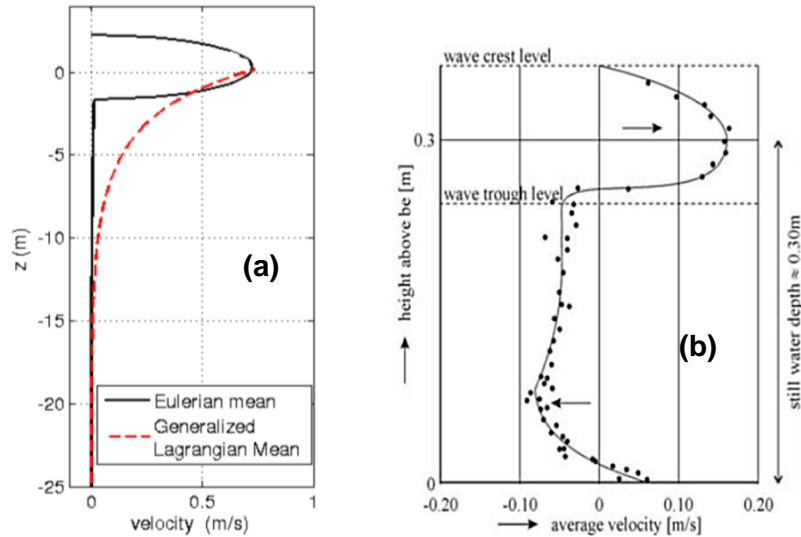
Figure 8: (a) Eulerian and Lagrangian vertical velocity profiles in deep water (figure from Ton (2017)). (b) Eulerian velocities in the surf zone (figure from Bosboom & Stive (2013)).
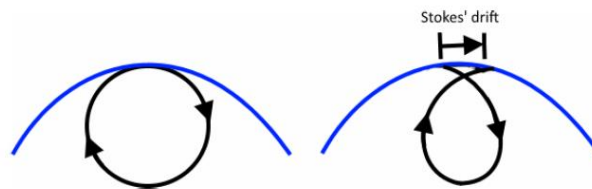
Figure 9: Particle motion during a wave period. Left: Closed orbit (no residual motion). Right: Open orbit (residual motion, Stokes drift). Figure from Ton (2017).

2.8. Anmok beach previous models

In the framework of the CoMIDAS-Deltares cooperation, some recent models of Anmok beach have been developed either in D3D (Deltares, 2016a; Ton, 2017), and/or XBeach (Deltares, 2016a; Koudstaal, 2016). The main differences between D3D and XBeach are summarized in the following bullets. For a full description of each model the reader is referred to Roelvink et al. (2010), Deltares (2014) and Deltares (2015b).

- The XBeach model resolves the long wave motions, whereas in D3D the bound long wave is only calculated at the outer boundary. The long wave motions are most of the swash waves that impact on the beach or dune's face. Incorporation of this phenomenon is necessary to accurately reproduce dune erosion (Roelvink et al., 2009).
- XBeach includes an avalanching algorithm which allows dry segments (grid cells) of sand to slump down, whereas D3D does not. It has been shown that this phenomenon is also important when the location of the dune's face needs to be modelled in an accurate manner (Roelvink et al., 2009).
- XBeach is a depth averaged (2DH) model, whereas D3D allows for a fully 3D modelling of flow with either the $z-layer$ or $\sigma-layer$ formulations (Lesser et al., 2004). This imposes a restriction when trying to model 3D phenomena as spiral flow or wind driven circulation. However for dune erosion models (including overwash and inundation regimes) the 2DH modelling approach with XBeach has proven to reproduce well both hydro- and morphodynamic behaviours (Roelvink et al., 2009; Roelvink et al., 2012; van Thiel de Vries et al., 2011; Pekkeriet, 2011; van Santen et al., 2012).

2.8.1. D3D

A D3D model of Anmok beach near the Gangneug port and a submerged breakwater (SBW) was developed by Deltares (2016a) in order to study the local hydrodynamics and sediment transport patterns. This model proved to reproduce well the nearshore tidal elevation and wave characteristics. It was also found that the SBW led to considerable reduction in sediment transport, yet the morphological changes around it were not investigated. Following this research Ton (2017) investigated the hydrodynamic patterns and morphological response around the SBW based on the field measurements of the year 2015. One important conclusion of this work is that the most relevant morphodynamic parameter is the mass transport formulation, either Generalized Lagrangian Mean (GLM) or Eulerian. It was found that the latter performs better for stormy conditions, whereas the former performs well during calm conditions. Each mass transport mode was run for 6 months periods, but it was suggested that running the Eulerian transport formulation only during storms might improve the accuracy of the predictions.

2.8.2. XBeach

An XBeach model was developed by Deltares (2016a) to assess the effect of individual storms at Anmok beach. Since no pre-and-post storm data was available, the models were used to qualitatively compare different storms with each other, and to assess the importance of non-stationary phenomena. Some of the main conclusions of this study are that extreme winter swell events were more relevant than typhoons, with respect to morphological changes. From these results it was suggested that infragravity waves are important when there is longshore variability, as they might help distribute the sediments along the coast. An important remark regarding future modelling was that higher-energy storms ($T_r \sim 1/100\ years$) had a higher impact on beach erosion than lower-energy storms, and therefore a threshold could be defined to model infragravity waves only when required.
A study on the effect of infragravity waves on wave run-up was undertaken by Koudstaal (2016), by analyzing several 1D models of synthetic storms. It was found that in this particular area a 1D model did not show the same results as a 2D model; however this conclusion was drawn from only a single storm simulation and it was recommended to repeat the same exercise with multiple storms in order to draw a more general conclusion. It is also explicitly stated that her study was focused on hydrodynamics only; hence all the models were run without a morphological update.

2.8.3. D3D-FM

D3D-FM is the latest suite developed by Deltares. This software is the successor of D3D-Flow and SOBEK flow suites, and is currently still in development. For this reason many of its functionalities are undergoing periodic changes, or are currently labelled as β (beta) since they are being validated in different projects. For an explanation of all the functionalities of this software escapes the reader is referred to Deltares (2016b) and Deltares (2016c). The most relevant changes (that apply to this thesis) compared to D3D-Flow are the following:

1. D3D-FM uses unstructured grids, such as triangles, squares, pentagons and hexagons. This allows for grid refinement in areas of interest, such as fronts with high gradients, and coarsening in areas where accuracy is less needed.
2. Networks with different dimensions (1D, 2D) can be coupled. Also grid restrictions are not present anymore.
3. The time integration of the advection term in the momentum equation is now solved explicitly, hence restricted by a CFL criterion. However the general speed of the models can still be improved (with respect to D3D) with a well posed grid refinement.
4. All geometric model inputs are now specified in coordinates rather than grid-indices. This allows for quicker changes in model grids without changing the rest of the inputs.
5. D3D-FM implements the basic model interface (BMI), which allows extract/replace model variables through an external interface or model wrapper. This is fundamental for an online model coupling not present in regular D3D.

Up to date there are not any models of Anmok beach developed in D3D-FM.

3. Model coupling methodology

In this chapter, first a description of the D3D-FM is presented, followed up by an explanation of the developed model coupling techniques.

3.1. D3D-FM brief description

The governing equations in D3D-FM are the same as the ones used in D3D, known as the shallow water equations. When expressed in a depth averaged (2DH) manner, there are two main equations to solve, which represent the conservation of mass (eq. [6]) and momentum (eq. [7]) (Kernkamp et al., 2011):

$$\frac{\partial h}{\partial t} = \nabla \cdot (H\vec{u}) = q \tag{6}$$

$$\frac{\partial \vec{u}}{\partial t} + adv(\vec{u}) + g\nabla\xi + c_f\vec{u}\|\vec{u}\| + 2\Omega \times \vec{u} = S \tag{7}$$

Where h is the total water depth, ξ is the water level, $\vec{u}$ is the depth-averaged horizontal velocity vector, $\nabla = [\partial_x, \partial_y]^T$ is the horizontal gradient operator, Ω is the earth rotation vector and $adv(\vec{u})$ is the advection term. The term on the right hand side q represents the sources terms, S are the external forcings. The remaining values are constants, being g the acceleration of gravity and c_f the bottom-friction coefficient.

The total water depth is defined as:

$$h = \xi - d \tag{8}$$

With d being the bottom level. In D3D-FM the same concept of a "staggered grid" is followed as in D3D, in the sense that water levels and velocities are not located in the same points in space. The net nodes are the points where the bed levels are imposed, and the flow nodes are the points where the water levels are defined (pressure points). These nodes are connected by links. The exact location of the flow nodes is defined by the cell circumcenter, which is the intersection of all the perpendicular bisectors of a grid cell as shown in Figure 10 (Stengs, 2013). This location may not coincide with the cell center of gravity. The velocity points are defined at the cell faces, in the intersection between flow and net links.
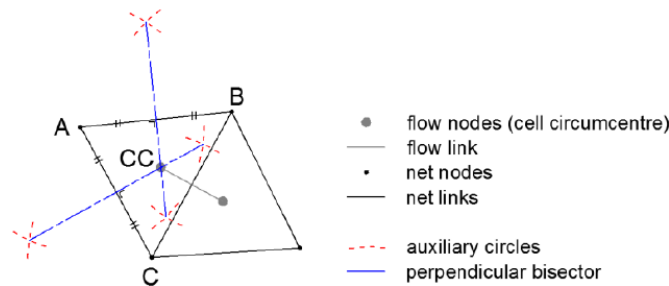
Figure 10: Orthogonal grid definition in D3D-FM. From Stengs (2013)

The numerical implementation is undertaken by means of a finite volume solver, where the continuity equation is solved implicitly for all points. The time integration of the advection term on the other hand, is solved explicitly, which results in a time step limited by the Courant number (CFL). This time step is changing during the computation and is automatically chosen to comply with the CFL criterion.

Suspended sediment transport in a 2DH mode is calculated by a depth integrated advection-diffusion equation, using semi-empirical formulas (van Son, 2009). The sediment concentration is estimated by solving eq. [9].

$$\frac{\partial h\bar{c}}{\partial t} + \bar{u}\frac{\partial h\bar{c}}{\partial x} + \bar{v}\frac{\partial h\bar{c}}{\partial y} - D_H\frac{\partial^2 h\bar{c}}{\partial x^2} - D_H\frac{\partial^2 h\bar{c}}{\partial y^2} = \frac{\overline{c_{eq}} - \bar{c}}{T_s} \tag{9}$$

Where h is the water depth, u and v are the x- and y- velocities, D_H is the horizontal dispersion coefficient, c is the sediment concentration, c_{eq} is the equilibrium sediment concentration and T_S represents an adaptation timescale. On the other hand, several expressions can be used to calculate bed load transport, being the formulae by Van Rijn (Deltares, 2016c) used as default.

For a morphological update, the change in the quantity of bottom sediments is calculated with expression [10] (Deltares, 2016c):

$$\Delta_{SED}^{C} = \frac{\Delta t F_{MORFAC}}{A^c}\Sigma_i S_u^i W_u^i \tag{10}$$

Where Δ_{SED}^{C} is change of quantity of bottom sediment at location c, Δt is the computational time step, F_{MORFAC} is the morphological acceleration factor, A^c is the area of computational cell at location c, S_u^i is the computed bed load sediment transport vector in u direction (normal to face i), and W_u^i is the width of the face i. It is important to indicate that the sediment transport points are located on the velocity points (intersection of cell faces and flow links) as shown in Figure 11. The resulting change in bottom sediment is added to the change due to suspended sediment sources and sinks (Deltares, 2016c).
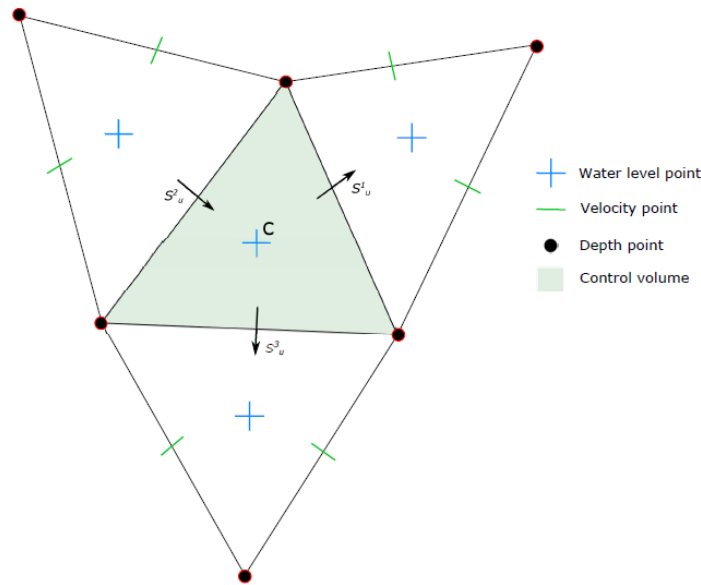
Figure 11: Morphological control volume and bed load transport in D3D-FM. Figure from Deltares (2016c).

To model wave evolution, a wave module called D-Waves is incorporated in flexible mesh suite, which is based on the third-generation SWAN model (**S**imulating **WA**ves **N**earshore) (Deltares, 2015a). This model is used to simulate the evolution of random, short-crested wind-generated waves. SWAN solves the spectral wave action balance, as shown in eq. [11] :

$$\frac{\partial N}{\partial t} + \frac{\partial c_x N}{\partial x} + \frac{\partial c_y N}{\partial y} + \frac{\partial c_\sigma N}{\partial \sigma} + \frac{\partial c_\theta N}{\partial \theta} = \frac{S_{tot}}{\sigma} \tag{11}$$

Where N is the wave action density (defined as $N = E/\sigma$), E is the energy density or wave variance spectrum, σ are the wave frequencies, θ are the wave propagation directions, $c_{x,y}$ are the wave propagation velocities in x- and y- directions, $c_{\sigma,\theta}$ are the wave propagation velocities in spectral

space (σ, θ), and S_{tot} contains the source/sink terms that represent all physical processes which generate, distribute, or dissipate the wave energy (The SWAN team, 2016).

A more detailed description of the whole set of equations solved by D3D-FM, D-Waves and D3D can be found in Deltares (2016c), Deltares (2014), Lesser et al. (2004) and Kernkamp et al. (2011).

It is important to stress that the morphology module in D3D-FM is still under development, and is not yet a standard part of the official release of D3D-FM suite. Up to date the only (published) successful use of the morphology module with bed level update has been carried out by Smits (2016), where erosion and sedimentation patterns in depth averaged (2DH) simulations were estimated and similar results in both software (D3D and D3D-FM) were obtained, when considering cohesive sediments.

3.2. Basic model interface (BMI)

The basic model interface (BMI) is mainly the work of Peckham et al. (2013), and it consists of a set of libraries for different programming languages (Java, Python, etc.) which allows to "wrap" models and steer the simulations with the "wrapper". This wrapper can be seen as a second layer for controlling the models, which allows for an intermediate exchange of variables during a simulation. In Figure 12 a simple comparison is shown between a model run with and without the BMI wrapper.
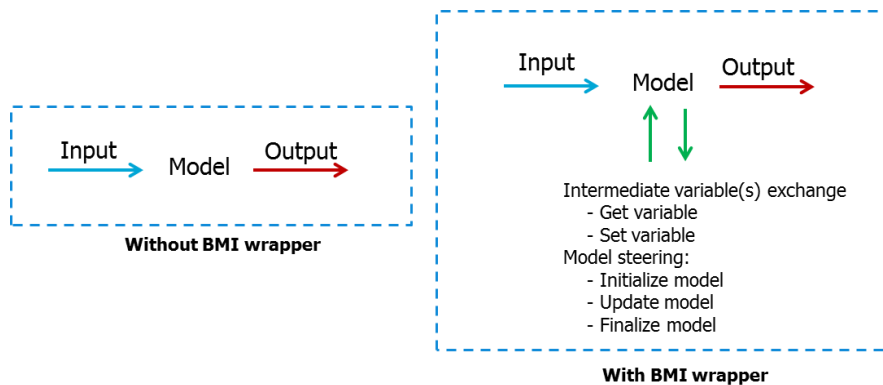
Figure 12: Simple comparison between a model run with and without the BMI wrapper.

The three basic functions of BMI are initializing the model; update its time dependant variables, and finalizing the model. To run a simulation through BMI, the software must be BMI-compatible. D3D-FM and XBeach are BMI-compatible, whereas regular D3D is not. In this thesis all the (coupled) models were steered through a Python BMI environment. One major disadvantage of steering models with BMI is that the simulations cannot (yet) be run in the Deltares computational cluster; hence the advantages of parallel multi-processing simulations are lost.

3.3. Model coupling technique

Commonly there are two ways of coupling models: offline (serial) and online (parallel). An offline coupling occurs when one simulation runs for a certain time span, it is then terminated, and its output serves as the input for the next simulation, as shown in Figure 13-a. In contrast, in an online approach information between models is exchanged every time step (or every certain pre-defined interval), as shown in Figure 13-b. This allows for a direct feedback between the physical processes of each model (Deltares, 2016c). The approach followed in this project is somewhat a blend of both approaches, as a serial coupling is used however the models are not terminated but rather put in *standby*, hence significantly reducing the time that would be required to initialize and finalize each simulation (Stengs, 2013). Due to the lack of a common name, this approach is called from hereafter *serial online coupling,* and is shown in Figure 13-c.
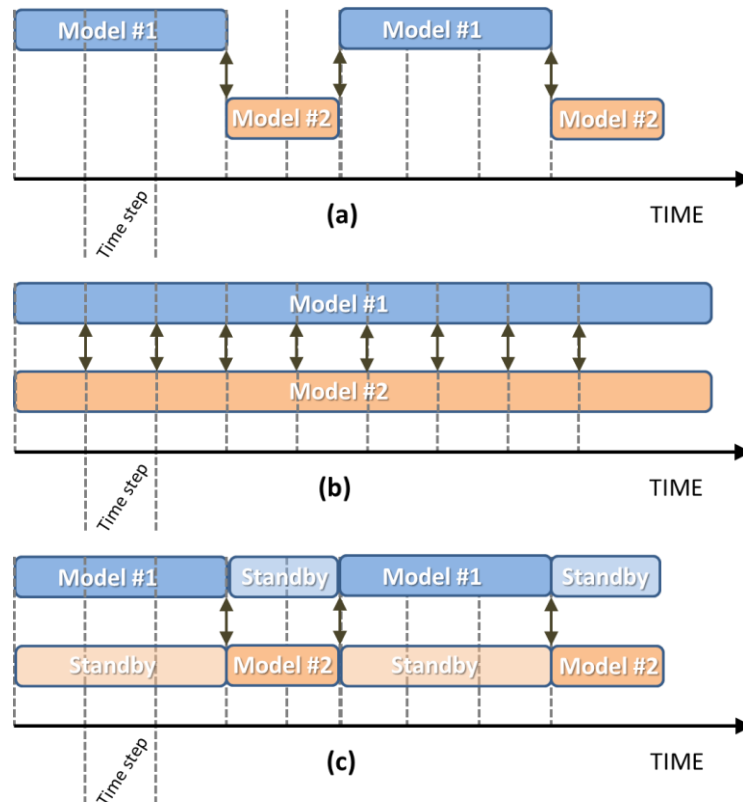
Figure 13: Coupling techniques between models. The arrows indicate the exchange of information between models. (a) Offline coupling; (b) Online coupling; (c) Serial online coupling.

Developing a serial online coupling model is a non-trivial challenge, for which two different techniques are used, dependent on the models that had to be coupled:
1) To couple two different instances or simulations of D3D-FM, a forking (cloning) technique was used, since special attention is required when attempting to call to the same software packages (libraries) at the same time.
2) To couple different software (D3D-FM and XBeach), a more straight forward routine is used, but special attention is required due to grid interpolation requirements.

The first technique was required since a restriction from BMI is that only one library (or software engine) can be initialized at a time. Hence, it was not possible to run simultaneously two different simulations of D3D-FM. To cope with this, a cloning technique known as forking was used, following a similar procedure as the one developed for XBeach (Hoonhout, 2015). This technique consists on cloning the *parent* or main simulation into *children* simulations and initialize each of them in a single processor. This is repeated for the required number of instances/parallel simulations. Then, every command available through BMI (e.g. model update, get variable, etc.) is sent into queues, which are handled in different processors. The data is later retrieved after all the queues have finished their respective assignments. This allows for a simple bookkeeping of information, avoiding a typical multiprocessing issue of trying to retrieve a variable from a task that is not yet finished. An example with two instances is shown in Figure 14, where the models are initialized and updated until they are finished, while information is being exchanged during this process.
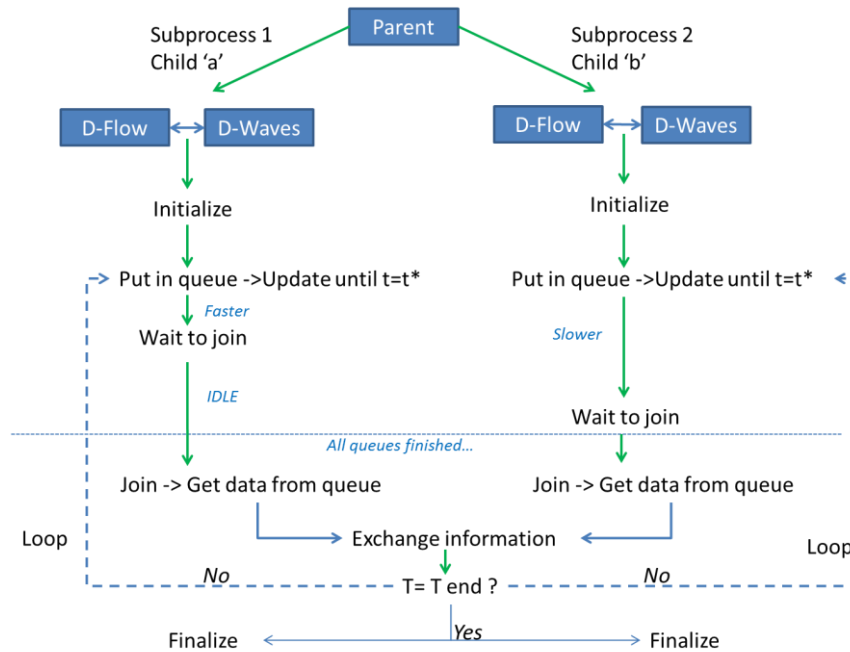
Figure 14: Example of forking/cloning technique with two instances. After initialization of the sub processes, each instance is updated until $t = t^*$, when exchange of information occurs. Since one instance is faster than the other, it must remain idle waiting for the slower one. When both queues are finished information is exchanged.

This forking coupling technique has the advantage of running many instances of the same software at the same time, but has the disadvantage that trying to couple different software is troublesome. Therefore, the coupling with different software was left out of the scope of work. Since all the different instances have the same hydro-morphodynamic mesh, spatial interpolation was not necessary. With this methodology many variables can be exchanged between simulations, however the most important one is the bed level. Exchanging information such as the water level or wave height is not strictly mandatory since these values are read from the boundary conditions, hence if the water level changes too much between instances, the new (and correct) value will take some time to spread into the model, generating an effect similar to a spin-up time. To reduce the hydrodynamic effect of these intermediate spin-up times, also the water level and water depth are exchanged. While trying to achieve an effective coupling it was found that D3D-FM cannot handle large instantaneous bed level changes in the order of $O(1-10)\ m$, which are the ones expected when running a serial online coupling under highly energetic environments. To cope with this, the bed level changes (as well as water level and water depth) were gradually (de)increased in a short but larger than instantaneous time span in the order of $O(60)\ min$, as schematized in Figure 14. This procedure increased the stability of the models by reducing large gradients in the variables exchanged, and is not problematic with respect to accuracy since in the long run bed level changes are expected to smooth out.
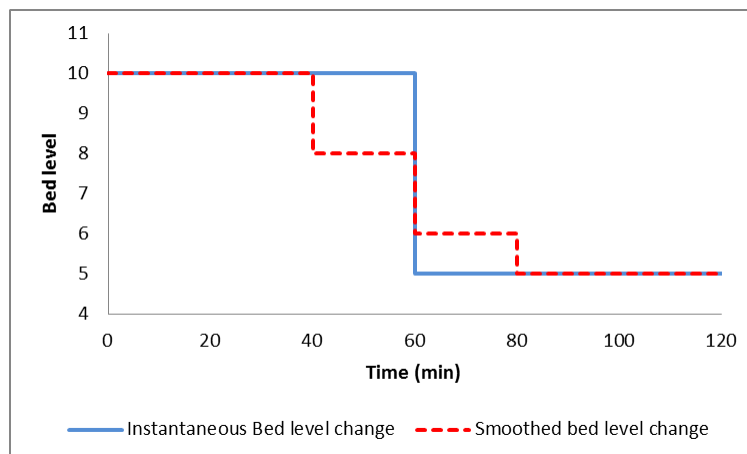
Figure 15: Example of ramp-up or tapering of bed level change between simulations.

18

The second coupling technique is similar to the one developed by Velhorst (2017), where a coupling between D3D-FM and Aeolis was developed. The main challenge of coupling XBeach and D3D-FM is that in most models the computational grids are not the same, and in this case a higher resolution is usually needed in the surf and swash zone for XBeach, where the long waves play a dominant role. Hence, if information is exchanged directly between these different meshes, an unwanted smoothening of the bathymetry would happen, as is shown in Figure 16-c, where the bathymetry from a coarser grid (Figure 16-b) is exchanged (set) into a finer grid (Figure 16-a). Even if no morphological changes happen in the simulation, the bed levels set in the finer model can have a resolution only as high as the coarser model resolution. To cope with this, *bed level changes* are exchanged between models, instead of *bed levels*. Hence, if no bed level changes occur, the original bathymetry is kept, and should bathymetrical changes happen, the high resolution is kept and a (in)decrease of the bed level is observed in the finer model, as shown in Figure 16-d.
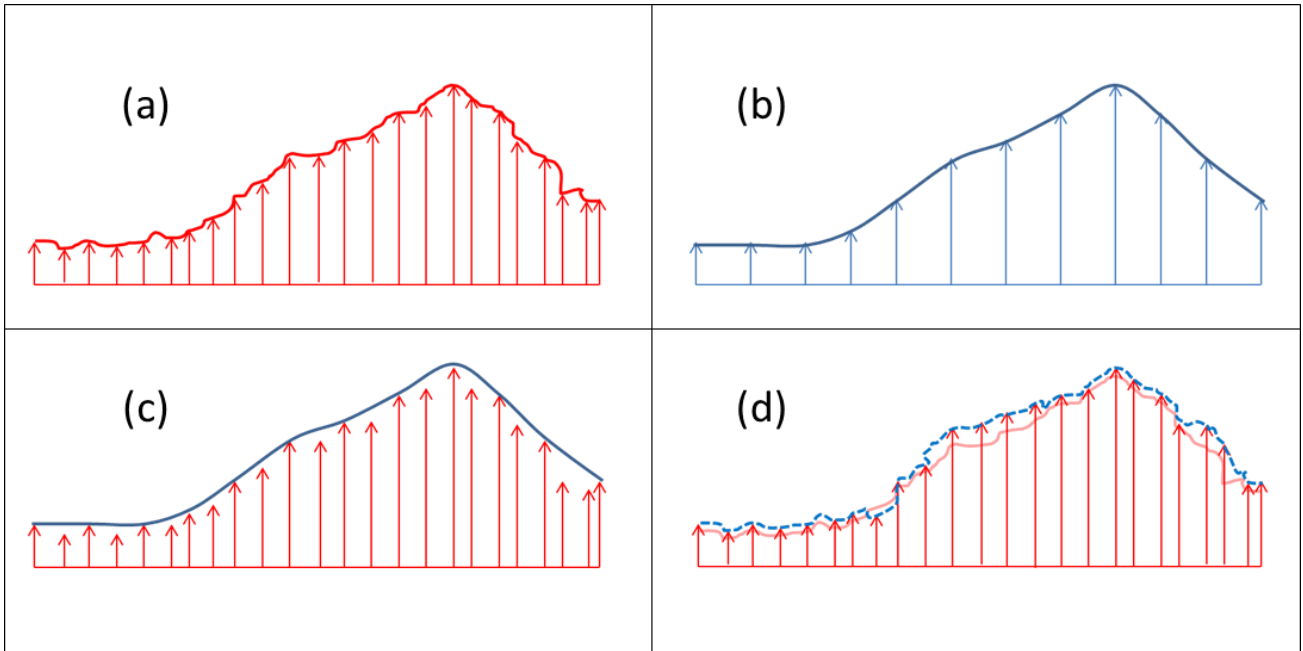
Figure 16: Smoothening as a result of interpolation. (a) Finer grid representing a cross section. (b) Coarser grid of the same location. (c) Finer grid smoothed after setting the coarser bathymetry as new bed levels. (d) Finer grid after setting bed level *changes* from coarser bathymetry.

One of the most important requirements of this coupling routine is that it must be mass conservative. When exchanging bed level differences, the area of the grid cells is already known (and invariant), hence the exchange of bed level differences is equivalent to exchange of mass.

This requirement is achieved using the methodology developed by Velhorst (2017), where the bed level differences are weighted with respect to the overlapping areas of the different grids. Hence, for example if a bed level change dZ_1 occurs in the finer grid (figures 17-a and 17-b), all this mass needs to be sent to the coarser grid. It is easy to see in Figure 17-c that the coarser grid cell will have a uniform and higher $dZ_3 > dZ_1$ bed elevation since its grid cell area (shown in red) is smaller than the total area of the finer grid cells (shown in blue). On the other hand, if there is a bed level change dZ_3 in the coarser grid (Figure 17-d), when exchanging this information the amount of mass will be spread depending upon the total weight (or overlapping area) of the receiving finer cells, as indicated by $dZ_6 > dZ_7 \approx dZ_5 > dZ_4$ and depicted in Figure 17-e
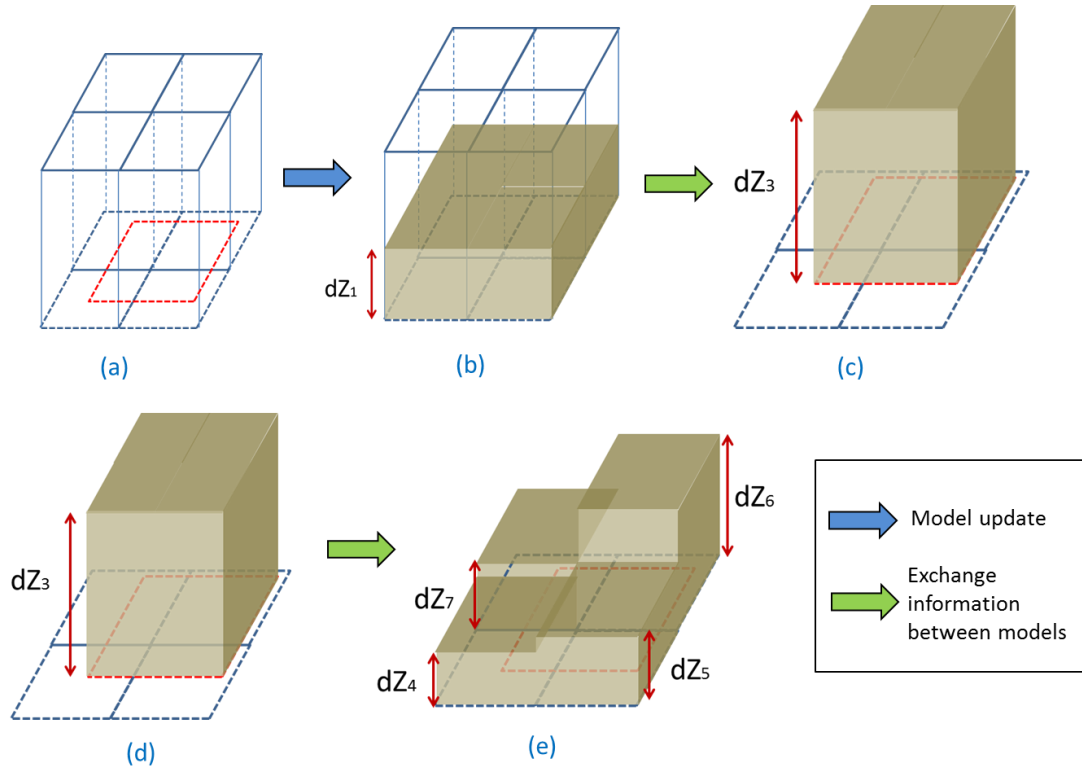
Figure 17: Schematization of bed level exchange between models. (a) Original grids. (b) Fine grid model update. (c) Information received by coarse grid model. (d) Coarse grid model update. (e) Information received by fine grid model. In all figures the blue grid is the fine grid and the red is the coarse one.

The exchange of bed levels can be summarized in eq. [12]:

$$(\Delta z \cdot Area)_{send} = \Sigma(\Delta z \cdot Area)_{receive} = \Sigma\Delta z_{send} \cdot \frac{Area_{send} \cap Area_{receive}}{Area_{receive}} \quad [12]$$

Where *send* are the values of the mesh that is sending the information, and *receive* the values of the mesh that is receiving the information. For exchanging water levels a correction factor f_{corr} is included in the right hand side of eq. [12], which is defined as the ratio of the receiving cell area over the area that does not overlap with any cell of the sending grid $f_{corr} = \frac{Cell_{area}}{Non\ overlapping_{area}}$, hence this factor is equal to 1 for all cells that are not located at the boundaries, and $f > 1$ for cells located at the boundaries. This procedure is chosen as it produces smooth water level gradients at the boundaries and is preferred over a water-mass conservative scheme to avoid model instabilities (Velhorst, 2017).

The information exchange between D3D-Waves and SWAN has been already developed by Deltares inside D3D-FM suite and cannot be accessed through a BMI interface, with the exception of the most basic functions (initialize, update, and finalize). Lastly, the coupling between the D3D-Flow and D3D-Waves is an online coupling through an external communication file, however it is not further explained in this thesis, and the reader is referred to Deltares (2014), Deltares (2015a) and Deltares (2016c).

The time coupling between models, as shown in Figure 13-c, will be done in such way that information will be exchanged whenever a severe storm approaches. As an example Figure 18 depicts the flow chart of information (such as bed level information) for a wave time series where a significant wave height threshold of 2.5 m has been set, i.e., anytime that the significant wave height exceeds 2.5 m information will be sent from one instance to the other and vice versa. This information exchange methodology applies for both coupling techniques previously discussed in this chapter.
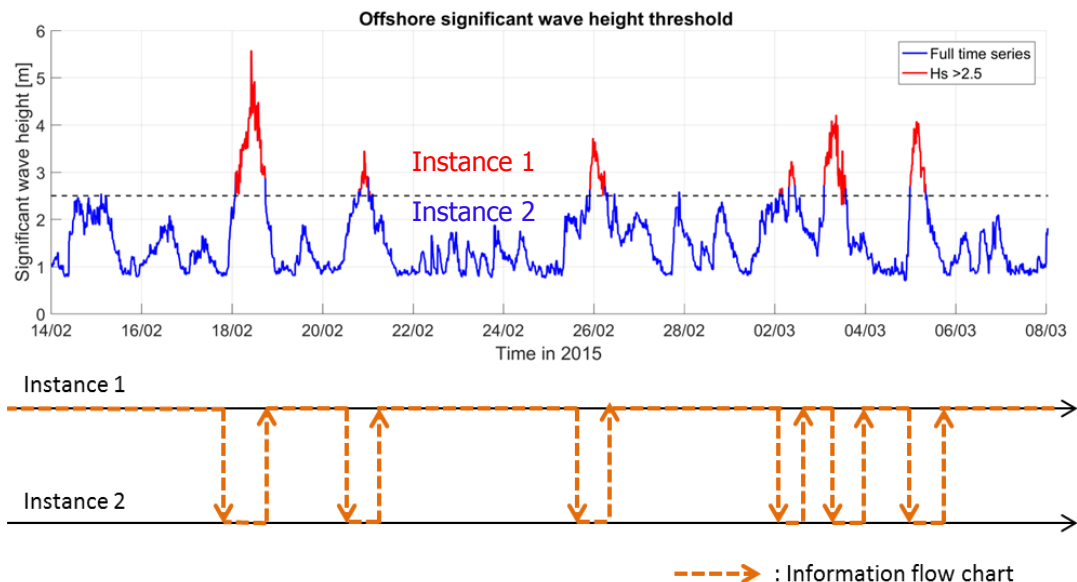
Figure 18: Time coupling flow chart example. The dashed orange line represents the flow of information (e.g., bed level). The black solid line represents the information that might be computed but is later replaced by the information received from other instance.

3.4. Coupling performance

The current version of D3D-FM used in this thesis (version 1.1.192.50908) has a major drawback when it comes to BMI steering in comparison with XBeach, which is lacking the option of performing large "jumps" in model time and not computing anything during the "*standby*" time as shown in Figure 13-c. Because of this restriction when performing the coupling, during the time that the model results are not important (as shown by the black lines in Figure 18) the model is still computing, hence misusing computational resources an affecting the overall performance. To set an example on the negative effect of this, a test case was performed by running a D3D-FM flow and wave simulation for 3 hours, in a model with approx. ~20,000 grid cells. The model was run with an increasing number of instances (parallel simulations), first by initializing and running all at the same time, and later by initializing all but running only one instance at a time, resembling what it would be to have the non-running instances in standby. Figure 19 depicts that by initializing more simulations, the increment in total processing time is marginal when compared to running more simulations in parallel. Furthermore, it can be seen that processing time does not follow a linear but a power trend with a power ~1.6; hence already with 2 parallel instances as shown by the red line, the processing time is a ~50% larger than what an offline coupling would take (green line), and a ~300% larger than running just 1 instance at a time (blue line). It is expected that future releases of D3D-FM include an option to overrule the CFL restriction and allow manually setting the model time with BMI, thus severely increasing the coupling performance.
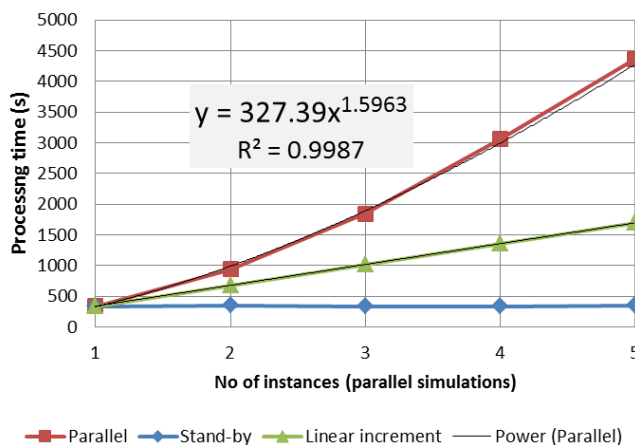
Figure 19: Processing time comparison for a single run v/s parallel runs with increasing number of model initializations

4. Modelling beach representations of Anmok beach

This chapter is divided into four main topics: hydrodynamic models, morphodynamic models, swash zone models and storm calibration models. For each of these first a description of the model set-up is presented, followed by the model results.

The purpose of the hydrodynamic models is to compare and validate the hydrodynamics at Anmok beach in D3D-FM. In the morphodynamic models section, the different mass transport formulations (Eulerian & GLM) are compared, and then a coupled simulation of these mass transports is developed. Later in this section XBeach is incorporated to solve the hydro-morphodynamic phenomena during severe storms. In the third section, a research version of D3D with specialized swash zone sediment transport formulations is assessed as a potential tool for enhancing the post-storm recovery mechanisms. Finally, a brief XBeach calibration is developed analyzing a (experimental) software parameter that is capable of reducing the dry beach erosion.

4.1. Hydrodynamic models

4.1.1. Model set-up

The first model to be tested is the hydrodynamic model of Anmok beach in D3D-FM, using the same grid, bathymetry and model set-up as the base case used by Ton (2017) in D3D. Figure 20 shows the initial model bathymetry as well as the location of buoys with measurements that will be used for hydrodynamic comparison. The offshore model boundary is located near the W1 buoy; hence the values recorded by this device are used as offshore boundary conditions (water level and wave spectra).
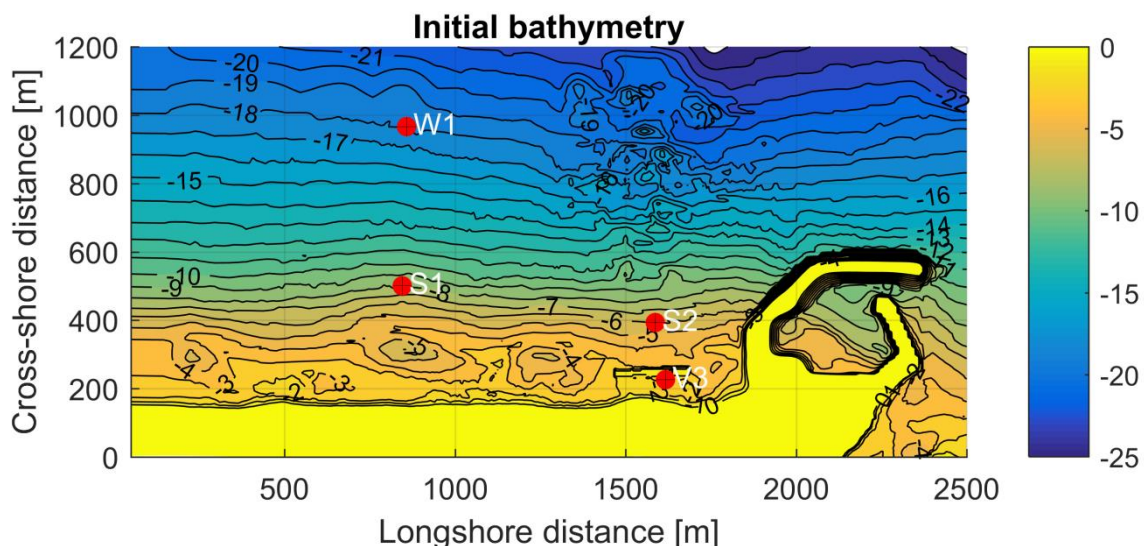
Figure 20: Initial hydrodynamic model bathymetry from January-2015.

The model is roughly 1,500 m long in the cross-shore direction, and 3,000 m long in the longshore direction. It has approx. ~46,000 rectangular grid cells with a varying resolution, ranging from 20x15 m offshore to 5x5 m in the nearshore. The initial bathymetries are based on the surveys from January-2015 for the calm season and June-2015 for the stormy season. The model domain is shown in Figure 21 along with a detail of the grid around the SBW. Neumann boundary conditions are imposed along the lateral boundaries.

The one year wave data in buoy W1 is shown in Figure 22. There is a period between April and May 2015 where the data is erroneous with the exception of the significant wave height and spectra. The hydrodynamic model is run for a 1 month period corresponding to February-2015 with a fixed

bathymetry, in order to have a fair comparison with the D3D model run by Ton (2017). All models are run in a depth averaged mode (2DH).
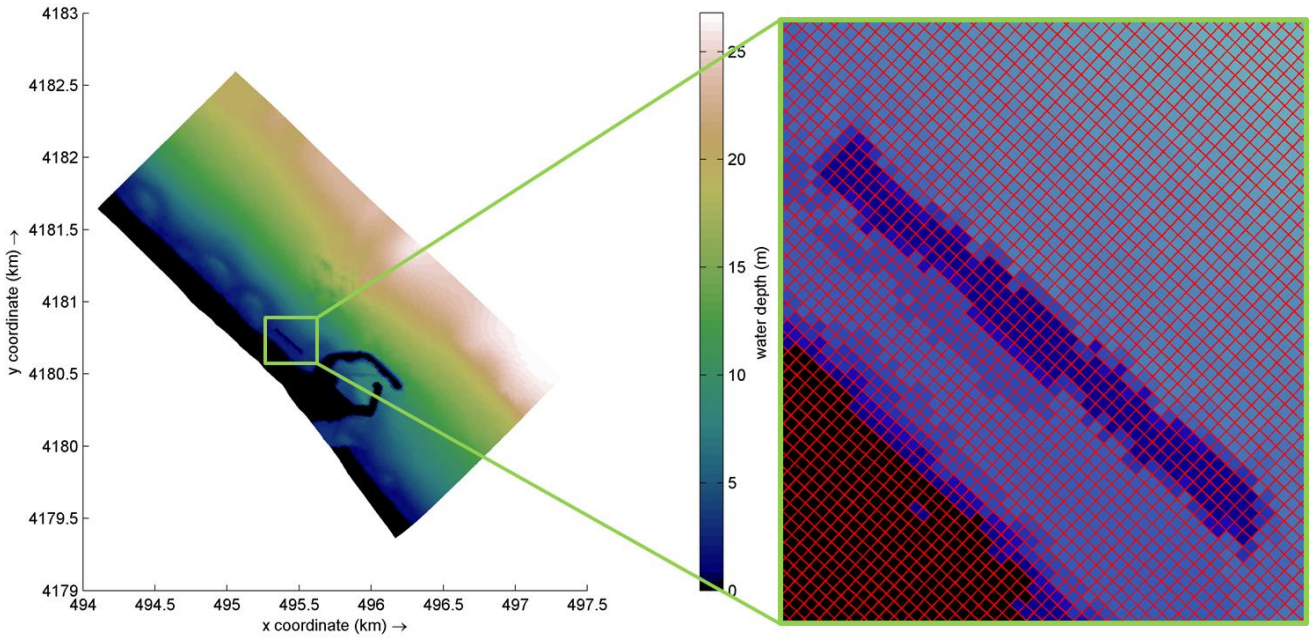
Figure 21: D3D model domain and zoom around the SBW showing the grid
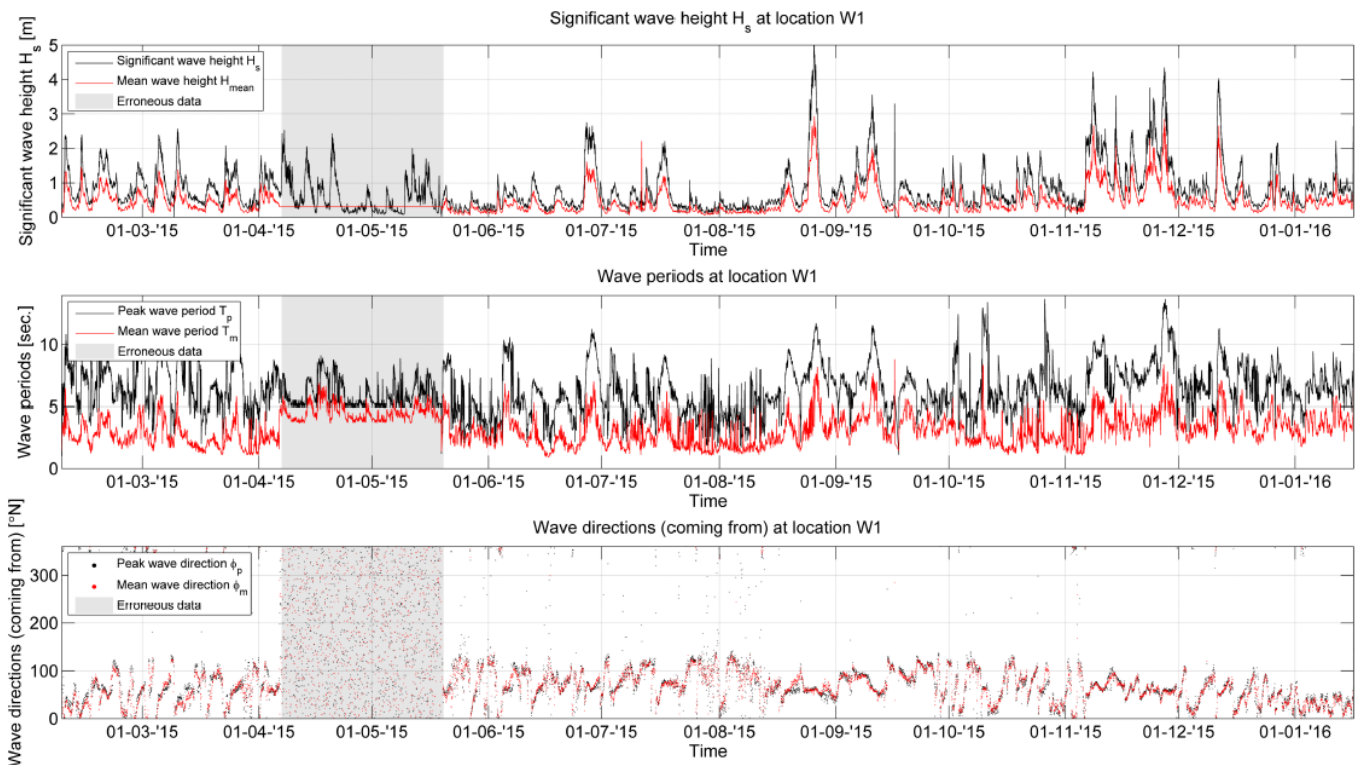
Figure 22: Wave data buoy W1. From Ton (2017)

As indicated by Ton (2017), to avoid instabilities due to variations in bathymetry along the boundaries, the horizontal viscosity was adjusted within a band of ~90 meters width along the domain boundaries, increasing its value from a default value of $1\ m^2/s$ to $100\ m^2/s$. The complete model settings are shown in appendix A.

23

4.1.2. Model results

The hydrodynamic model validation is a required step in order to develop a sound morphodynamic model; however a thorough hydrodynamic validation/comparison deviates from this thesis' main objective. The most important findings of the hydrodynamic models developed in D3D and D3D-FM are summarized in the next bullets. The full description of the hydrodynamic results is presented in appendix B.

- The wave spectra simulated by both software (D3D & D3D-FM) is exactly the same everywhere except behind the SBW. At this location some minor frequency shifts are observed during highly energetic events ($H_s > 2\,m$). Despite this, the total energy simulated by both suites is almost identical throughout the whole simulation period.
- The water level predicted by the different software is in excellent agreement, with maximum differences in the order of ± 5 cm. There is a $\sim 0.4\,m$ difference between the model predictions and the measurements, already noticed by Deltares (2016a) and Ton (2017), which is attributed to uncertainties in the instruments' reference level and/or the highly dynamic morphological development of the area. When corrected by a constant value the models and measurements have a good agreement.
- The currents predicted by both models are similar in the deeper water region (at the location of buoy W1), however it was found that in the nearshore D3D is more sensitive than D3D-FM to wave-driven currents for the same model settings. In general the agreement between both suites is good, although when the tide opposes the wave's direction, and the waves are highly energetic, some differences between the simulated currents are found. Since the mismatches are only occasional it is not expected that they significantly affect the morphodynamics.
- In a late stage of this thesis it was found that the wave boundary conditions had a directional error with respect to the magnetic north of approx. 8 deg. To have a fair comparison with the results obtained by Ton (2017) and for the sake of time this direction was not corrected in the present models.

4.2. Morphodynamic models

4.2.1. D3D model set-up

For the morphodynamic model, a base case was obtained by running a D3D model with the same parameters and data as the calibrated model developed by Ton (2017). For this model, in order to achieve a reasonable running time, all the waves with $H_s < 0.9\,m$ were removed from the wave time series, and then the hydrodynamic boundary conditions were compressed by a factor 3. This allowed running the simulation with a morphological acceleration factor or *morfac* of 3. The combination of this input reduction and morphological acceleration allowed reducing the hydrodynamic modelling time from 1 year to 1 month, having approximately the same morphodynamic results. The main parameters from the calibrated model are shown in Table 1, indicating the final values determined by Ton (2017). The full model settings are shown in appendix A.

Table 1: Calibrated D3D model parameters. From Ton (2017)

Parameter	Calibrated result
Mass transport formulation	Eulerian (and GLM for calm season)
Transport formula	Van Rijn 1993
Wave bed load factor (*BEDW*)	0.05
Wave suspended load factor (*SUSW*)	0.05
Maximum wave height to depth ratio (γ_{max})	0.55
Mean sediment diameter (d_{50})	500 μm

In Figure 23 the measured bathymetries from the year 2015 are shown, from which sedimentation and erosion patterns can be estimated as shown in Figure 24. This data is required to estimate the Brier Skill Score (BSS) and for further analyses.
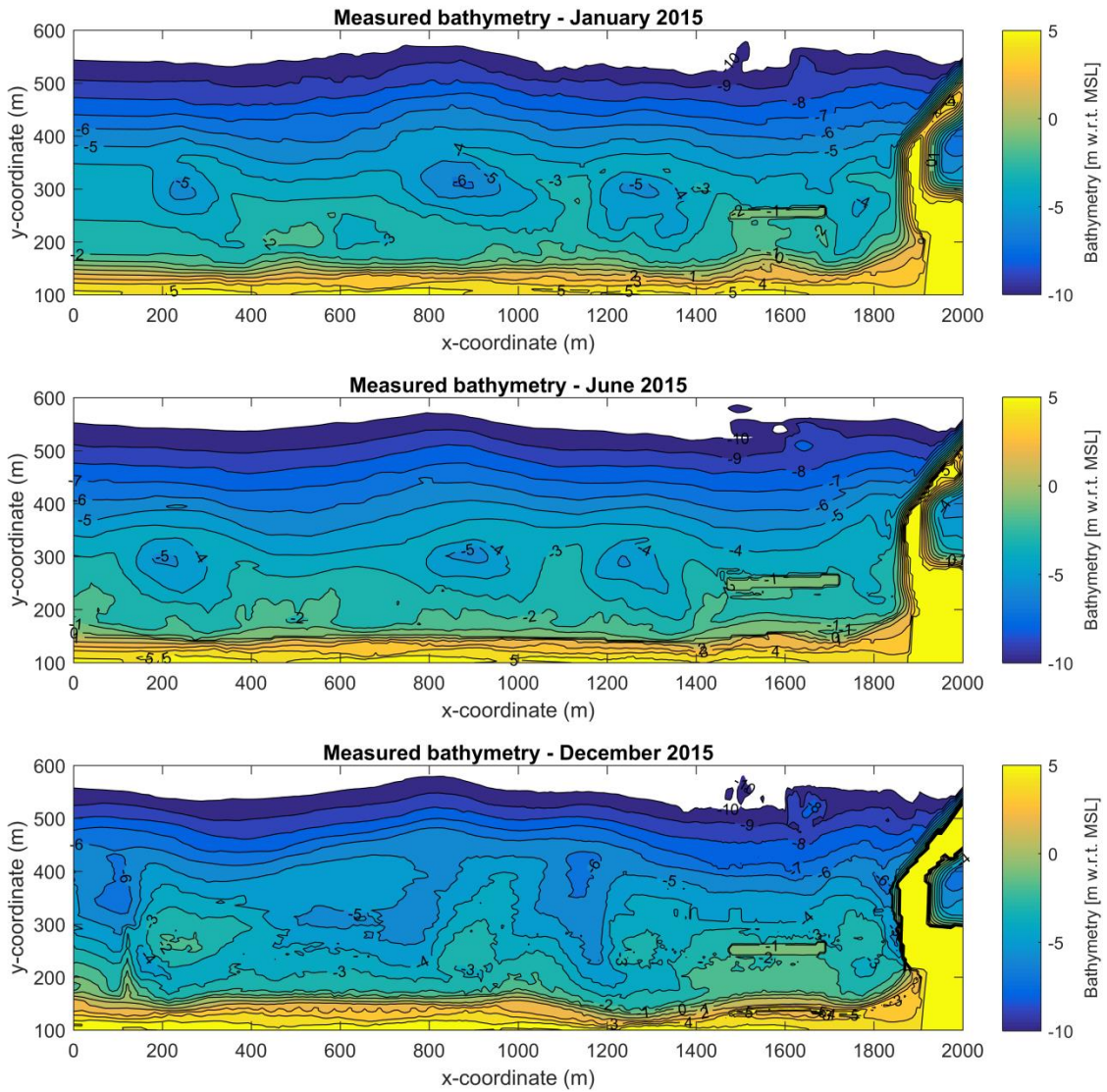
Figure 23: Measured bathymetry of Anmok beach around the SBW
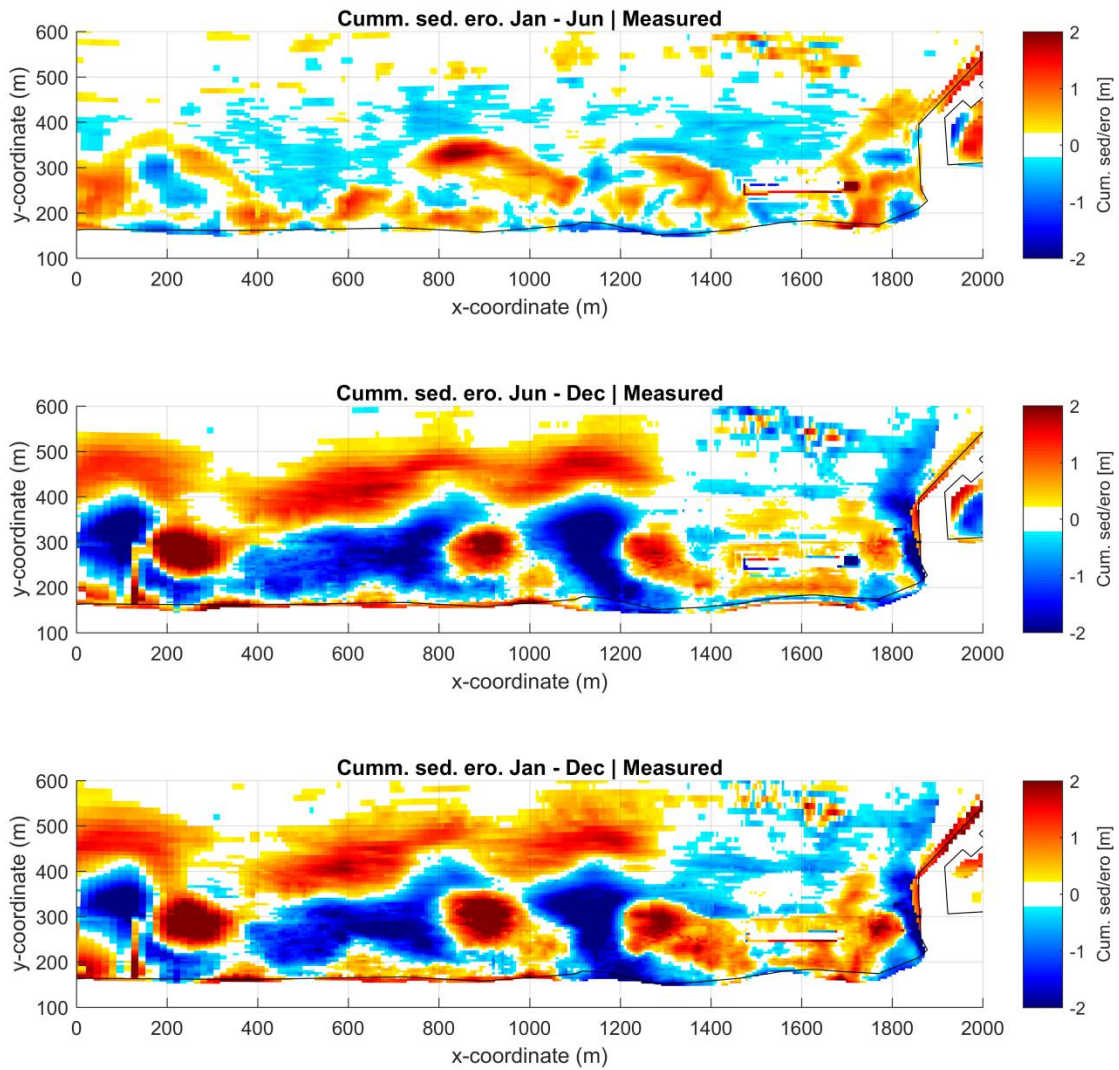
Figure 24: Measured cumulative sedimentation/erosion patterns of Anmok beach close to the SBW

Table 2 summarizes the list of models that were performed to determine the morphological base case.

Table 2: D3D models list to estimate the base case results

Model No.	Description
1	GLM mass transport – 1 year
2	EUL mass transport – 1 year
3	GLM (6 months) followed by EUL (6 months) - (offline coupling)

4.2.2. D3D model results

Figures 25, 26 and 27 show the cumulative erosion/sedimentation patterns for the 1 year GLM run, EUL run and offline coupled GLM-EUL model respectively. It is observed from a qualitatively point of view, when comparing with the measurements from Figure 24, that the GLM model performs better during the calm period (January-June) and the Eulerian model has a better performance in the stormy season (June-December). The offline-coupled model performs better than the individual models in a qualitative manner, since it is able to represent both periods. However, an exception is observed at the swash zone for all cases, where the Eulerian model predicts excessive erosion and the GLM model predicts an unmeasured accretion.
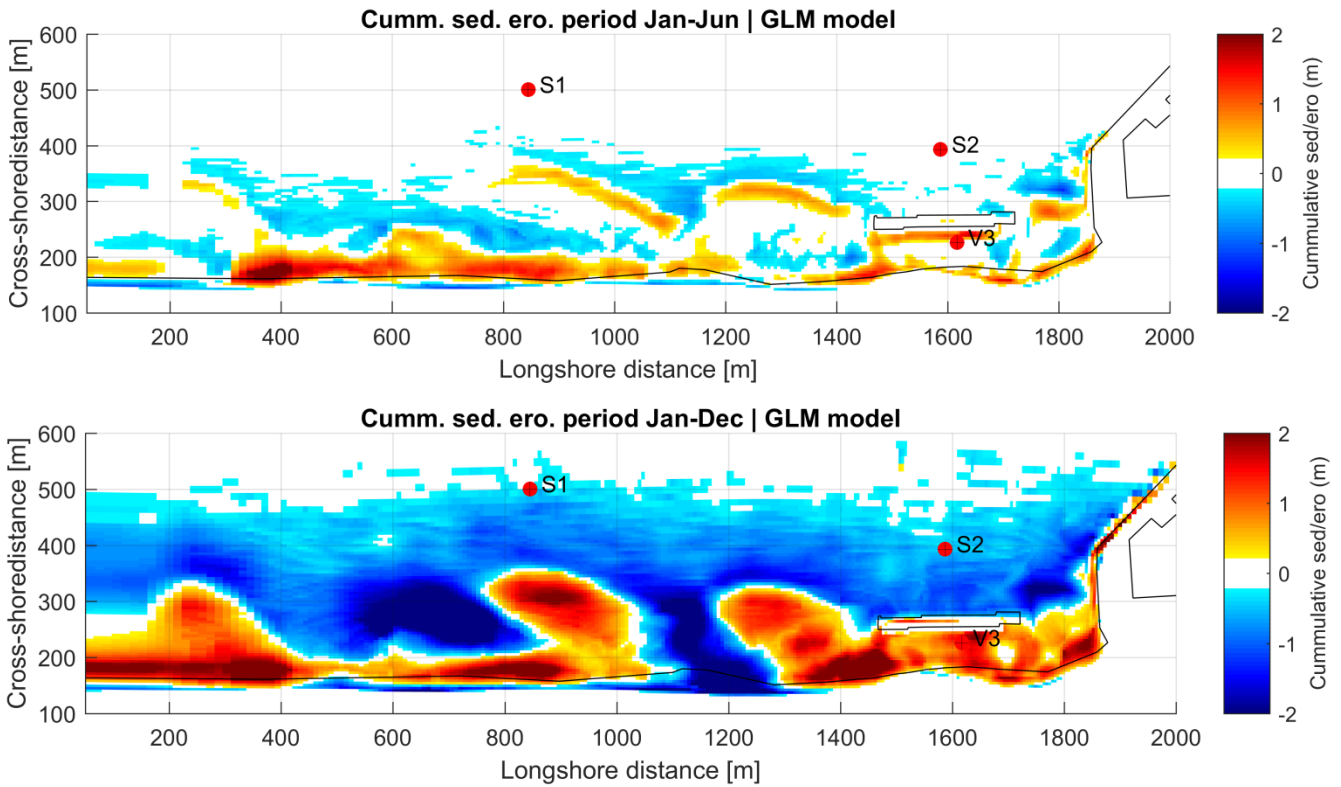
Figure 25: Modelled cumulative sedimentation/erosion patterns. D3D GLM model. Top: Calm season. Bottom: Calm and stormy season
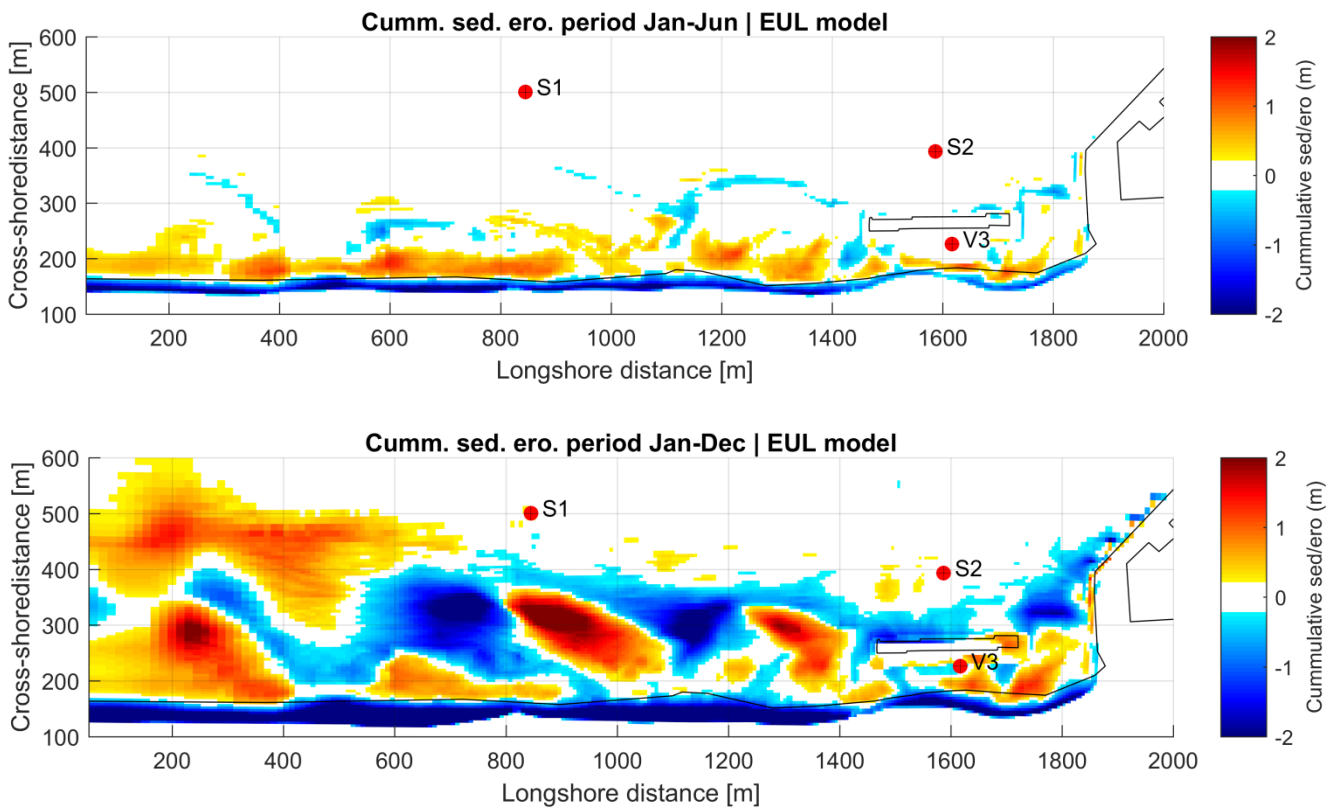
Figure 26: Modelled cumulative sedimentation/erosion patterns. D3D EUL model. Top: Calm season. Bottom: Calm and stormy season
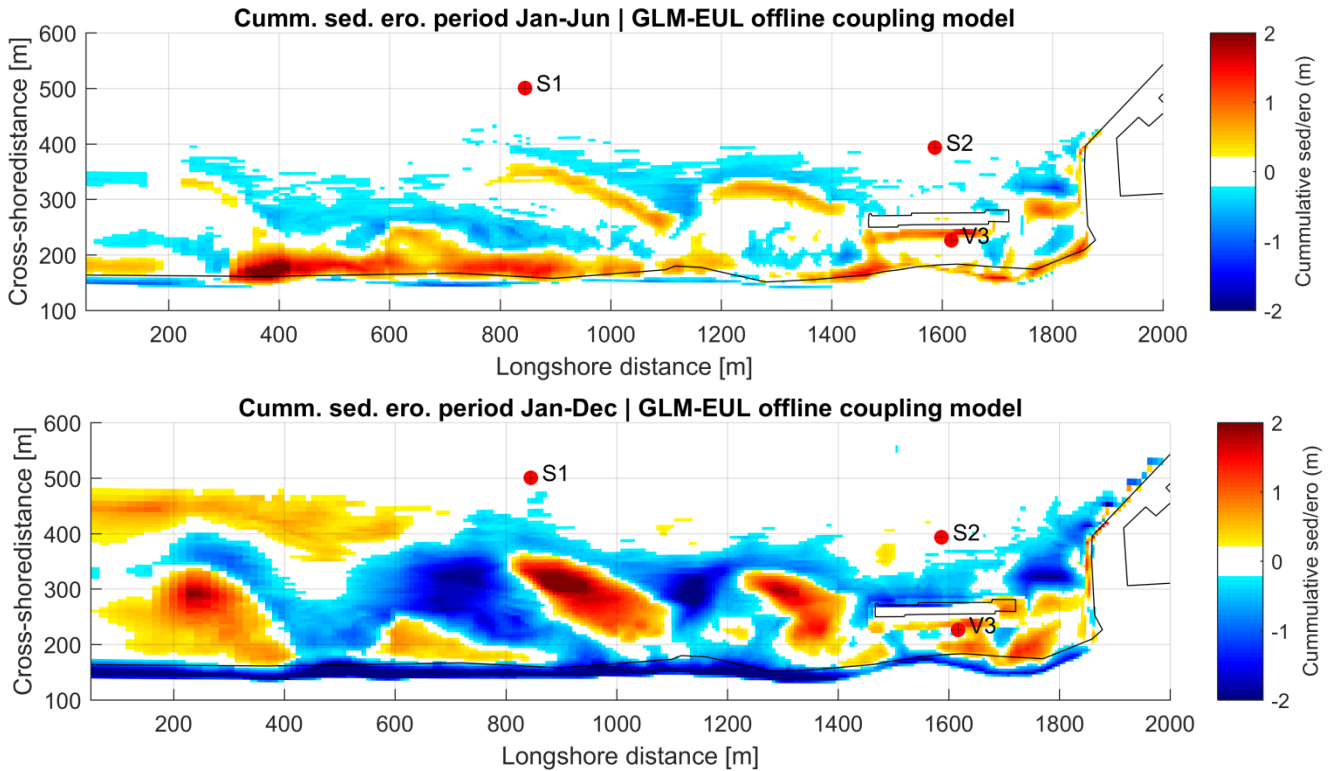
Figure 27: Modelled cumulative sedimentation/erosion patterns. D3D offline coupled model.
Top: GLM (calm season); Bottom: Calm (GLM) and stormy (EUL) season coupled model.

To quantify the quality of the morphological predictions in an objective manner, the BSS is used. This statistical score is defined by Sutherland et al. (2004) as:

$$BSS = 1 - \frac{\langle(z_c - z_m)^2\rangle}{\langle(z_0 - z_m)^2\rangle}$$

[13]

Where z_c is the computed bed level by the model, z_m is the measured bed level and z_0 is the initial bed level. A value of 1 corresponds to a perfect match between the computed and measured bed levels, whereas a low (or negative) value means a great divergence between these bathymetries. A general classification of the BSS values is shown in Table 3:

Table 3: BSS classification

Classification	BSS
Excellent	1.0-0.8
Good	0.8-0.6
Reasonable/fair	0.6-0.3
Poor	0.3-0
Bad	<0

Since the BSS score is severely skewed by areas where no morphological change occur, five areas were selected starting from the shoreline and going farther offshore, as shown in Figure 28. The results are shown in Table 4 and summarized in Figure 29. It can be seen that in general the scores vary between "bad" and "poor" at best, which is in line with the results obtained previously by Ton (2017) . The GLM model seems to give better results in June and a similar result as the Eulerian model in December. However, from a qualitatively point of view, the sedimentation/erosion patterns in December are better represented by the Eulerian model. When looking at the offline coupled results, it can be seen that the result is qualitatively equal or better than the single models for both periods, and the BSS is better than the individual models when considering the whole year. This outcome strengthens the idea that a more frequent (serial-online) coupling could have a better performance.

As an additional exercise the BSS was evaluated excluding the swash zone (indicated as area 1 in Figure 28) since this area is not well represented by any of the models and brings down the overall skill. As seen in Figure 29, the model that has the best behaviour over the whole year is the coupled one, hence reinforcing the hypothesis that this simulation is the one that performs best, especially when the qualitative results are taken into account.
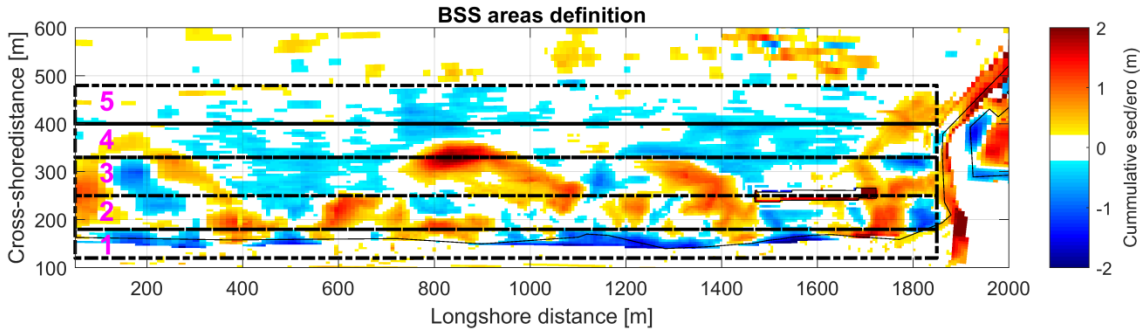
Figure 28: Areas selected for BSS analyses, as indicated with the black dashed lines.

Table 4: BSS results for D3D models

	MODELS					
	GLM		EUL		GLM-EUL (coupled)	
AREA	Jan-Jun	Jan-Dec	Jan-Jun	Jan-Dec	Jan-Jun	Jan-Dec
1	-0.31	-0.15	-0.61	-2.41	-0.31	-1.06
2	-0.02	0.01	0.12	0.29	-0.02	0.47
3	0.26	0.52	0.08	0.59	0.26	0.47
4	0.30	-0.54	-0.03	0.11	0.30	0.09
5	0.18	0.18	-0.04	-0.04	0.18	-0.44
Weighted averaged	0.10	0.03	-0.08	-0.20	0.10	-0.06
Weighted averaged (w/o swash zone)	0.15	0.05	0.03	0.20	0.15	0.12
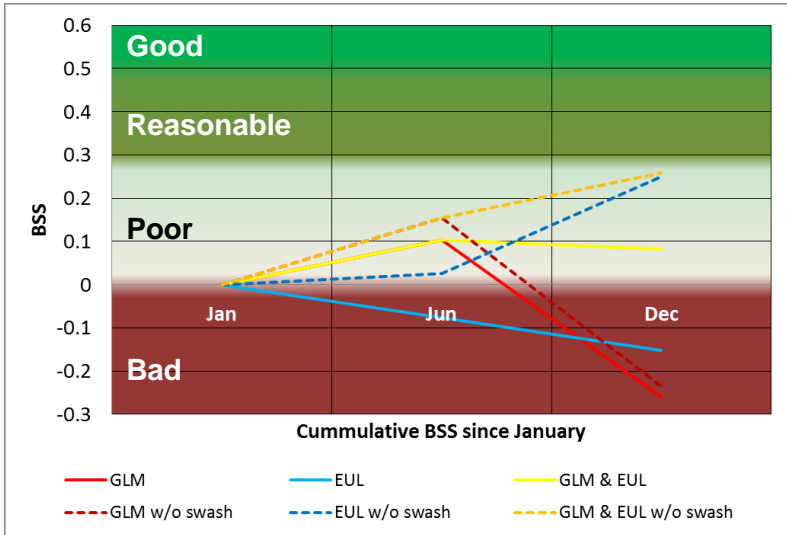
Figure 29: BSS results plotted against BSS classification

Since the second period (June-December) presents the largest changes in bed level changes as seen in Figure 24, it is considered much more relevant in morphological terms than the first half of the year. Therefore, the stormy season is selected as the base case to be analyzed with respect to any

additional model calibrations, which are required in order to achieve stable simulations in D3D-FM. The sedimentation/erosion patterns of all periods (Jan-Jun-Dec) are shown in appendix C.

As a different way to quantify these morphological changes, an area of interest was selected between the SBW and approx. 400 m east of the left model boundary, as depicted in Figure 30. In this area, cross-shore bars of cumulative sedimentation/erosion in the area of interest are calculated and then grouped and averaged in the cross-shore direction every 4 grid cells. By doing this it is possible to quantify the trends in bed level changes in the cross-shore profile, and compare it with the measurements of each period.

The results for the June-Dec, Jan-June and Jan-Dec periods are depicted in figures 31, 32 and 33 respectively. What can be recognized from the measurements during the stormy season is a general trend of erosion between 0 and 350 m in the cross-shore direction, which suffers an inversion showing sedimentation farther offshore (Figure 31-a). This behaviour is somewhat well represented by the Eulerian D3D model (Figure 31-c, with the exception of the shoreline). On the other hand, the GLM D3D model shows an inverse pattern, with erosion offshore and sedimentation in the nearshore (Figure 31-b).

When looking at the calm season results (Figure 32), opposite behaviour is observed in the measurements, with accretion until ~350 m in the cross-shore direction, followed by erosion. This is at some level better represented by the GLM model (Figure 32-b), whereas the Eulerian model over predicts the erosion at the shoreline and under predicts it everywhere else (Figure 32-c).

Finally, Figure 33 shows the full year results, for the stand-alone models and the offline-coupled D3D model. What is depicted in the measurements is a behaviour similar to the stormy season period, with erosion between 0 and 350 m, followed by deposition (Figure 33-a). From the three models the only one that follows this trend is the coupled model (Figure 33-d), with the exception of the shoreline where severe erosion is predicted.
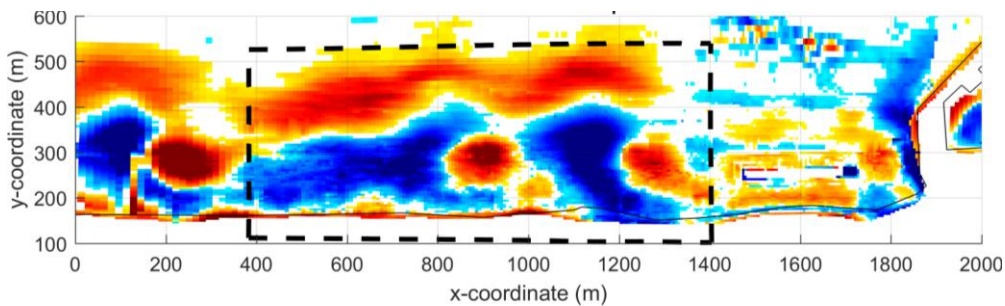
Figure 30: Sedimentation/ Erosion quantification - Area of interest
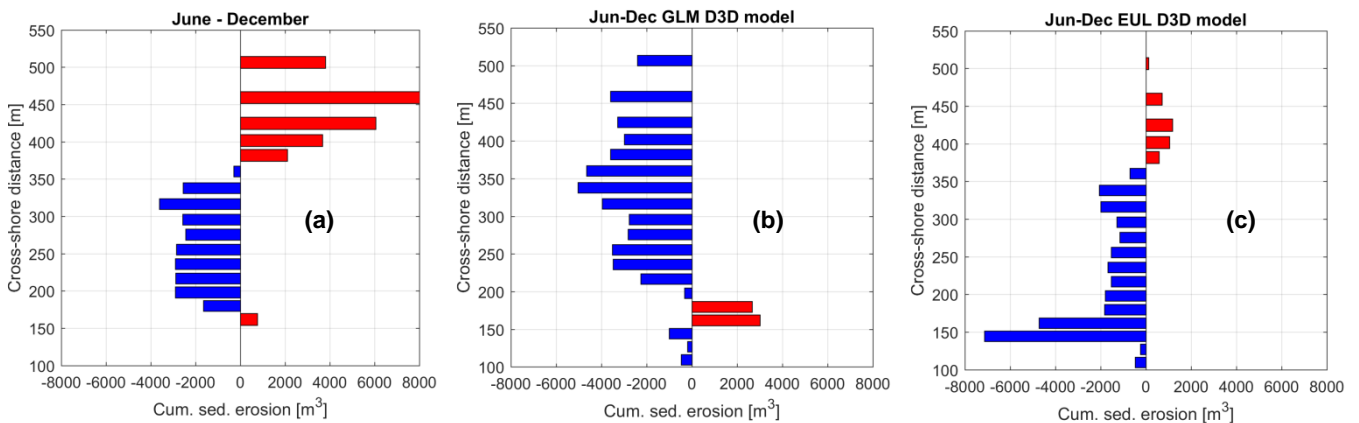
Figure 31: Cross-shore sedimentation/erosion bars for June-December. (a) Measured; (b) D3D GLM model; (c) D3D EUL model.
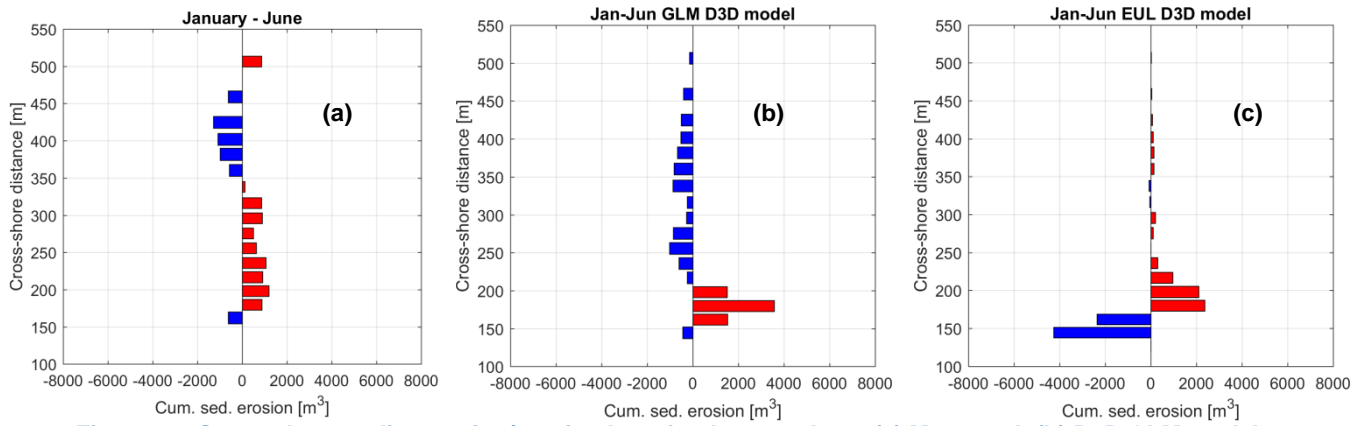
Figure 32: Cross-shore sedimentation/erosion bars for January-June. (a) Measured; (b) D3D GLM model; (c) D3D EUL model.
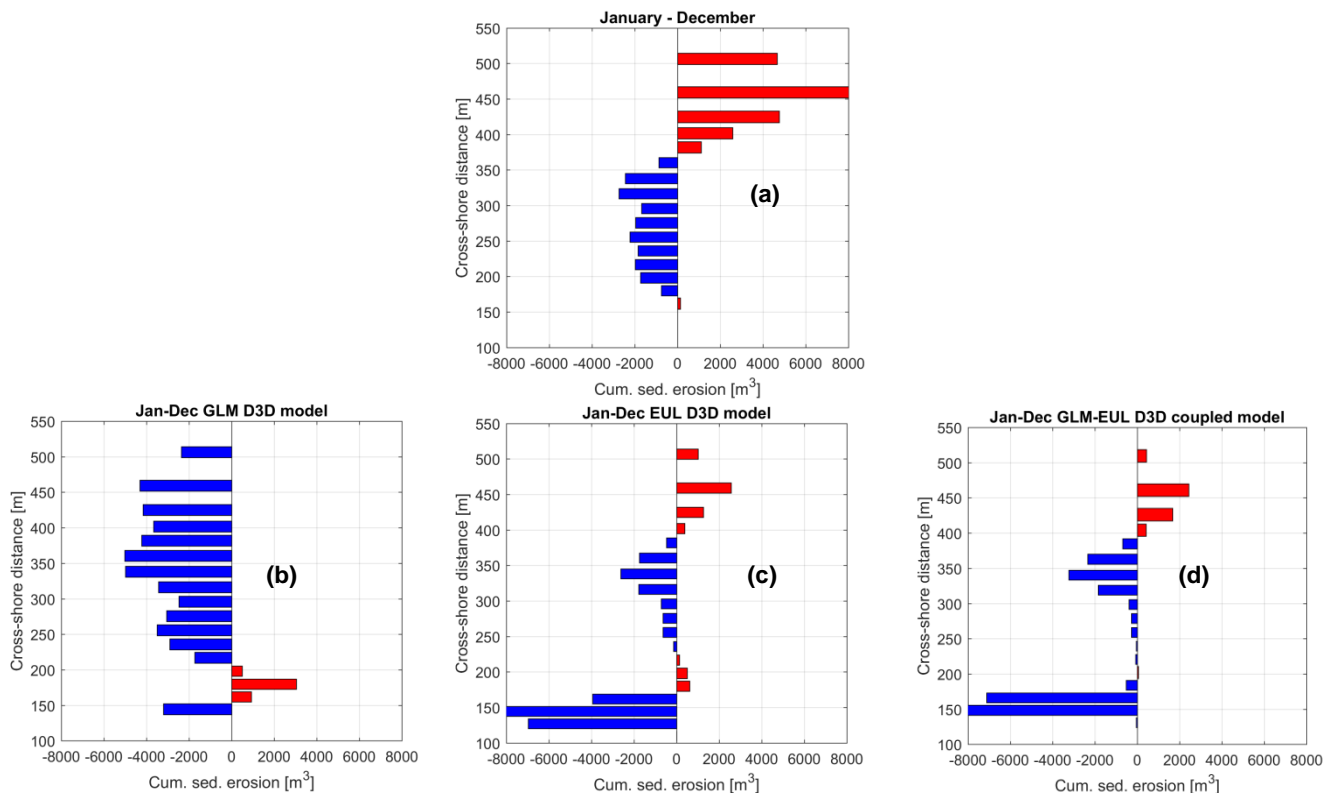
Figure 33: Cross-shore sedimentation/erosion bars for January-December. (a) Measured; (b) D3D GLM model; (c) D3D EUL model; (d) D3D GLM-EUL offline coupled model;

4.2.3. D3D-FM model set-up

The model in D3D-FM has the same grid, boundary conditions and parameters as the D3D model, with some exceptions:

1. The wave breaker parameter γ_{max} is changed from 0.55 to 0.8. This is because in D3D this parameter applies to the root mean square wave height (H_{RMS}) whereas in D3D-FM this parameter applies to the significant wave height (H_s).

2. The threshold water depth for determining whether a cell is wet or dry (*EPSHU*) was lowered from 0.05 to 0.01.

3. The bathymetry at the boundaries was changed from a fixed bathymetry to a bathymetry that allowed changes (UPDINF=true).

4. Close to the offshore boundary there are "spikes" as part of a very irregular bathymetry, which is believed to be due to the presence of rocky outcrops. This created model instabilities in the form of high velocity "jets" which propagated into the model. To cope with this the bathymetry

31

close to the boundaries was smoothed as shown in Figure 34. This is not expected to influence the nearshore sediment transport patterns in the model.

5. The maximum volumetric reference concentration (CAMAX) was lowered from its default value of 0.65 to 0.05.
6. The wave-related suspended sediment transport factor (SUSW) was lowered from 0.05 to 0.02.

From the previous list the first 4 items were found to be critical to achieve model stability, since small changes in these coefficients/settings usually led to model instabilities followed by the software "*crashing*". The last 2 items of the list are related to achieve more sensible results, avoiding for instance large bed level gradients at the boundaries.

It is important to mention that the viscous boundaries of $100 \, m^2/s$ (just like in the D3D simulations) were crucial for model stability, since not a single simulation could be completed without this inclusion, and in some cases it had to be increased to $\sim 1000 \, m^2/s$ during extremely high energetic storm periods.
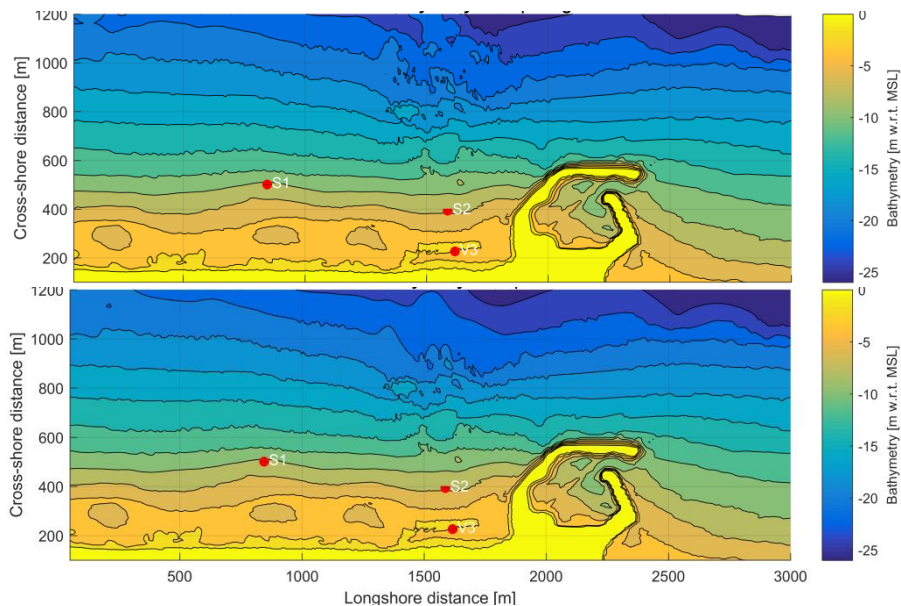
Figure 34: Model initial bathymetry in June. Top: Original bathymetry. Bottom: Smoothed bathymetry. Contour lines every 2 m. Differences are observed around (x,y)=(1500,1100).

The models chosen to be run are shown in Table 5. The first 4 models correspond to stand-alone simulations which will be compared with the results of the D3D simulations, whereas the last one is a coupled model from where improvement/worsening of the morphodynamic results can be assessed.

Table 5: D3D-FM morphological models list

Model No.	Description	Simulation period
1	GLM stand-alone model	Jun-Dec
2	EUL stand-alone model	Jun-Dec
3	GLM stand-alone model	Jan-Jun
4	EUL stand-alone model	Jan-Jun
5	GLM-EUL coupled model	Jun-Dec

To run the coupled simulations an information exchange criterion had to be determined as explained in section §3.3 and Figure 18. For this purpose the offshore significant wave height was chosen, as the wave forcings are the main drivers for morphological changes at this beach. Since the main goal of this thesis project is to develop a coupling methodology and not to re-calibrate or over-calibrate the independent models previously developed by other authors, and also taking into account that BMI

does not allow running simulations in a cluster, for the sake of time only one wave-threshold scenario is currently evaluated based on the results of the uncoupled simulations.

This scenario considers a significant wave height threshold of 2.5 m as shown in Figure 35. Thus, when this value is exceeded, information is sent into the Eulerian model, and when the wave height is inferior, information is sent back to the GLM model. In Figure 35 only the stormy season period (equivalent to Jun-Dec) is shown, since in §4.2.2 it was shown that this is the dominant period when it comes to morphological changes. Also, during the calm period the wave height never exceeds the aforementioned threshold.
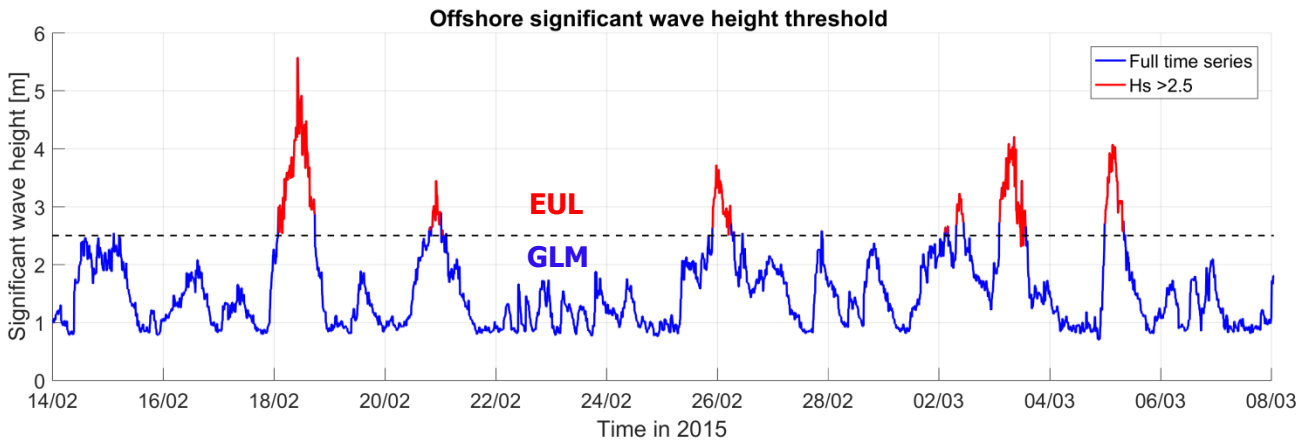
Figure 35: Offshore significant wave height time series and threshold for model coupling information exchange

4.2.4. D3D-FM model results

The sedimentation/erosion patterns of models 1 and 2 (from Table 5) are shown in figures 36 and 37. What can be seen directly is that the difference between both models is less notorious as compared with the D3D simulations, at least from a qualitatively point of view. To confirm this in a quantitative way, the same procedure of sedimentation/erosion cross-shore bars was replicated, for the same area of interest shown in Figure 30.

When looking at these results of the Delft3D-FM simulations, it can be recognized that the GLM model (Figure 38-b) follows a similar trend as the D3D simulation, whereas the Eulerian model (Figure 38-c) presents less erosion between ~200 and ~400 m in the cross-shore direction, and the general trend of offshore accretion and onshore erosion is not present. The Eulerian simulation shows definitively less erosion in the farther offshore area ($> 400\,m$), but it does not reach the point to reverse the trend into actual accretion. What the Eulerian simulations (in both suites) have in common is an over-prediction of erosion at the shoreline
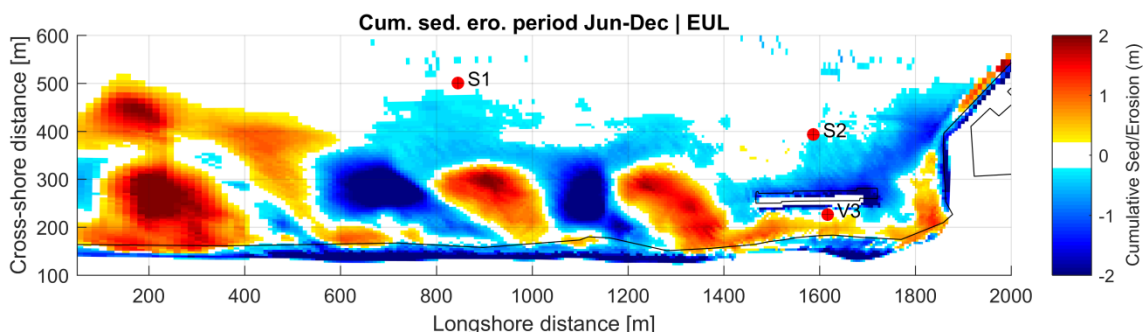
Figure 36: Modelled cumulative sedimentation/erosion patterns. D3D-FM EUL model.
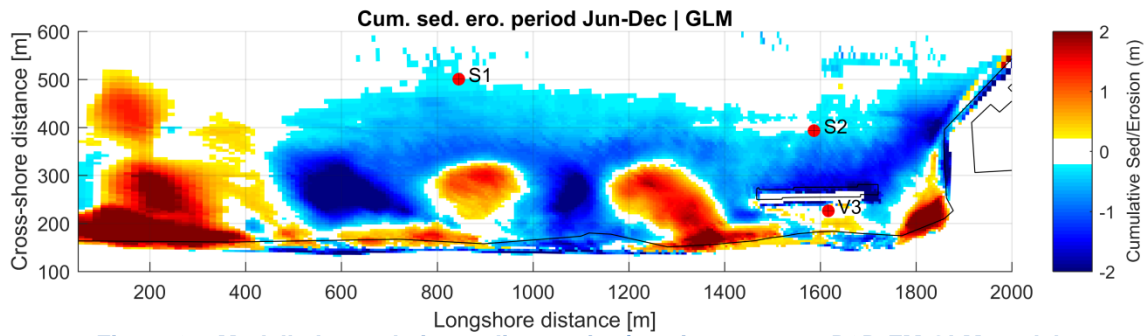
Figure 37: Modelled cumulative sedimentation/erosion patterns. D3D-FM GLM model.
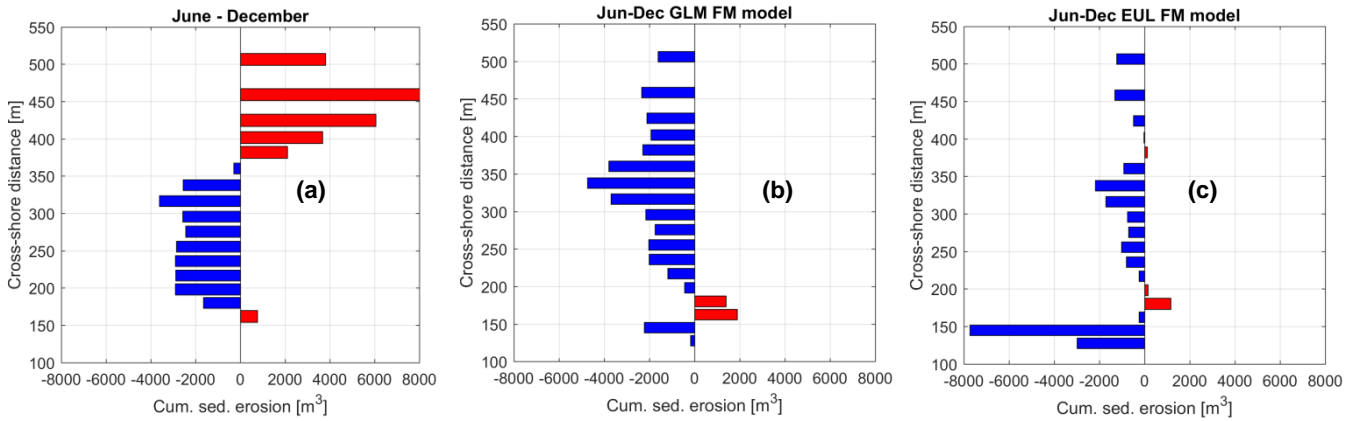
Figure 38: Cross-shore sedimentation/erosion bars for June-December. (a) Measured; (b) D3D-FM GLM model; (c) D3D-FM EUL model.

When comparing the final bathymetries between EUL and GLM simulations for both software (figures 39-a and 39-b), it can be seen that the impact of using different mass transport formulations is stronger in D3D, as the relevant morphological changes extend up to ~500 m in the cross-shore direction, whereas in D3D-FM they only reach about ~400 m. Also the shoreline erosion is stronger in D3D. Despite these differences in magnitude the general patterns when changing from one mass transport formulation to the other are consistent for both modelling suites.
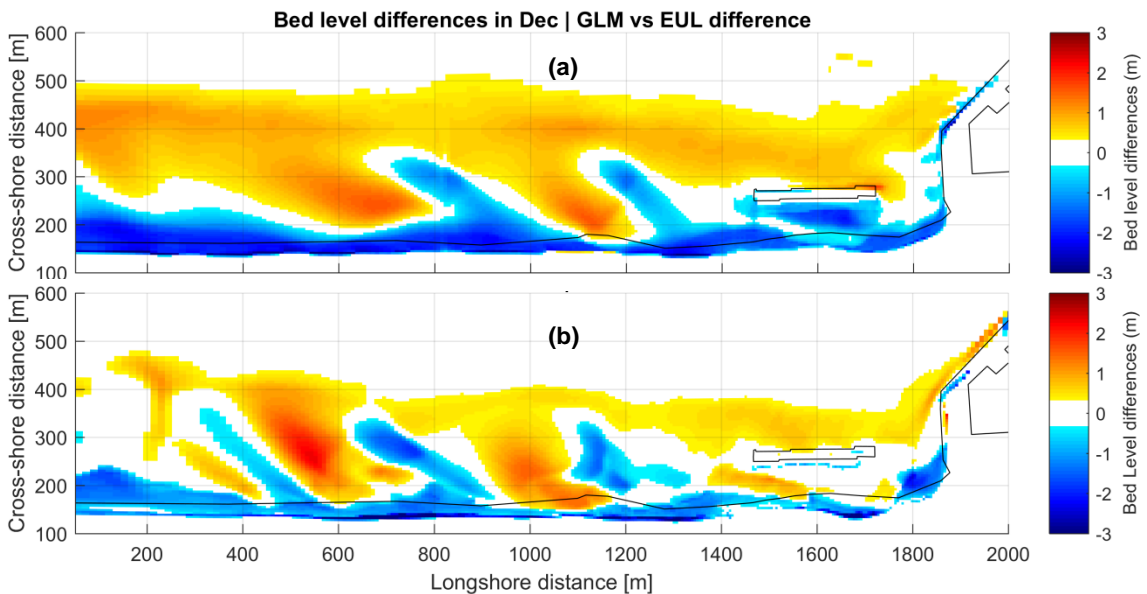
Figure 39: Bed level differences between GLM and EUL simulations for the stormy season. Differences calculated in December. (a) D3D model; (b) D3D-FM model.

34

When running the GLM model for the calm season, a good agreement between D3D and D3D-FM was found, as is depicted in Figure 40. When running the same period with Eulerian transport, a similar result is found but with higher erosion near the shoreline (Figure 41). The cross-shore sedimentation/erosion bars were calculated for the same area of interest as before, and the results are depicted in Figure 42. Here it can be seen that both the GLM and Eulerian simulations have a pattern that resembles the measurements, with sedimentation in the nearshore and erosion offshore, but with the difference that the Eulerian simulation shows relatively large erosion at the shoreline. The major difference between models and data is that in the measurements the inversion of the trend happens at ~350 m in the cross-shore, whereas in the simulations it is seen at ~220 m. The bed level differences between the GLM and Eulerian simulations (in both software) are shown in Figure 43, where it can be recognized that the changes in the offshore region (~300-600 m) are less significant in D3D-FM, and only the swash zone is noticeable affected. With these results it can be inferred that the present version of D3D-FM has less dynamic results when using the Eulerian mass transport when compared to regular D3D. Part of this could also be attributed to the fact that some model parameters had to be changed in D3D-FM in order to achieve a stable simulation (as explained in section §4.2.3). To assess this, a simple 2D alongshore uniform coast model was tested with the exact same settings in both software, and it was confirmed that when using an Eulerian mass transport formulation, the morphological changes were approx. 80% smaller than the ones observed in D3D. This test model is further explained in appendix F.
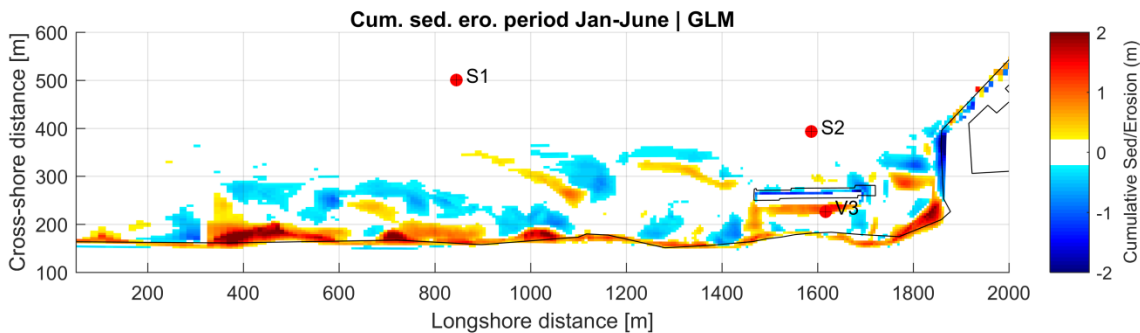
Figure 40: Modelled cumulative sedimentation/erosion patterns. D3D-FM GLM model.
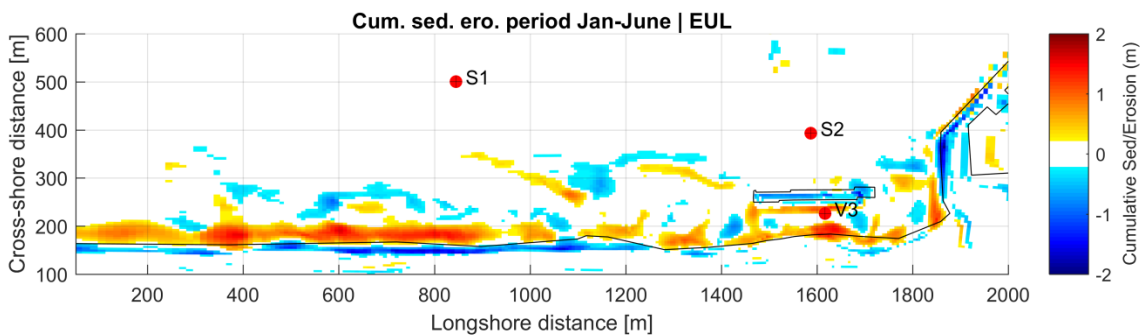
Figure 41: Modelled cumulative sedimentation/erosion patterns. D3D-FM EUL model.
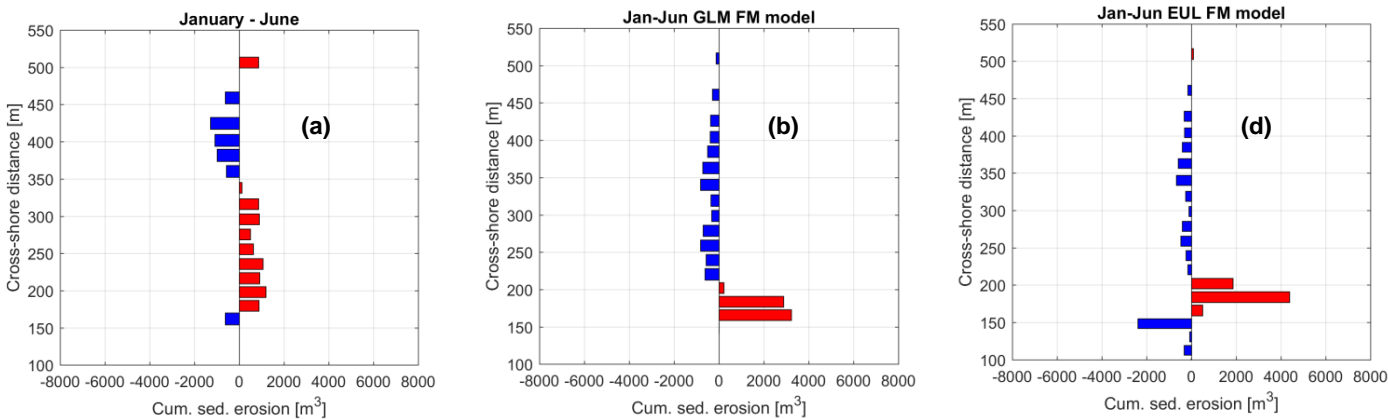
Figure 42: Cross-shore sedimentation/erosion bars for January-June. (a) Measured; (b) D3D-FM GLM model; (c) D3D-FM EUL model.
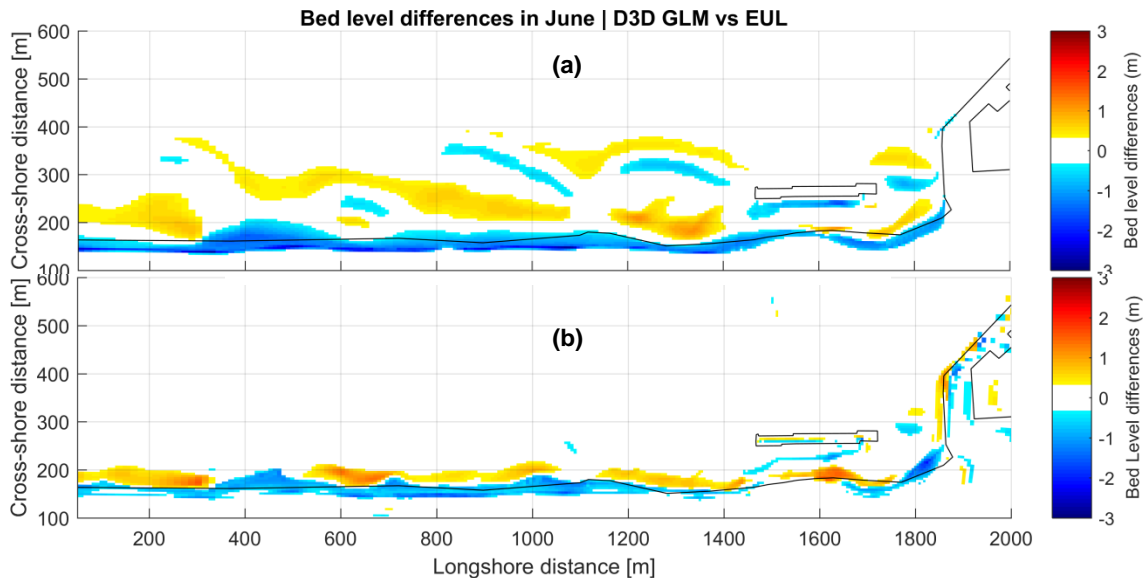
Figure 43: Bed level differences between GLM and EUL simulations for the calm season. Differences calculated in June. (a) D3D model; (b) D3D-FM model.

The BSS values were estimated for both seasons as shown in Table 6. What can be seen is that for both seasons the BSS results qualify as "poor" at best, which is in the same order of magnitude as the results obtained with the D3D model.

Table 6: BSS results for D3D-FM uncoupled models

	MODELS			
	GLM		EUL	
AREA	Jan-June	June-Dec	Jan-June	June-Dec
1	-1.10	-0.80	0.05	0.01
2	-0.48	-0.68	-0.27	0.02
3	0.22	0.23	0.23	0.42
4	0.28	-0.34	0.27	0.25
5	0.15	-0.43	0.16	-0.08
Weighted averaged	-0.14	-0.38	0.09	0.13
Weighted averaged (w/o swash zone)	0.04	-0.24	0.09	0.13

Based on the results from the uncoupled D3D-FM models, it is expected that the coupled model will have less shoreline erosion than the Eulerian model, but also less offshore accretion. This is indeed observed in the coupled model results as depicted in Figure 44, where a 2.5 m wave height was used as information exchange threshold. Figure 45 shows the sedimentation/erosion bars, which have the same trend as the stand-alone EUL model (Figure 38-c), but less shoreline erosion is seen, and somewhat smaller offshore accretion also takes place. It is believed from these results that choosing a higher wave height threshold (hence less frequent coupling) would steer the results towards the GLM outcome, whereas a lower wave height threshold (more frequent coupling) would mobilize the final morphology towards the Eulerian results. The present result is promising as it means that the coupling methodology works, and different settings could be applied to each condition (storm and calm representations) in order to improve and fine-tune the morphological predictions. It is also interesting to notice that in the present coupled model the Eulerian mass transport is used only about ~14% of the time, and yet its morphodynamic impact is dominant since the final sedimentation erosion patterns (Figure 44) looks similar to the ones obtained by running the Eulerian model 100% of the time (Figure 36). The bed level difference between these two simulations is depicted in Figure 46, and is clearly smaller than the GLM-EUL differences (Figure 39-b). This does not come as surprise since it is expected that the large storm events steer the main morphological changes at this beach.
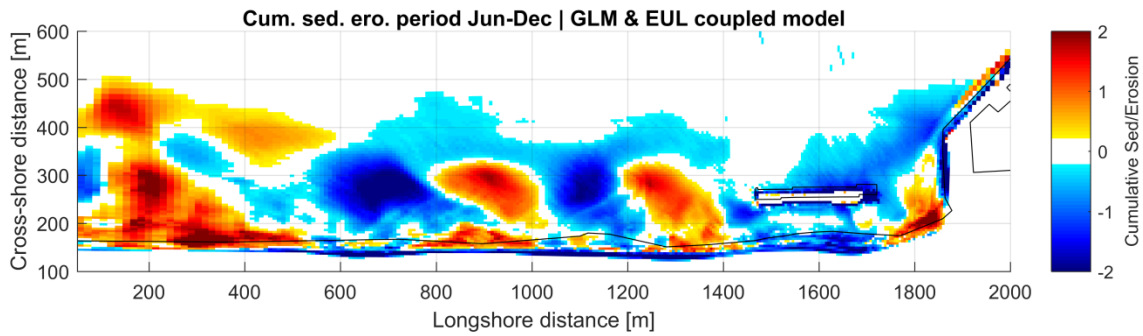
Figure 44: Modelled cumulative sedimentation/erosion patterns. D3D-FM GLM-EUL coupled model, H_S threshold=2.5 m.
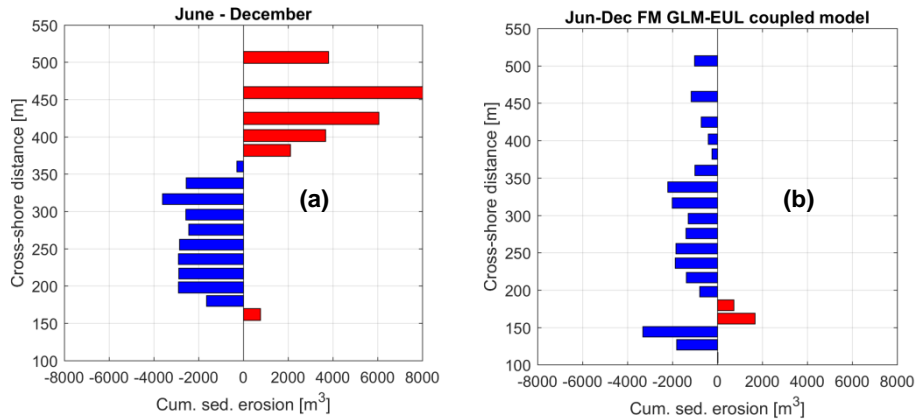
Figure 45: Cross-shore sedimentation/erosion bars for June-December. (a) Measured; (b) D3D-FM GLM-EUL coupled model, H_S threshold=2.5 m
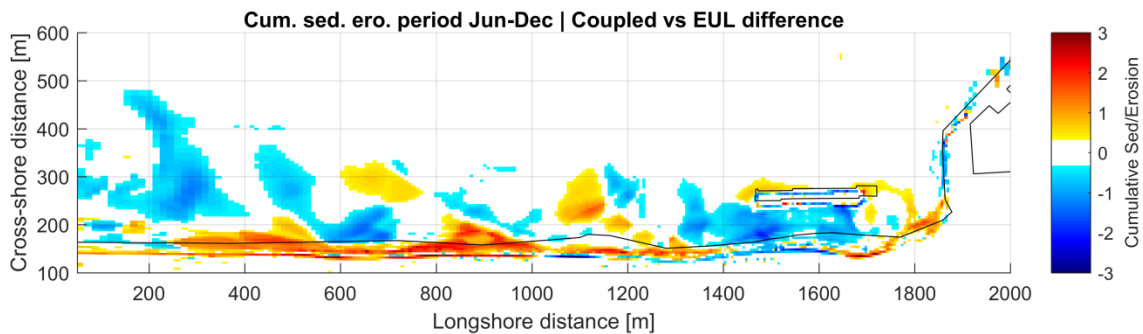
Figure 46: Bed level differences between the GLM-EUL coupled simulation (H_S threshold=2.5 m) and the uncoupled Eulerian simulation. Differences calculated in December. D3D-FM models.

4.2.5. D3D-FM & XBeach model set-up

The next modelling step consists on coupling D3D-FM with XBeach, running the first model during calm periods and the second one for highly energetic events. The XBeach model to be used is an extension of the model developed by Koudstaal (2016) but now including morphological updates.

The domain has approximately ~50,500 grid cells with a varying resolution, having a maximum resolution of 1.7x5.0 m in the nearshore. The domain is approx. 800 m larger than the D3D model in each side, as shown in Figure 47. Here it can be seen where the different grids overlap. The particle diameters were considered equal to the D3D model ($d_{50} = 500\ \mu m, d_{90} = 750\ \mu m$). At the offshore boundary a time series of SWAN spectra were considered, using the same (measured) input as in the D3D models. On the sides, Neumann boundary conditions were considered.

In surf beat mode, for such a large domain the computational time becomes extremely large, especially when considering the disadvantage that BMI does not allow to run XBeach with several cores (also known as MPI-mode). Hence to achieve a manageable running time in the order of

~1 week, XBeach was used only for the highest energetic events, defined by an offshore wave-height threshold of 3.5 m as shown in Figure 48. Unlike D3D-FM, XBeach in combination with BMI does allow to *skip* the times when the software is idle, hence allowing to compute only the required periods, shown in red in Figure 48. This resembles the serial online coupling as explained in section §3.3 and Figure 13-c.

To achieve an effective coupling several runs had to be made, coming to the conclusion that the ramping-up or tapering of the bed level differences exchange had to be spread over 1 hour for $\Delta bl < 4.0\ m$ and 2 hrs for $\Delta bl > 4.0\ m$, as this turned out to be a critical parameter to achieve stability in D3D-FM at the moment of receiving the information. Also to analyze the effects of long waves on the morphological changes, a simulation in stationary mode was run with similar settings. Unfortunately, when running XBeach in stationary mode a spectral boundary condition is not allowed, hence the representative wave height, period and direction had to be extracted from the SWAN input files in order to be used as boundary conditions for the stationary solver. Other minor changes had to be made (for example the wave braking formula) when selecting the stationary solver. The full model(s) settings are shown in appendix A.

The coupled models list is shown in Table 7.

Table 7: D3D-FM & XBeach coupled models list

Model No.	Description	Simulation period
1	XBeach in stationary mode, $H_s > 3.5\ m$	Jun-Dec
2	XBeach in surf beat mode, $H_s > 3.5\ m$	Jun-Dec
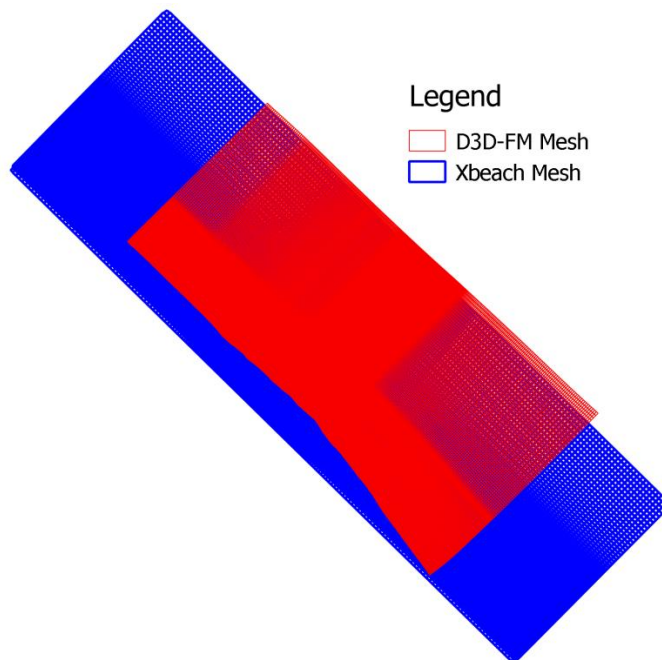
Figure 47: XBeach and D3D-FM grid overlapping
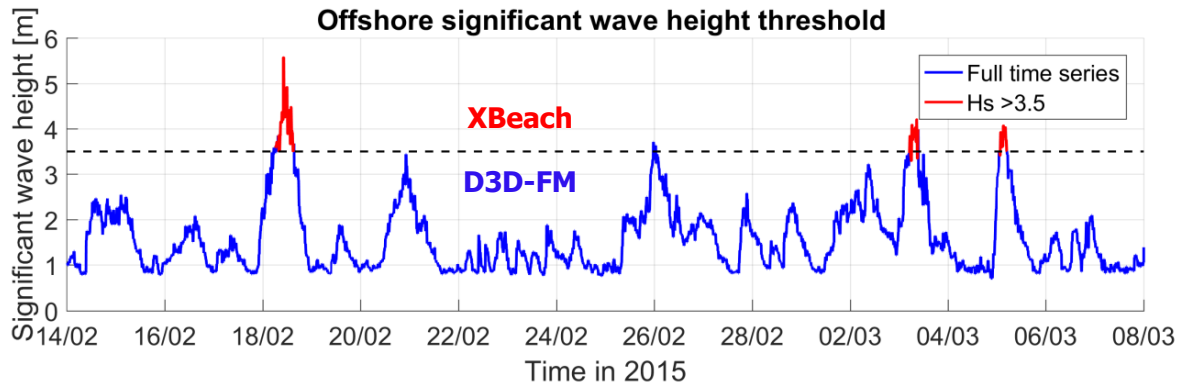
Figure 48: Offshore significant wave height for XBeach information exchange.

4.2.6. D3D-FM & XBeach model results

The final sedimentation/erosion patterns of the stationary and surf beat models are shown in figures 49-a and 49-b respectively; while in Figure 50 the cross-shore quantitative erosion/accretion bars in the area of interest are presented. What can be seen in both figures is that there is a large erosion of the shoreline, which is not observed in the measurements. To analyze the direct effect of the long waves on beach erosion, the first storm with $H_s > 3.5\,m$ (as shown by the first red peak in Figure 48) and its aftermath were plotted for two cross sections over time. Figure 51 shows the cross-shore evolution next to the SBW (~60 m to the west), while Figure 52 shows a cross section approx. 500 m west of the SBW, around the center of the area of interest. What can be recognized is that erosion in the surf beat model reaches higher elevations, up to 5 m.a.s.l., and also reaches a point located farther onshore (~100 m in the cross-shore direction). This is believed to be caused by two effects: the increased run-up due to long waves, and the avalanching algorithm implemented in XBeach, which can cause slumping of dry material (Figure 51-b). When comparing the same cross section with the stationary wave solver (Figure 51-a), it is seen that the beach erosion reaches a maximum elevation of 2 m.a.s.l., at a cross-shore distance of approx. ~130 m, suggesting that due to the lower run-up, the dry beach did not erode (neither as direct erosion nor due to avalanching).

When looking at the temporal evolution after the storm (when $H_s < 3.5\,m$), which is solved by D3D-FM, some patterns that are difficult to analyze are seen. When the model with surf beat is considered (figures 51-b and 52-b), there is a trend of erosion in the shoreline and deposition farther offshore, whereas in the stationary models the opposite holds. The 2D sediment distribution makes it difficult to draw general conclusions, but something that is observed in both models is that all the changes caused by XBeach in the dry beach (mainly erosion), approx. between 0 and 5 m.a.s.l., are not altered later by D3D-FM. In other words it can be said that all the shoreline erosion generated by XBeach cannot be later restored by D3D-FM. Hence, the (sediment) recovery mechanisms are not as strong as required, since when comparing with the measurements, near the shoreline little or no erosion is observed. This behaviour is something that is also observed in the D3D model with Eulerian transport, where severe erosion at the shoreline is predicted during storms, but then during less energetic conditions the recovery mechanism is not strong enough to accrete to beach to its original bed level.
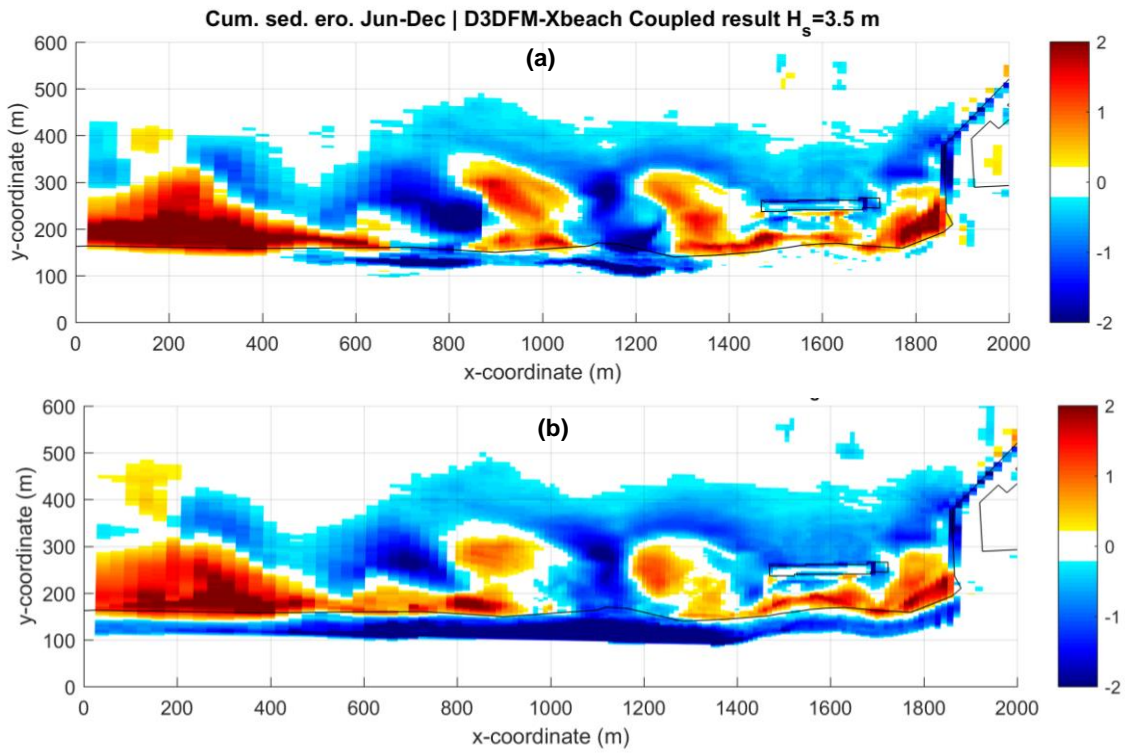
Figure 49: Modelled cumulative sedimentation/erosion patterns. D3D-FM & XBeach coupled model. (a) XBeach in stationary mode; (b) XBeach in surf beat mode
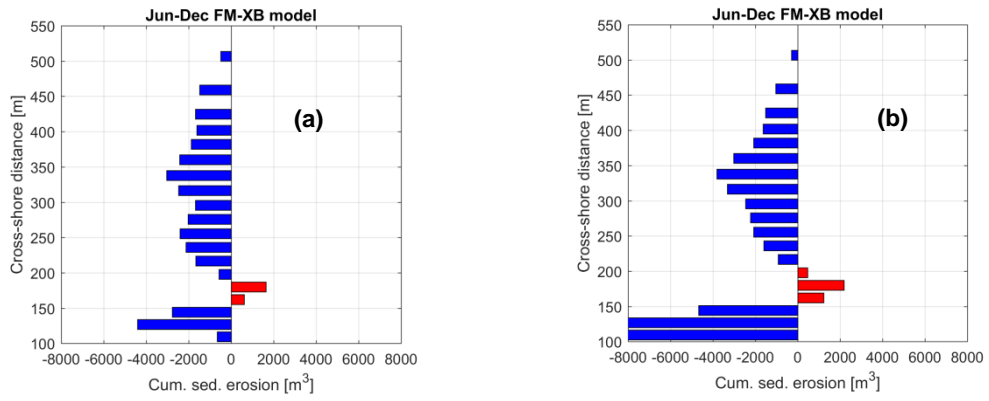
Figure 50: Cross-shore sedimentation/erosion bars for June-December. D3D-FM & XBeach coupled model. H_s threshold = 3.5 m. (a) XBeach in stationary mode; (b) XBeach in surf beat mode
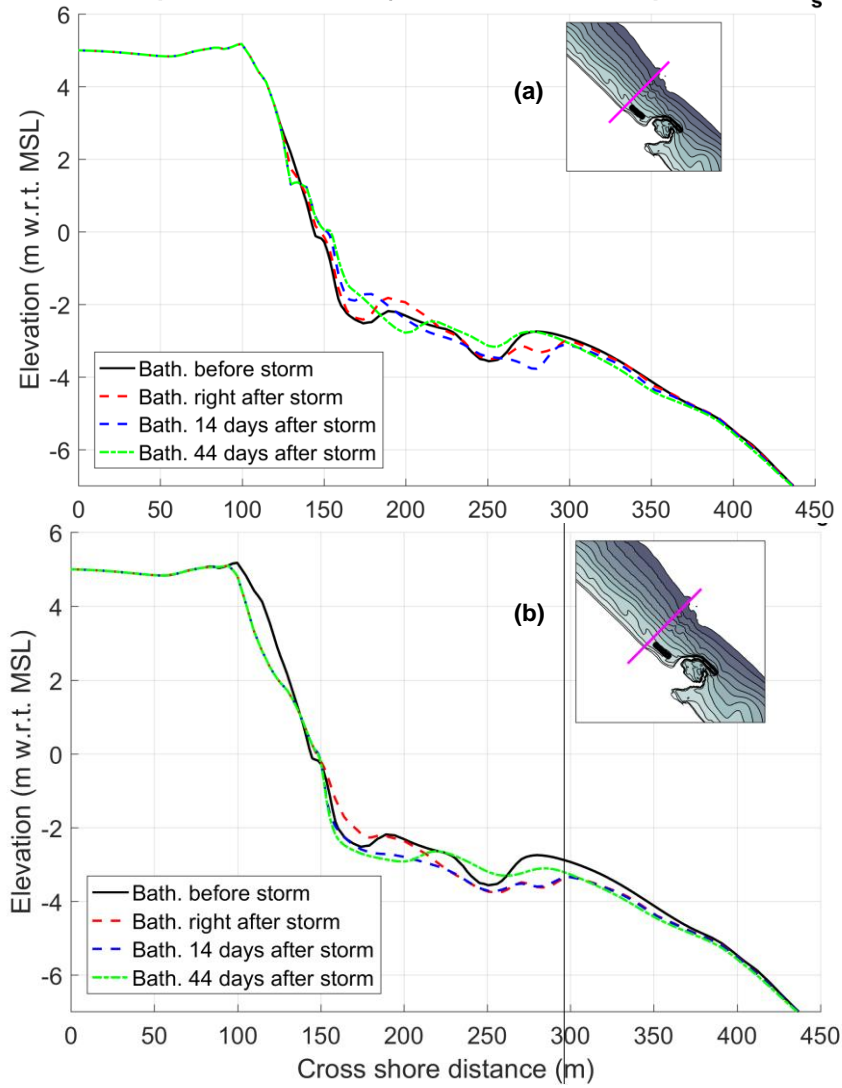
Figure 51: Beach development after storm. Location ~60 m west of the SBW. D3D-FM & XBeach coupled model. (a) Stationary model; (b) Surf beat model
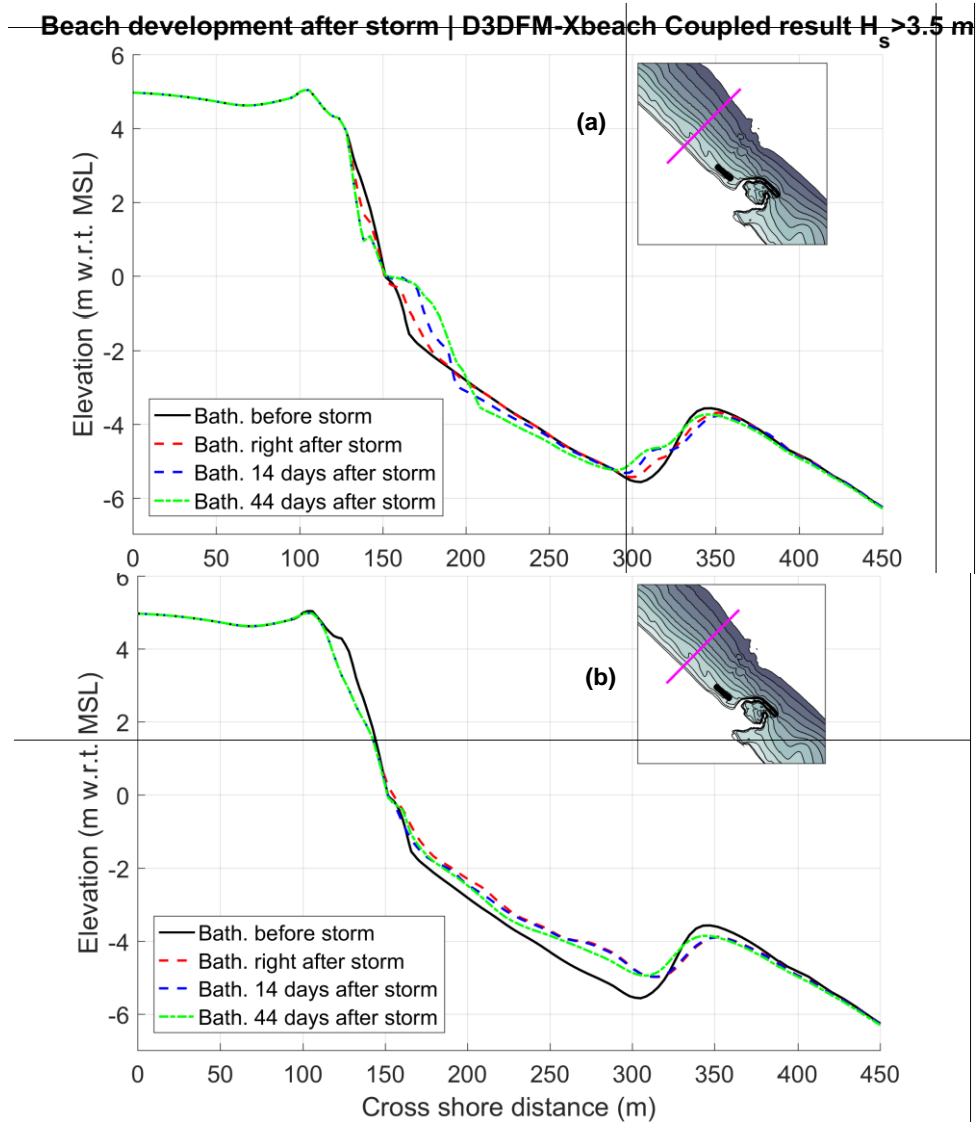
Figure 52: Beach development after storm. Location ~500 m west of the SBW. D3D-FM & XBeach coupled model. (a) Stationary model; (b) Surf beat model

4.2.7. D3D-FM & XBeach model additional scenarios

Based on the results from section §4.2, an additional wave height threshold of 2.5 m was tested as shown in Figure 53, keeping all the other model settings intact. This is the lowest wave height that allows running XBeach for a reasonable amount of time, and it is useful for assessing the sensitivity of this threshold on the coupled-model results.
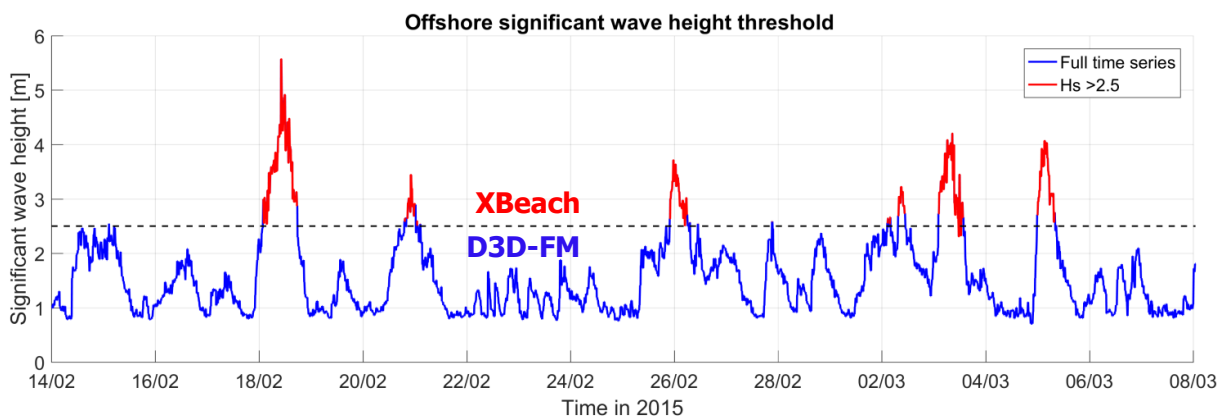
Figure 53: Offshore significant wave height time series and threshold for model coupling information exchange

Once again two models were developed, one in stationary mode and another in surf beat mode. The cumulative sedimentation/erosion results are shown in Figure 54, and the cross-shore quantitative bars in the area of interest are depicted in Figure 55.
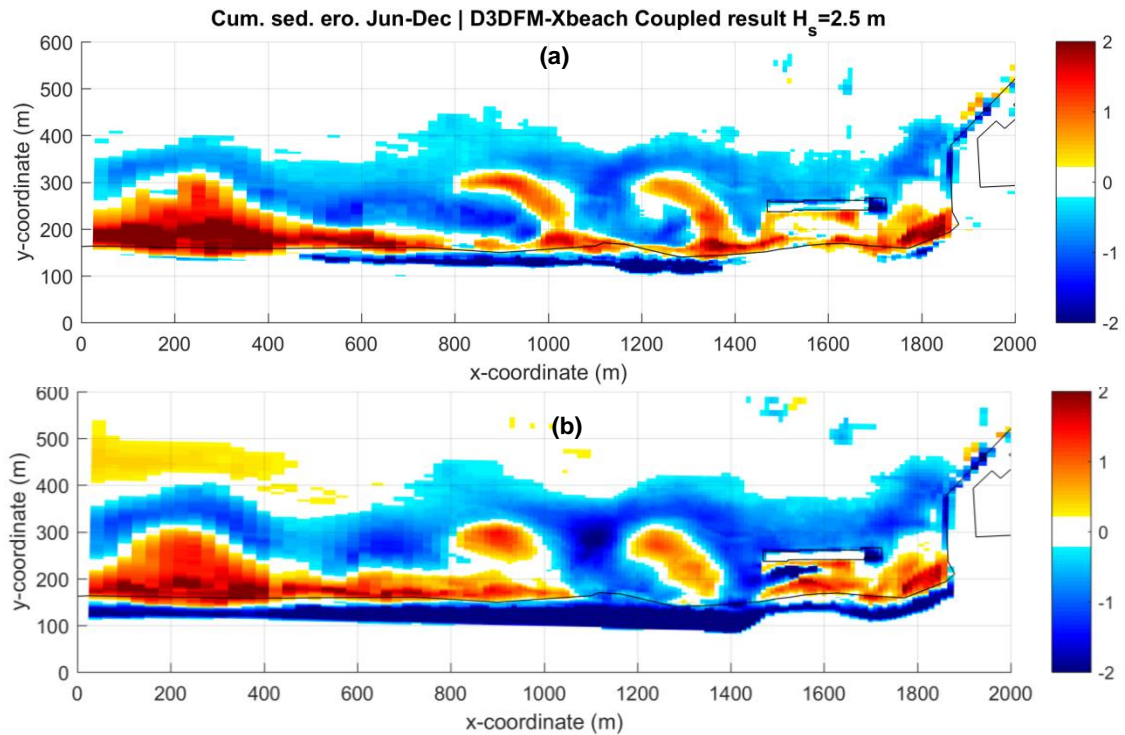
Figure 54: Modelled cumulative sedimentation/erosion patterns. D3D-FM & XBeach coupled model. (a) XBeach in stationary mode; (b) XBeach in surf beat mode
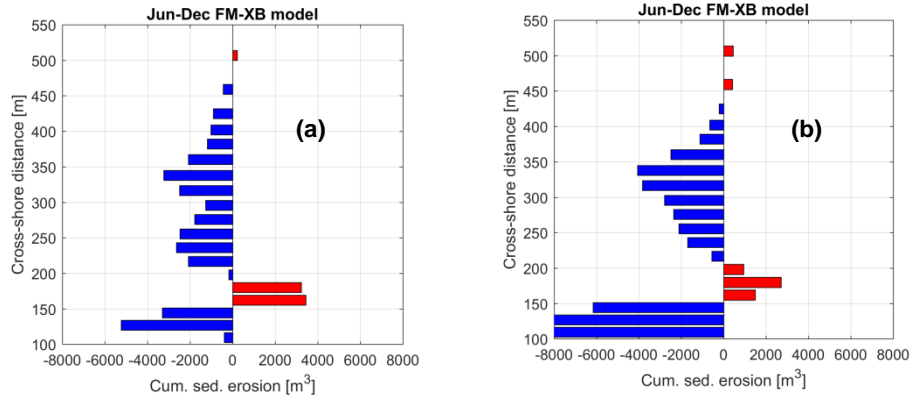
Figure 55: Cross-shore sedimentation/erosion bars for June-December. D3D-FM & XBeach coupled model. H_s threshold = 2.5 m. (a) XBeach in stationary mode; (b) XBeach in surf beat mode

What can be seen from figures 54 and 55 is that when choosing a lower wave height threshold, higher erosion is seen in the shoreline, both for the stationary and surf beat models. In the first case this can be attributed to the fact that an Eulerian mass transport is run for a longer period (hence beginning to assimilate the 6 months Eulerian simulation in D3D, depicted in Figure C-92), whereas in the surf beat model the combination of a higher run-up (due to infragravity waves) and avalanching algorithm plays a dominant role. As a way to confirm this, the water level (and bed level) was plotted for a cross section approx. 80 m west of the SBW at a certain time during the first storm (Figure 56). It can be seen that the stationary model has an almost steady water level around 0 m.a.s.l., with only few centimeters of run-up at the shoreline. On the other hand the surf beat model reaches higher waterline elevations in the order of ~2 m, which is due to long waves interactions, since in this analysis neither tides nor surge are included.

To assess the relevance of the avalanching algorithm, the same model with a 2.5 m wave height threshold was run but now with the avalanching algorithm deactivated in XBeach (*avalanching=0*).

A cross section west of the SBW is shown in Figure 59 where a bed level comparison of the XBeach simulations with and without avalanching is depicted right after the first storm. It can clearly be seen that despite both models are simulating long waves, the erosion is much higher when the dry beach is allowed to erode through avalanches. The final model bathymetries from these additional scenarios are shown in appendix D.
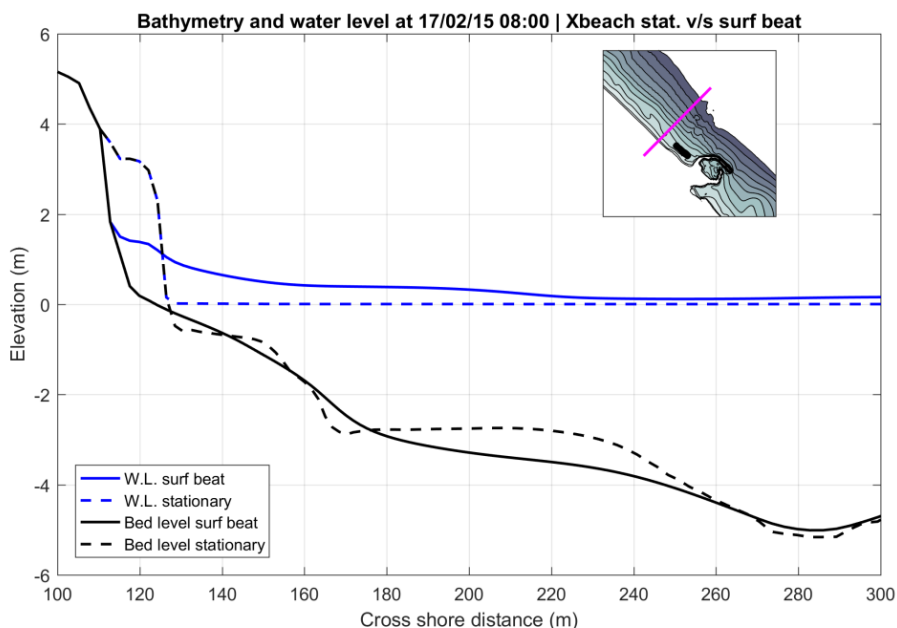
Figure 56: Water level comparison due to long waves. Location west of the SBW. XBeach stationary and surf beat models. Tides and surge not included.

When comparing Figure 50-b with Figure 55-b, it can be seen that with the lower wave height threshold a higher accretion is seen offshore, which starts to resemble the measured results (Figure 31-a), but at the cost of sacrificing the accuracy in the nearshore where higher erosion is predicted.

As was mentioned in Chapter 1, the cumulative effect of storms might potentially have a severe impact in the shoreline, and can be of critical importance for man-made facilities located at the beach. As a way to estimate the shoreline location in the models and measurements, an adaptation of the momentary coastline method ("MKL" from herein)[1] (van Koningsveld & Mulder, 2004) was performed, as explained further in appendix H. The result from this procedure is shown in Figure 58, where two important features or trends can be identified: 1) the shoreline estimated from the coupled model (XBeach in surf beat mode) is located ~20-40 m landwards with respect to the shoreline predicted by the uncoupled model and measurements, and; 2) the shoreline predicted by the coupled model right after the first storm (where $H_s > 5.5\,m$), which is mainly the result from the XBeach model, is similar to the shoreline predicted by the uncoupled D3D-FM model but at the end of the stormy season. These findings show that the erosion of a single storm is relevant, especially when compared with the erosion caused by a stationary long-term simulation; however it can be completely overshadowed by the cumulative effect of including several storms during the simulation.

With these results the conclusion that can be drawn is that lowering the wave height threshold will improve the results in the offshore area but will worsen the results in the nearshore, therefore running coupled simulations with even lower wave heights will not improve the overall morphodynamic predictions, and it will take longer computational time. The main hypothesis at this point regarding why the results of the coupled model are not better than the stand-alone simulations is that by adding a storm model (such as XBeach) during the highest energetic periods, the dry beach erosion is enhanced, but no additional mechanisms are included later for post storm recovery, thus the results end up being skewed. This could very well be the real behaviour of the beach at locations where

---

[1] *Momentane KustLijn* or MKL in dutch

structural erosion happens or is expected to happen, but in places where this is not the case a morphological imbalance is created. A possible solution for this is address in the following chapter.
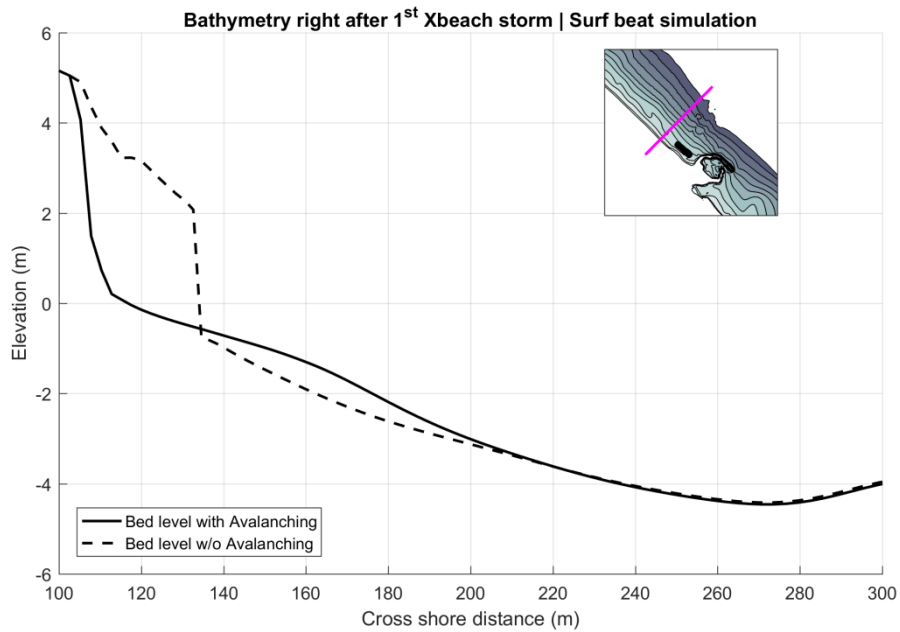
Figure 57: Erosion comparison due to avalanching. Location ~80 m west of the SBW. XBeach surf beat simulations. Tides and surge not included.
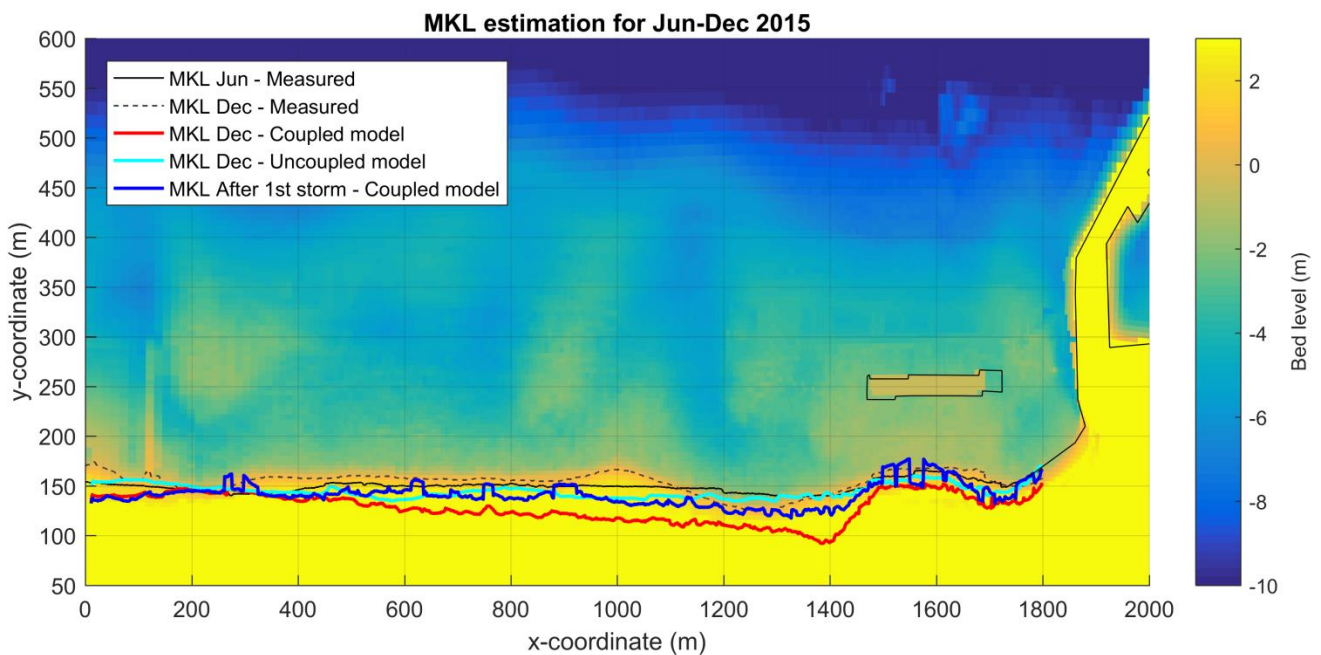
Figure 58: Momentary coastline (MKL) adaptation at Anmok beach for measurements and models. The coupled model refers to the D3D-FM & XBeach (surf beat) simulation with a $H_s\ threshold$ = 2.5 m. The bed level at the background is the measured bathymetry from December 2015.

4.3. D3D swash zone transport models

The results from section §4.2 indicate that by coupling D3D-FM with XBeach large erosion near the shoreline is predicted, especially when considering long waves. What is seen in these models is that large erosion of the supratidal beach happens during highly energetic periods, but there is not enough post-storm beach recovery, which is expected to happen in the simulations in order to be in agreement with the measurements. A simple sketch of what post-storm recovery should be like is depicted in Figure 59.

Since the models that have been ran so far under predict the post-storm recovery mechanisms, a special version of D3D has been compiled for this thesis project (version 6.02.11.000000), which includes a "mask" or pre-defined model area where the sediment transport is no longer computed by the formulas included in regular D3D (Van Rijn 1993, Engelund-Hansen, etc.) but following the relations of Larson & Wamsley (2007) as shown in eq. [3] and [4] (from section §2.6). These relations were developed for computing sediment transport rates in the swash zone, both in cross-shore and longshore directions. The run-up height, which is a parameter used to estimate the highest wet point in the swash zone, is obtained following eq. [1] (shown in section §2.6).
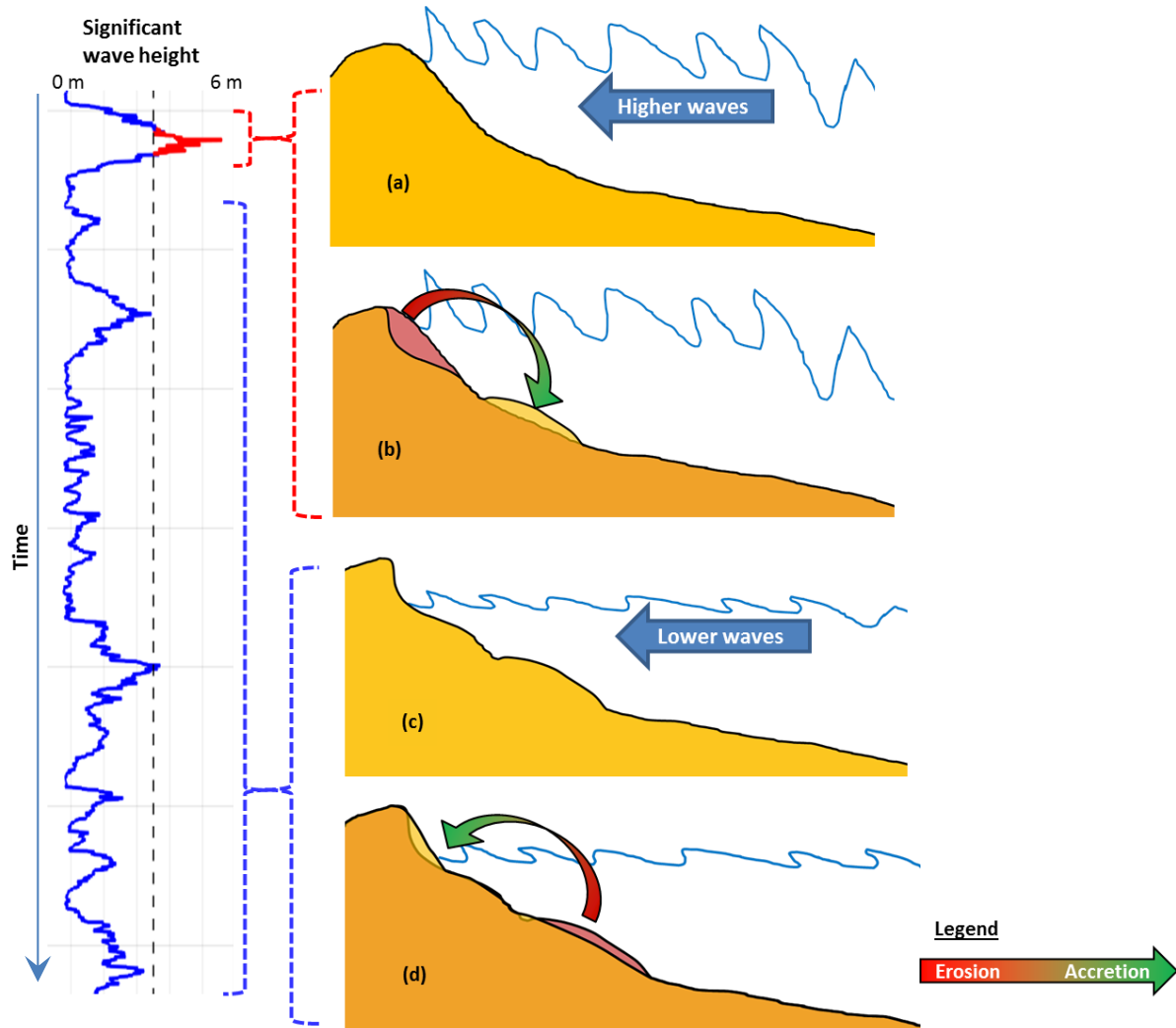
Figure 59: Beach erosion and post-storm recovery sketch as function of time. (a) High wave attack for a short period; (b) supratidal beach erosion and deposition in the inner surf zone; (c) low wave attack for a longer period; (d) post-storm recovery due to swash onshore transport (and other mechanisms).

4.3.1. Model set-up

To run this version of D3D first a "mask" must be defined where the swash zone sediment transport equations will take place. For this purpose a zone of 160x1800 m^2 mask was defined along the shoreline, from the dry beach down-to the SBW as shown in Figure 74.
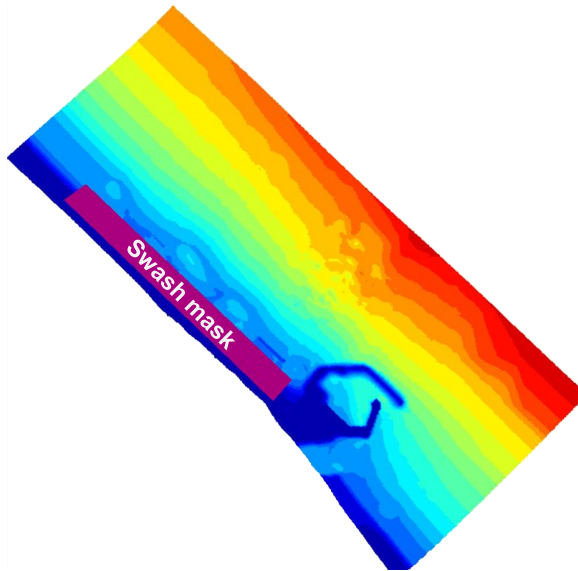
Figure 60: Swash zone "mask" or definition for D3D input.

Beside this mask, seven additional parameters are required as input to run this module, as briefly explained next:

1. K_c: Empirical coefficient for cross-shore transport (from eq. [3])
2. K_L: Empirical coefficient for longshore transport (from eq. [4])
3. $\tan(\beta_e)$: Local equilibrium slope of the foreshore
4. H_{sfac}: Amplification (reduction) factor for the maximum wave run-up (estimated with eq. [1])
5. $Nr_{smooth\ steps}$: Numerical parameter regarding the number of iterations for slope-smoothing
6. $Search_{width}$: Width (in number of cells) where the swash equations will look for a water depth <= 1.0 m
7. $Mask_{depth}$: Maximum (water) depth for computing swash transport

Since this is the first time that this module is used, several simulations were ran to assess the sensitivity of the aforementioned seven parameters, trying first with the default values, and later with larger and/or smaller values bearing in mind that the goal is to enhance the onshore sediment transport. The simulation period is the stormy season of 2015. All the other simulation parameters are the same as the D3D GLM base case simulation. The additional swash model parameters are summarized in Table 8.

Table 8: Sensitivity analysis for swash zone sediment transport D3D simulations. The changes with respect to the default values (Model No. 1) are highlighted.

Model No	SWASH mask	K_c	K_L	$tan(\beta_e)$	H_{sfac}	Nr_{Smooth}	$Search_{Width}$	$Mask_{Depth}$
0	off	N/A	N/A	N/A	N/A	N/A	N/A	N/A
1	on	0.2	0.1	0.1	1	3	10	-1
2	on	**0.002**	0.1	0.1	1	3	10	-1
3	on	**1**	0.1	0.1	1	3	10	-1
4	on	0.2	**0.002**	0.1	1	3	10	-1
5	on	0.2	**1**	0.1	1	3	10	-1
6	on	0.2	0.1	0.1	**5**	3	10	-1
7	on	0.2	0.1	0.1	**0.1**	3	10	-1
8	on	0.2	0.1	**1**	1	3	10	-1
9	on	0.2	0.1	**0.01**	1	3	10	-1
10	on	0.2	0.1	0.1	1	3	**50**	-1
11	on	0.2	0.1	0.1	1	3	10	**-5**

Model No	SWASH mask	K_c	K_L	$tan(\beta_e)$	H_{sfac}	Nr_{Smooth}	$Search_{Width}$	$Mask_{Depth}$
12	on	0.2	0.1	0.1	1	30	10	-1
13	on	1	1	0.1	10	3	10	-1
14	on	1	0.1	0.1	10	3	10	-1
15	on	0.2	0.1	0.1	100	3	10	-1
16	on	10	10	0.1	10	3	10	-1
17	on	10	10	0.1	100	3	10	-1
18	on	0.2	0.1	0.1	1000	3	10	-1
19	on	0.2	0.1	0.01	1000	3	10	-1
20	on	1	1	0.01	1000	3	10	-1
21	on	10	10	0.01	100	3	10	-1
22	on	1	1	0.01	100	3	10	-1
23	on	0.2	0.1	0.01	100	3	10	-1
24	on	10	10	0.001	1000	3	10	-1
25	on	10	10	0.001	100	3	10	-1

The first 12 models are developed with the purpose of assessing the relevance of the different parameters on the final morphological results. The last 13 models are a combination of the previous simulations in an attempt to obtain higher nearshore accretion (enhancing the post-storm recovery mechanism).

4.3.2. Model results

To assess the relative impact of including the swash zone sediment transport equations, the bed level differences between the D3D-swash zone model with default settings (model No. 1 from Table 8) and the D3D base case model (without swash zone formulations, model No. 0) is shown in Figure 61:
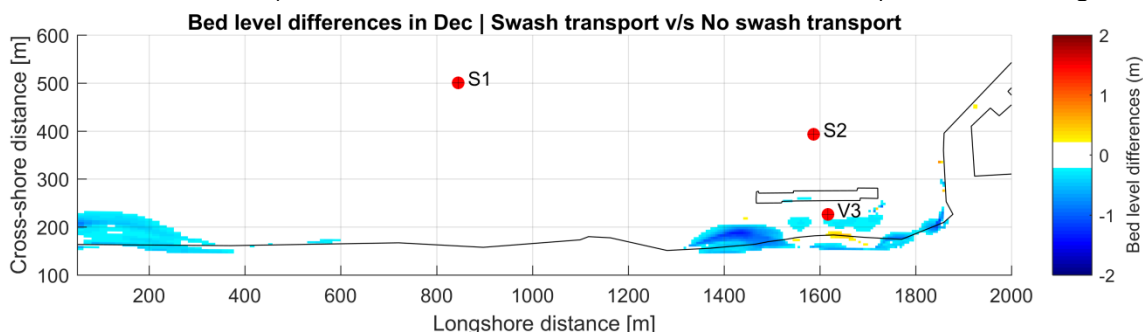
Figure 61: Bed level difference between model 01 and no-swash (base case) D3D simulations at the end of the stormy season. Blue indicates that the swash-formulation model has a final bed level lower than the base case, while red indicates the opposite.

What is seen in Figure 61 is that applying the swash mask with default settings does not improve the overall morphodynamic results, and at the same time it is not fulfilling its purpose of acting as a post-storm recovery model by pushing more sediment onshore. The sedimentation and erosion patterns of all the simulations listed in Table 8 are shown in appendix E.

In figures E-101 until E-112 it can be seen that increasing the cross-shore and longshore sediment transport empirical coefficients K_c and K_l, as well as the run-up factor H_{sfac}, generates a small amount of accretion in the shoreline (models 3, 5 and 6), whereas increasing the equilibrium slope β_e produces significant erosion (model 8). The use of a milder slope does not show the opposite effect, as it does not produce any additional shoreline accretion. The three final parameters Nr_{smooth}, $Search_{width}$, and $Mask_{depth}$ seem to be related to numerical stability more than physical processes as no notorious changes are depicted when comparing their outcome with the results of the default swash simulation (model 1).

Based on these initial results a series of parameter combinations were tested, presented in figures E-113 to E-125. What can be seen in these images is that the run-up factor H_{sfac} is the most effective parameter when it comes to transporting sediment onshore, however it must be changed in combination with the other coefficients to be noticeable. Even when it is increased by 1 or 2 orders of magnitude it does not have a positive impact on the shoreline (viz., accretion) if the rest of the parameters remain roughly constant. The best results are obtained when H_{sfac} becomes of the order $O(1000)$ and $K_c \approx K_l$ are of order $O(1-10)$. However to achieve stable runs, the equilibrium slope in these runs had to be decreased to $\beta_e \sim O(0.01 - 0.001)$.

These results represent just a rough calibration and not a fine-tuning, however the results are promising in the sense that shoreline accretion is observed when modifying some empirical coefficients in the swash zone sediment transport formulations. Nevertheless some remarks have to be made regarding these results:

1. The simulations with the highest shoreline accretion (models 19 to 25) have a run-up factor H_{sfac} up to 1000. This means that the maximum water depth reached by the wave run-up is increased by an unrealistic value; hence this can only be seen as a numerical modelling artifact. Since this large value was not capable of bringing sediments farther upslope it is assumed that there is an implementation error at the moment.
2. The cross-shore and longshore coefficients K_c and K_l were increased up to a value of 10. This action significantly increases the sediment transport in the swash zone; however these *calibrated* coefficients are approx. 4-5 orders of magnitude larger than the ones obtained by Larson et al. (2004) and Larson & Wamsley (2007). Therefore these high values might also be seen as a "brute force" method to "bring" sediment onshore in the simulation, and probably deviate from reality.
3. Even with these highly amplified coefficients, the shoreline accretion at the different locations does not reach any elevation higher than ~0.5 to 1.5 m.a.s.l. Some cross sections are shown in figures 62 and 63, as a way of exemplification, depicting only the simulations with noticeable shoreline accretion. From these results it can be concluded that the severe erosion caused by XBeach at elevations of 2-5 m.a.s.l. (in the supratidal or dry beach) cannot be later recovered by the D3D-swash transport module alone. To achieve effective post-storm recovery results, the accretion caused by the latter model should reach higher elevations. Thus, an alternative could be to add an additional mechanism with capabilities to transport the sediments deposited between 0-1.5 m.a.s.l. farther into the dry beach. A first candidate at this stage would be a better parameterization of the swash model and its ability to wet the beach at higher elevations. A second candidate is the inclusion of an Aeolian transport model.
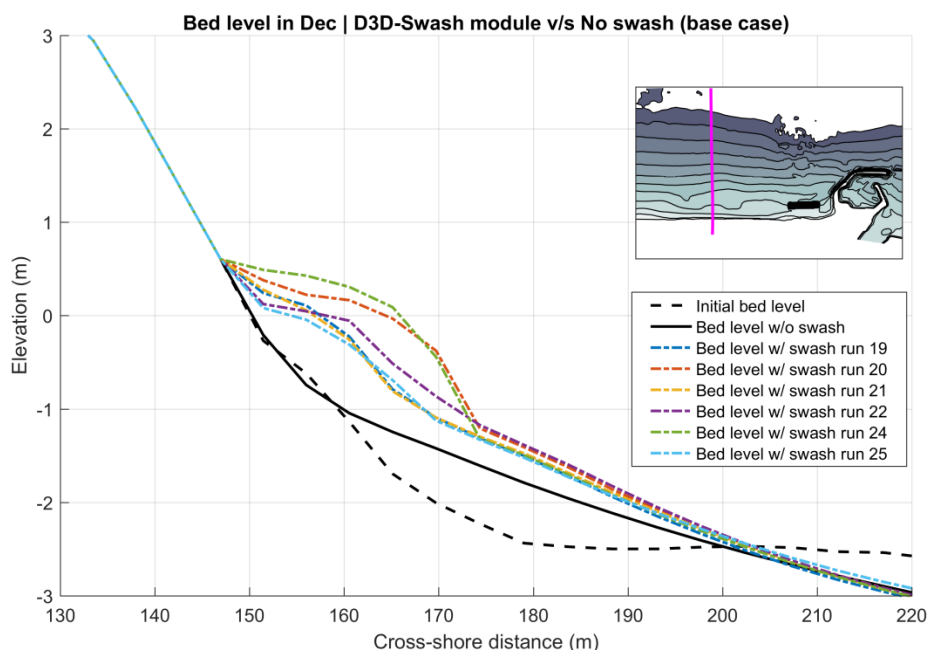
Figure 62: Bed level at the end of the period Jun-Dec for different D3D-swash module simulations, following the enumeration from Table 8. Cross section located approx. 600 m west of the SBW.
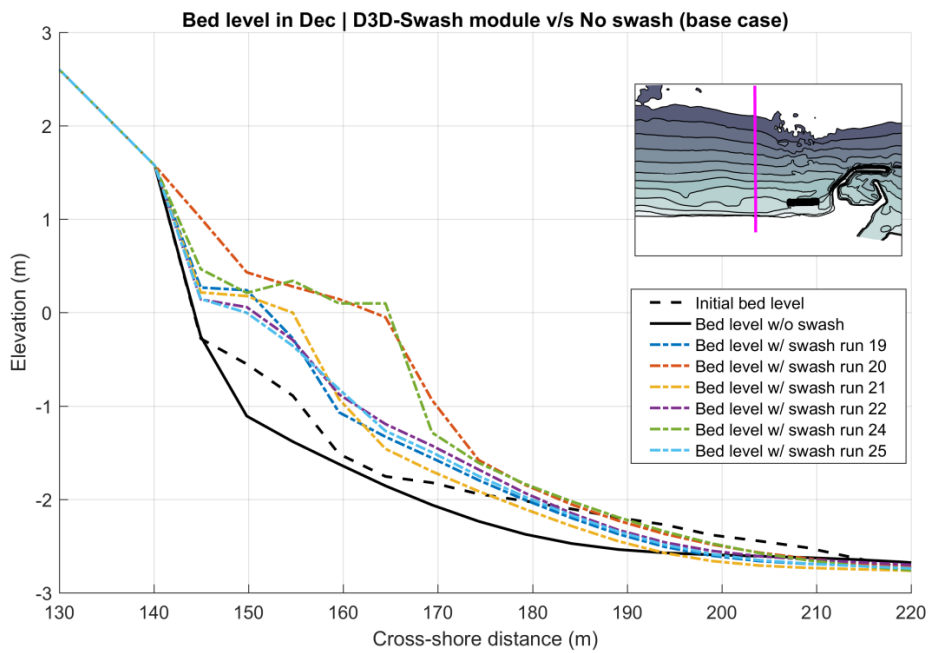
Figure 63: Bed level at the end of the period Jun-Dec for different D3D-swash module simulations, following the enumeration from Table 8. Cross section located approx. 200 m west of the SBW.

4.4. Storm calibration models

In section §4.2 it was found that the coupling of a long-term morphodynamic model (D3D-FM) and a storm model (XBeach) enhances the dry beach erosion, and an additional mechanism is required to restore the balance between storm erosion and post-storm recovery in case that no structural erosion is present. Then in section §4.3 an attempt to simulate this recovery was undertaken by means of running a research version of D3D with specialized swash zone sediment transport formulations, however the supratidal beach erosion could not be fully restored.

As an alternative path and final attempt to improve the morphodynamic hindcast results, in this chapter a brief calibration of the storm model is undertaken, which has the objective of reducing the over predicted dry beach erosion.

4.4.1. Model set-up

For the purpose of the calibration, two measured bathymetries from the year 2016 and separated by a one month period are used as initial and final bed levels, as shown in Figure 64. These bathymetries include LiDAR points in the dry beach up to an elevation of approx. 5 m.

50
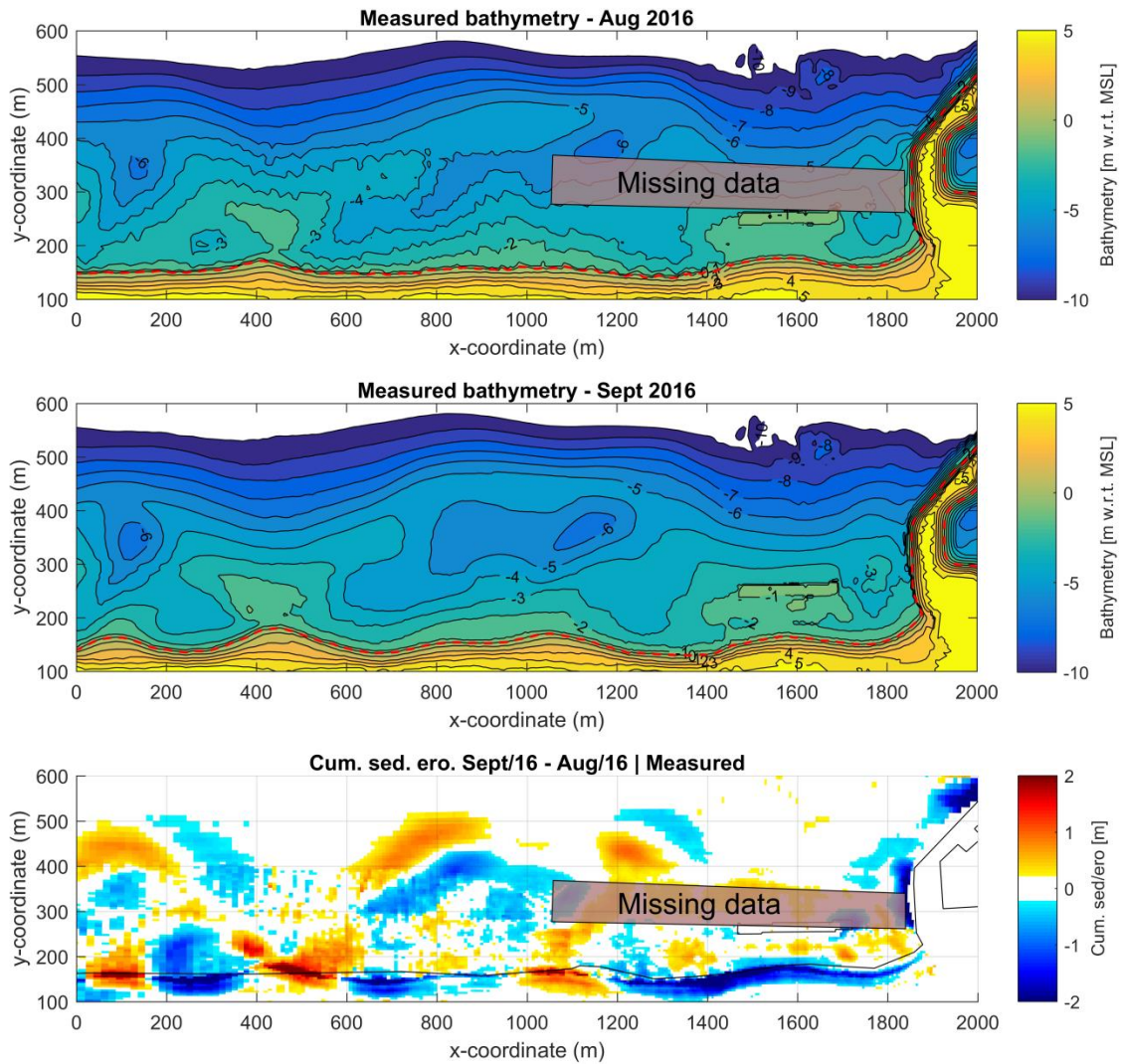
Figure 64: Measured bathymetry of Anmok beach in 2016. The 0 m contour is highlighted in a red dashed line. (Top): August; (Center): September; (Bottom): Cumulative sedimentation/erosion Aug-Sept.

The 2016 wave data (significant wave height, period and direction) was available with a 1 month gap of information, however this was not relevant since the lack of data happens before the measured bathymetries (Figure 74-a). Following the same procedure that was done for all the simulations so far in this project, the waves with a height $H_s < 0.9\ m$ were removed from the analysis, and the final wave time series was compressed by a factor 2, leading to a final hydrodynamic modelling time of 8 days, which is morphologically equivalent to the 1 month period (20 Aug until 25 Sept 2016) when using a morphological scale factor of 2. The post-processed wave data is shown in Figure 74-b.
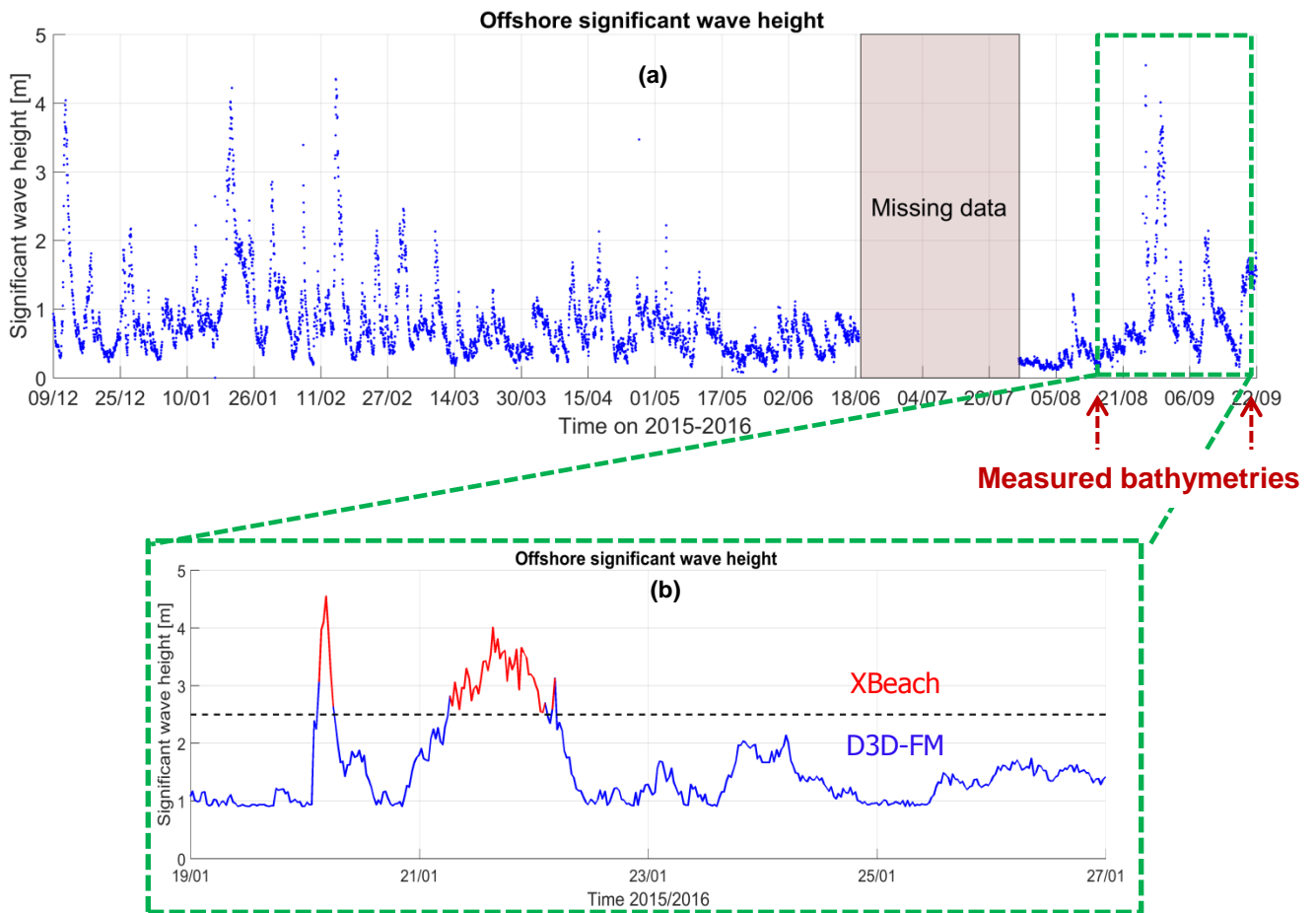
Figure 65: Wave data buoy W1 in the year 2016. (a) Raw data; (b) Processed wave data in the period of interest.

It can be seen from Figure 74-b that in the period of interest two relevant storms occur, reaching an offshore wave height of $H_s > 4\,m$. It is believed however that the erosional impact of these two storms is dominant during this month, and the post-storm recovery processes will only a play a minor role during this reduced timeframe. Based on the results from sections §4.2 and §4.3, and to avoid unmanageable long XBeach computations, an offshore significant wave height threshold of $H_s = 2.5\,m$ was chosen to switch between models. A total of six different simulations were set-up, and the parameter chosen to diminish the dry beach erosion was a variable called "*bermslope*", which is an undocumented research XBeach variable that attempts to "force" or achieve a user-given slope (available in XBeach version 1.22.5123). This variable can be seen as an equivalent to the equilibrium slope (β_e) from the D3D-swash zone module. In all the cases the same grid and lateral boundary conditions as the 2015 model were used. The offshore waves were forced in the form of a time series of Jonswap spectra. The list of models from this calibration is shown in Table 9.

Table 9: Storm calibration model list, Aug-Sept 2016 data

Model No.	Description
1	Uncoupled D3D-FM model.
2	D3D-FM & XBeach coupled model. XBeach default values.
3	D3D-FM & XBeach coupled model. XBeach without avalanching.
4	D3D-FM & XBeach coupled model. XBeach bermslope=0.1
5	D3D-FM & XBeach coupled model. XBeach bermslope=0.3
6	D3D-FM & XBeach coupled model. XBeach bermslope=0.5

The best outcome of these 6 models is then be applied to the 2015 coupled model, in order to assess if this reduction in the dry beach erosion improves the overall morphological predictions in a longer model.

4.4.2. Model results

The sedimentation/erosion patterns from these models are shown in appendix G. When comparing the results from the simulations with the measurements (Figure 64 - bottom panel), it can be seen that the uncoupled D3D-FM model has almost no impact in the dry beach (Figure G-129), whereas the opposite is true for the XBeach-coupled simulation with and without avalanching (figures G-130 and G-131 respectively). In these two models excessive dry beach erosion is predicted, in a very similar manner as the 2015 stormy season coupled results from section §4.2. When applying the *bermslope* parameter, it can clearly be seen that the results improve significantly depending on its value. For a low value of 0.1 (Figure G-132), there is still considerable (unmeasured) erosion at the dry beach, although somewhat less severe than the simulation without this parameter. For a bermslope of 0.3 and 0.5 (figures G-133 and G-134), the supratidal erosion is considerably reduced, although it is still larger than the D3D-FM uncoupled simulation. Furthermore, depending on the alongshore location, some accretion is even observed at the dry beach, and an alternate pattern of sedimentation/erosion is obtained, which has a better resemblance with the measurements. Since the results from simulations 5 and 6 are quite similar, some cross sections (identified in figure 66) were plotted and are depicted in figures 67 to 69, in order to have a better understanding of the simulations' differences, and also for comparison purposes with the default XBeach model (model No. 2). What is seen in these figures is that little difference is observed between models 5 and 6, with simulation 6 having slightly less beach erosion than simulation 5. It is also interesting to notice that farther offshore (cross-shore distance > ~250 m) all the models predicts the same bed levels, however in the dry beach (Elevation > 0 m.a.s.l.) simulation No. 2 differs substantially from simulations 5 & 6 and the measurements, predicting up-to 2 m of (unmeasured) erosion at some locations.

Based on these results and bearing in mind that the goal of this calibration is to reduce the beach erosion produced by XBeach, the calibration from model No. 6 (*bermslope*=0.5) was chosen to re-run the stormy season (Jun-Dec) of the year 2015. The final sedimentation/erosion patterns along with the quantification bars in the area of interest are shown in figures 70 and 71. What is seen in these results is that the shoreline erosion is severely reduced when compared to the coupled simulation with default parameters in XBeach (Figure 54-b), and also the alternate pattern of shoreline accretion between 200-800 m in the alongshore direction followed by a large erosion around 1200 m is now better represented. However, the offshore accretion is not represented at all and the shoreline erosion is still larger than the measured values. Also the use of this special (research) parameter generated model instabilities, particularly near the non-erodible boundaries, and large localized erosion next to the SBW and at the model boundaries had to be frequently and manually corrected to allow the simulation to finish. Thus the results from this simulation are not considered fully valid, but they provide a first attempt in modelling a coupled system of storm erosion and post-storm recovery in an intermediate (6 months) time scale without producing a large morphological imbalance or erosion at the dry beach.
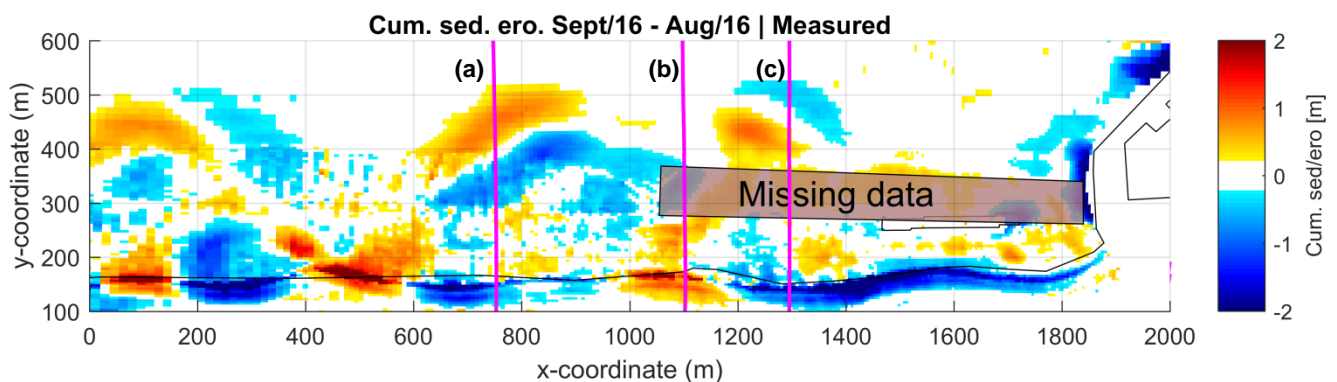
Figure 66: Alongshore location of cross-sections for 2016 model comparison on top of the measured sedimentation/erosion patterns.
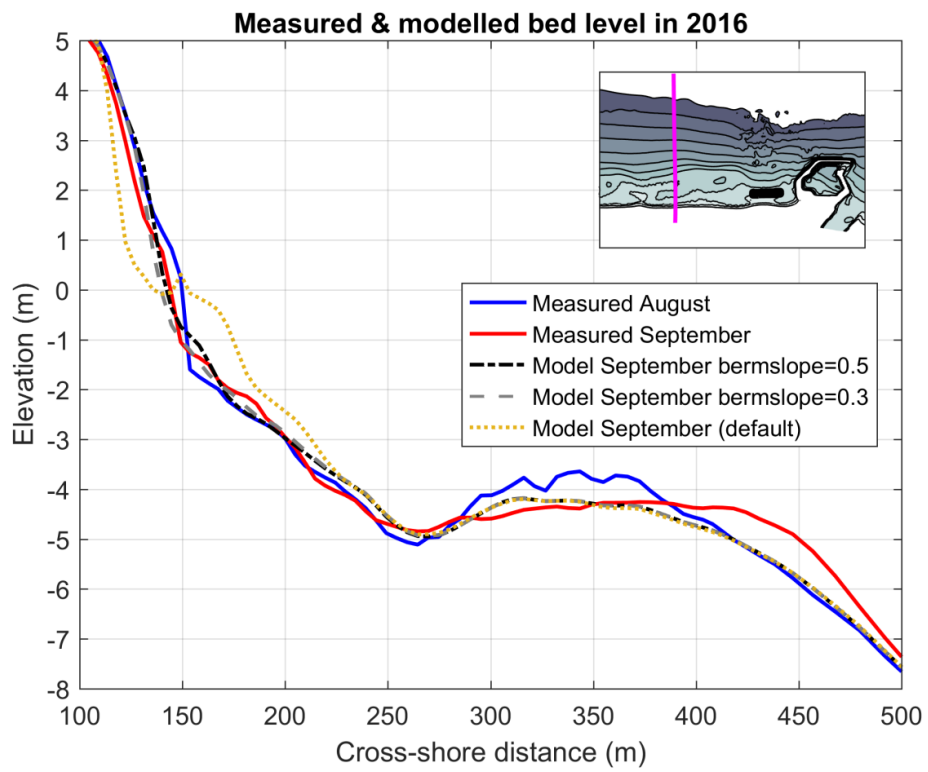
Figure 67: Cross-section *(a)* from figure 66. Measured and modelled bed level comparison.
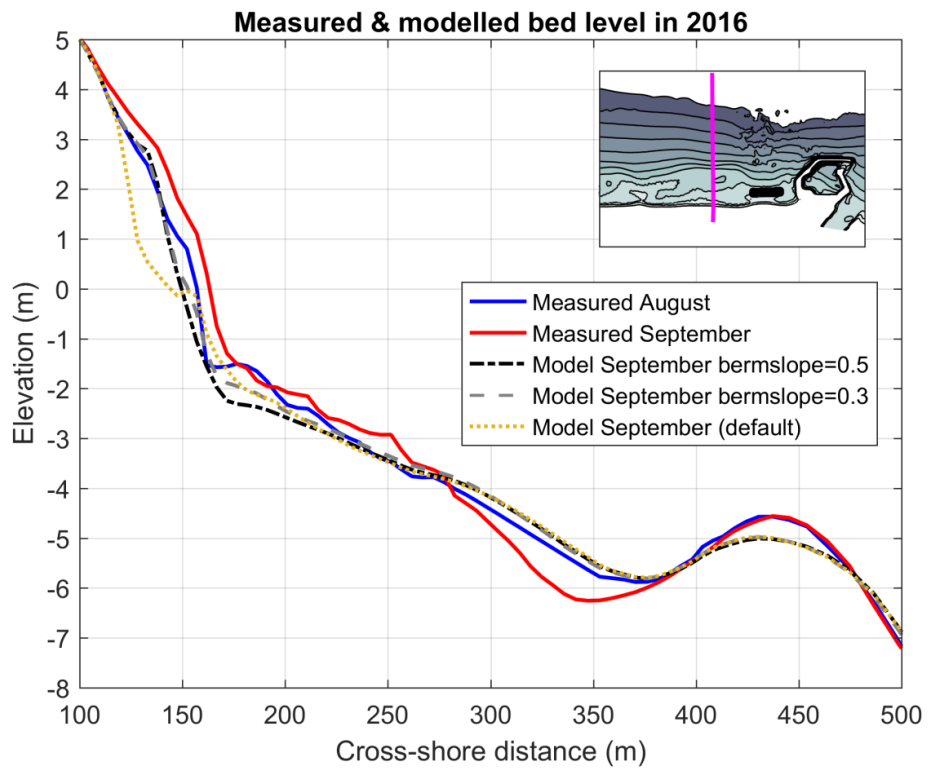
Figure 68: Cross-section *(b)* from figure 66. Measured and modelled bed level comparison.
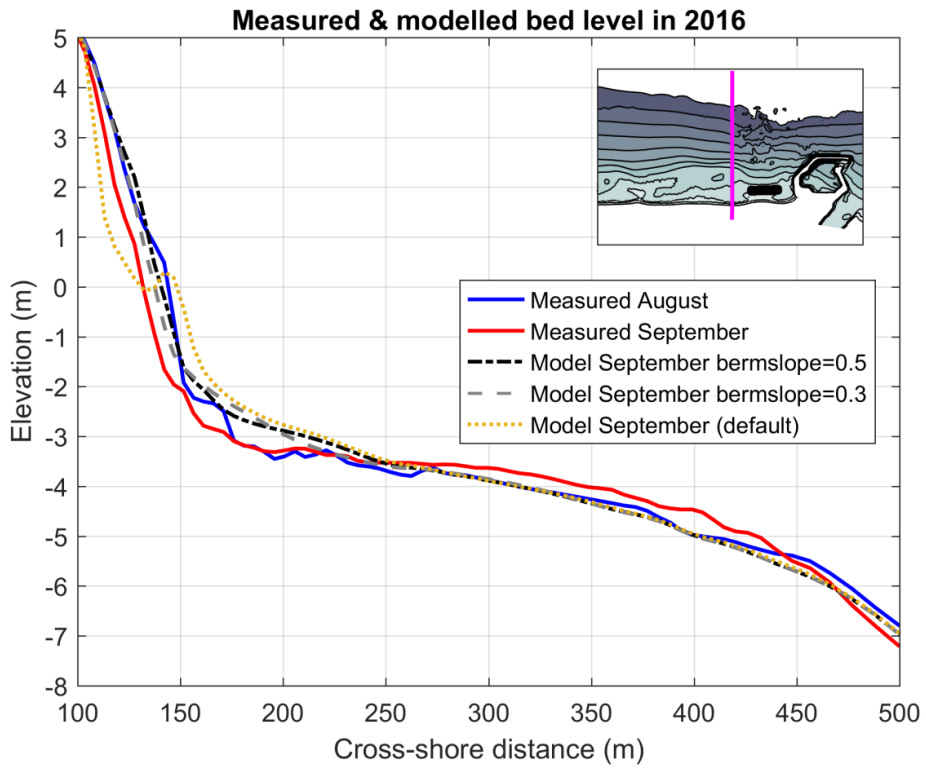
Figure 69: Cross-section *(c)* from figure 66. Measured and modelled bed level comparison.
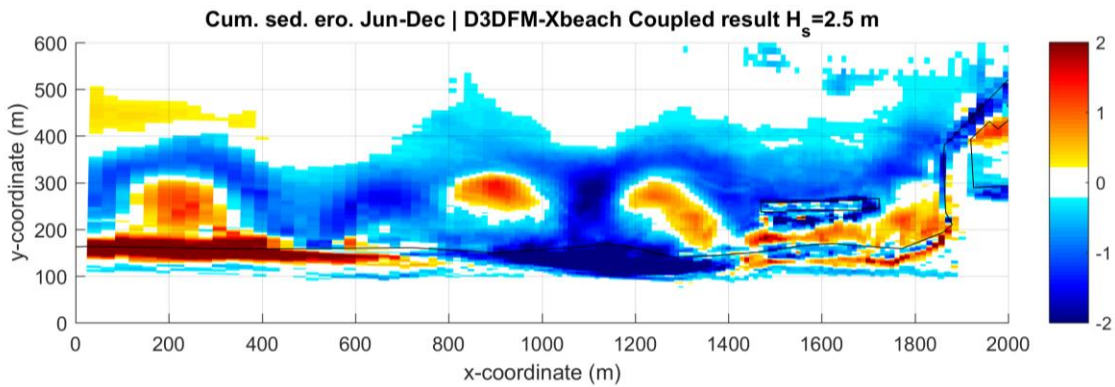
Figure 70: Modelled cumulative sedimentation/erosion patterns. D3D-FM & XBeach coupled model, period Jun-Dec 2015. XBeach *bermslope* = 0.5
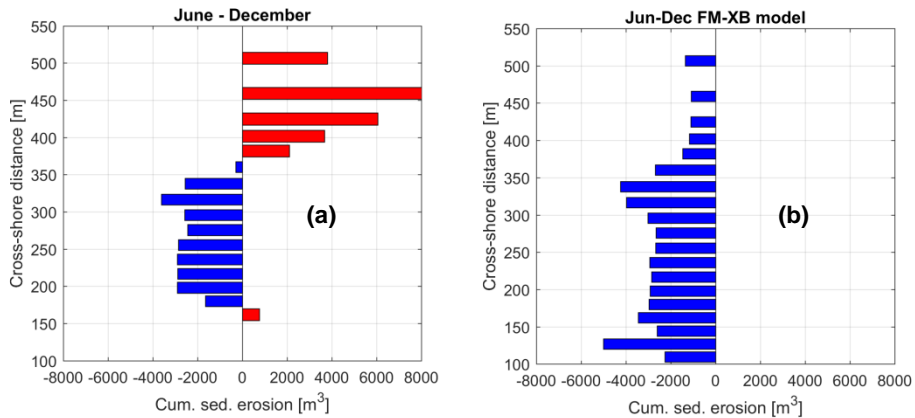
Figure 71: Cross-shore sedimentation/erosion bars for Jun-Dec 2015. D3D-FM & XBeach coupled model.
H_s **threshold = 2.5 m. (a) Measured results ; (b) Xbeach with *bermslope* = 0.5 results**

5. Discussion

The previous chapters have focused on presenting the data and model results from Anmok beach, showing the contrast between different models mainly focusing on the difference between coupled and uncoupled simulations. During this process decisions and/or assumptions about certain model parameters were made, but only briefly discussed.

In this chapter these results are further analyzed, and the key assumptions are discussed. This chapter is divided in five parts: the comparison between D3D and D3D-FM; the discussion of Eulerian and GLM coupled model results; the discussion of the stationary and surf beat coupled model results; the discussion of the dry beach erosion and recovery processes, and; a brief analysis of computational performance.

5.1. D3D & D3D-FM

A base case model was determined in D3D and later reproduced in the new suite D3D-FM. After the validation of hydrodynamics it was found that in general the new software achieves similar results in most of the comparisons of water levels, wave energy (spectra) and flow velocity magnitude. However, it was found that the D3D-FM is less sensitive to wave-driven currents in the nearshore when they oppose the tide direction. This is something new that had not been seen before, and it could be attributed to the complex bathymetry and highly energetic boundary conditions that affect Anmok beach. The wave module is still a β-functionality in D3D-FM that has not been officially released, hence there is a possibility that the mismatch between both models is related to a programming error that could be fixed.

After the hydrodynamic validation, the morphodynamic base case was attempted to be replicated in D3D-FM. By doing this it was found that the new software is still highly sensitive to some numerical parameters such as cell wet/dry threshold, or the maximum wave height breaker parameter γ_{max}. This was expected since the new morphology module is also classified as a β-function. One of the underlying purposes of this work was to validate this module in a complex field scenario such as Anmok beach, assessing the (dis)advantages of using the new software. It is interesting to notice that this work is one of the first to successfully make use of the new morphology module, as of today's date there is only one published work where it was effectively used before (Smits, 2016). However in Anmok beach the conditions are much more energetic than the aforementioned publication, as for instance the bed shear-stresses modelled by Smits (2016) are roughly one order of magnitude smaller than the ones obtained in the present project (Smits, personal communication).

The main advantage of D3D-FM is the implementation of the Basic Model Interface (BMI), which allows coupling the software with different instances of itself or with different software such as XBeach. This interface is not present in regular D3D hence an online coupling between models is not possible.

Among the disadvantages of using D3D-FM it was found that the same base case model takes roughly ~50% larger computational time; however this is before grid optimization. Further discussion on software performance is addressed in section §5.5. The most relevant disadvantage of D3D-FM for this work was the less dynamic morphological response when computing sediment transport using the Eulerian velocities for mass transport. This was meant to be a key process to analyze in this work. Due to the fact that the uncoupled results were not as good as expected, the coupling of GLM with Eulerian mass transport became a secondary goal. The results of this procedure are discussed in section §5.2. Another disadvantage of D3D-FM is that for such an energetic and complex environment as Anmok beach the new software shows instabilities that were not present in regular D3D. They were circumvented by doing an analysis of the most sensitive numerical parameters through trial and error. Despite the fact that the changes in these parameters could have affected in some way the final morphodynamic results, they were necessary to achieve stable runs.

5.2. Eulerian & GLM mass transport coupling

Two D3D models were run with Eulerian and GLM mass transport, and together they defined the base case to analyze. It was found that the best results were obtained by running a model where the first 6 months (calm season) use a GLM transport and the last 6 months (stormy season) use an Eulerian transport. It was also found that the morphological changes of the stormy season dominate over the changes in the calm season.

When attempting to replicate these models in D3D-FM it was found that the GLM model showed similar results, whereas the Eulerian model was different. When comparing all the model results it was discovered that the Eulerian mass transport implementation in D3D-FM produced less dynamic results than in D3D. This was expected because the morphological changes when moving from a GLM to an Eulerian simulation were not as strong as the ones observed in D3D. To test this, a simple 2D alongshore uniform coast model was developed. The results of this 2D model confirmed this expectation. One of the original goals of this thesis was to develop a coupling methodology that would allow running Eulerian mass transport only during severe storms, and GLM mass transport the rest of the time. According to the hypothesis of Ton (2017) and the results from a full year D3D base case, the morphological results were expected to improve. Regardless of the limitations found, with the results from the present study this hypothesis is rejected. The coupled model results in D3D-FM ended up having a morphological result that was better than the GLM-only results, but not as good as the Eulerian-only results. This was mainly because less erosion at the shoreline was obtained, but at the cost of having less accretion in the offshore region. Despite the results not being as promising as hoped, one major achievement of this thesis is the development of a coupling methodology between two instances of D3D-FM through a process known as "forking". To exchange information between models, a significant wave height threshold of 2.5 m was selected to maximize the Eulerian mass transport processing time but not abuse it, and it is on the same order of magnitude (~3.0 m) as other thresholds used in similar studies for defining storm events (Pender & Karunarathna, 2013), (Callaghan et al., 2008). The processing time of the coupled model increased by a factor ~2.5, and the overall performance is further discussed in section §5.5. One of the main advantages or added value that can be recognized from this particular coupling technique is the significant reduction in bookkeeping efforts. For the 2.5 m wave height threshold only 1 model was run, whereas to do the same simulation following an offline approach a total of 13 serialized models would have been required, which increases the chances of making a human error.

In both the Eulerian and GLM simulations the quantification of the results by the BSS turned up to be not practical. The models had very low scores in the order of ± 0.1, which qualifies as "Poor" at best. The main reason behind these low scores is that the BSS is a simple quantification measure that fails to capture the relevance of the complex bathymetry and shoreface dynamics present at Anmok beach, such as the crescentic bar system. These low scores were also achieved by Ton (2017), who used alternative ways to estimate the model's performance. Following a similar line of work the model performance was assessed based on a qualitative analysis of the sedimentation/erosion patterns, and in a quantitative manner by means of cross-shore sedimentation/erosion bars in an area of interest located away from the boundaries.

A hypothesis for a solution to get better results with a GLM-EUL coupled model in D3D-FM is to calibrate two different models simultaneously: a GLM model for the calm periods ($H_s < threshold$) and an Eulerian model for the storm events ($H_s > threshold$). This however would implicate spending more time in each model calibration to a point of, even, duplicating the workload of this activity. Additional scenarios regarding the wave height threshold could be tested without compromising the overall performance in D3D-FM, since the processing time in this case time is expected to remain constant. One very interesting result from the GLM-EUL coupled model is that when running the Eulerian mass transport only during the storms, which accounts for ~14% of the total simulation time, the morphological changes obtained do not differ significantly with the uncoupled Eulerian simulation. This confirms the results from section §4.2.2 that indicates that storms at this beach are the most important morphological drivers.

As an alternative way to analyze the effect of including Eulerian mass transport only during storms, a coupling between D3D-FM and XBeach in stationary mode was developed, with the main limitation that XBeach has longer processing times. For this computational reason only two wave height thresholds were assessed (of 3.5 and 2.5 m). These values where selected to have a better understanding on how sensitive the morphodynamic results are with respect to this parameter. The lowest value was selected for practical reasons as is the lowest value that allows running XBeach for an acceptable amount of time (during 6 storms), while the largest value would run it "briefly" only for 3 storms. The results from these models show that the longer the (XBeach) Eulerian mass transport is used, the higher the erosion in the nearshore, while the overall results do not significantly improve with respect to the 6 months D3D Eulerian simulation. One possible reason for this could be that the model settings of the Eulerian computation were calibrated for a mean scenario, in different words, the calibrated parameters for the winter season also take into account calm periods in between the storms. Because of this is likely that the calculated sediment transport during the storm itself is less than expected, while the calculated sediment transport during the calm periods is larger than in reality.

From the results obtained it can be inferred that a more frequent coupling between both software ($H_{s\,threshold} < 2.5\,m$) would not generate better predictions near the shoreline, since higher erosion starts to appear (as is seen in the D3D Eulerian simulation). A case that was not tested but is expected to generate results similar to the D3D Eulerian simulation is a 6 months XBeach simulation in stationary mode and with the avalanching algorithm turned off. Unfortunately, the processing time of such simulation would make it prohibitive to perform in a practical sense.

5.3. Stationary & surf beat coupling

In this thesis two methodologies were developed to couple models: one that coupled two (or more) instances of D3D-FM as discussed in section §5.2 and; a second methodology that allowed coupling different software (BMI compatible) such as D3D-FM and XBeach. In this section the results from the second coupling technique are discussed.

There were two purposes behind the coupling of D3D-FM and XBeach. One was to compute the storm events with XBeach in stationary mode, which is similar to apply an Eulerian mass transport during these events, as previously discussed in section §5.2. The second purpose was run the storm events in surf beat mode, which allows assessing the effect of including long waves. To exchange information between models two wave height thresholds were tested (of 3.5 m and 2.5 m). When comparing the results between the stationary and surf beat simulations, it was found that the inclusion of long waves generates excessive erosion of the dry beach for both thresholds. The results indicate that lowering the wave height threshold for a coupled simulation should improve the offshore morphodynamic results, but would generate even larger dry beach erosion. The reasons for this erosion are believed to be the increase in wave set-up and run-up due to long waves, and the inclusion of the avalanching algorithm in XBeach, which allows slumping of dry material from the supratidal beach.

To assess the impact of long wave set-up/run-up in beach erosion, the water levels were compared between the stationary and surf beat simulations (Figure 56), confirming that the surf beat model does present higher waterline elevations, hence wetting and eroding more sand. This finding is in line with the results obtained by Deltares (2016a), as shown in Figure 72, where in different storms the maximum waterline was compared between stationary and surf beat models of Anmok beach. The finding from that work is that the maximum difference in water levels between both models ranges between 2.8 m to 1.3 m, which is in the same order as the results obtained in this thesis. To assess the effect of the avalanching algorithm on supratidal beach erosion, an additional model in surf beat mode but without avalanching was developed (Figure 57 and Figure D-99). The considerably milder dry beach erosion confirms the dominant role of the avalanching mechanism in dry beach morphology.
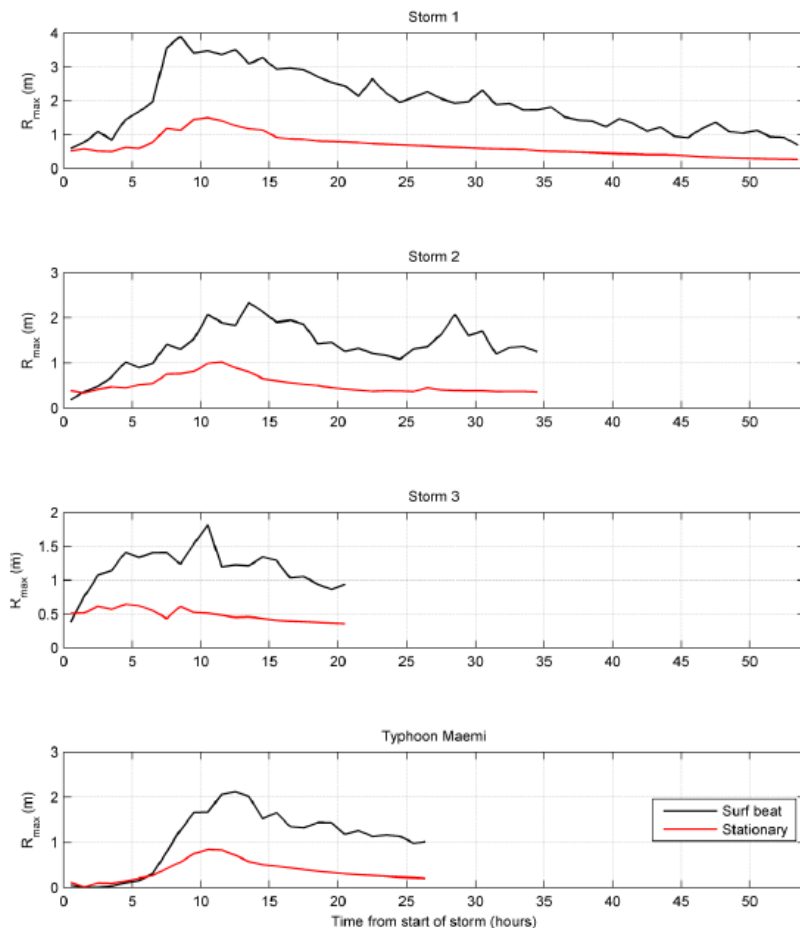
Figure 72: Time series of maximum waterline elevation for different storm events. XBeach stationary (red) v/s surf beat (black) simulations. Location approx. 1000 m west of the SBW. Figure from Deltares (2016a)

With the present results, it can be said that the coupling of a long-term morphodynamic model (D3D-FM) with a storm model such as XBeach does not generate better morphodynamic results with respect to an uncoupled D3D Eulerian simulation in Anmok beach. The main reason for this is that the inclusion of long waves generates additional beach erosion, but no additional mechanisms for post-storm recovery are being included. In different words, by adding a storm model during high energy events, but not adding a post-storm recovery model in the subsequent calmer periods, the model is being skewed, and an imbalance is produced where the "additional model" physics become dominant. The question that arises now is: *what if a post-storm recovery model would be coupled instead of a storm model? Would the results be skewed towards higher shoreline accretion?* This idea seems plausible, but more research is needed to prove it. A conclusion that can be drawn from the present results is that an uncoupled model will generate better average morphodynamic results with respect to a coupled model where only some of the physical processes are considered. Specifically in this case, if a storm model such as XBeach is chosen to be included, then the recommendation is to also include a post-storm recovery model which enhances the supratidal beach accretion. This additional model could comprise processes such as aeolian sediment transport and/or a different representation of the swash zone and wave run-up. This conclusion is in line with what has already been addressed by different authors: den Bieman (2012) concluded in his study that the coupling of a storm model and an aeolian (stationary) post-storm recovery model was imbalanced due to the inability to accrete the large erosion caused during the storms. In a different line of work, Pender & Karunarathna (2013) concluded that a storm/post-storm coupled simulation could be reasonably well achieved only if different model settings were considered in each simulation, although the uncoupled models still produced better results. What seems to be a widespread recommendation, and is also suggested in thesis, is that whenever a coupled model is chosen to be run, a simultaneous calibration of all the involved models is expected to give better results than an independent calibration of each model-component separately followed by a coupling procedure (den Bieman, 2012; Pender & Karunarathna, 2013; Velhorst, 2017).

An important finding from the coupled model results is that the shoreline erosion caused by the cumulative effect of storms is relevant. Bearing this in mind it is recommended to develop a coupled simulation with XBeach (surf beat) as storm model if for instance a "worst case scenario" regarding beach erosion or coastline retreat is looked upon. Likewise, if the intra-seasonal (medium term) variation of the beach width or shoreline location is of importance, it seems warranted to perform a coupled simulation. The results from this work show that the extreme erosion or severe coastline retreat caused by cumulative storms is underestimated when represented by a long-term morphological model only. Since in practice engineers must choose at the end what software to use, the added value of coupling simulations or a rough suggestion on "when to couple models" is summarized in Figure 73.
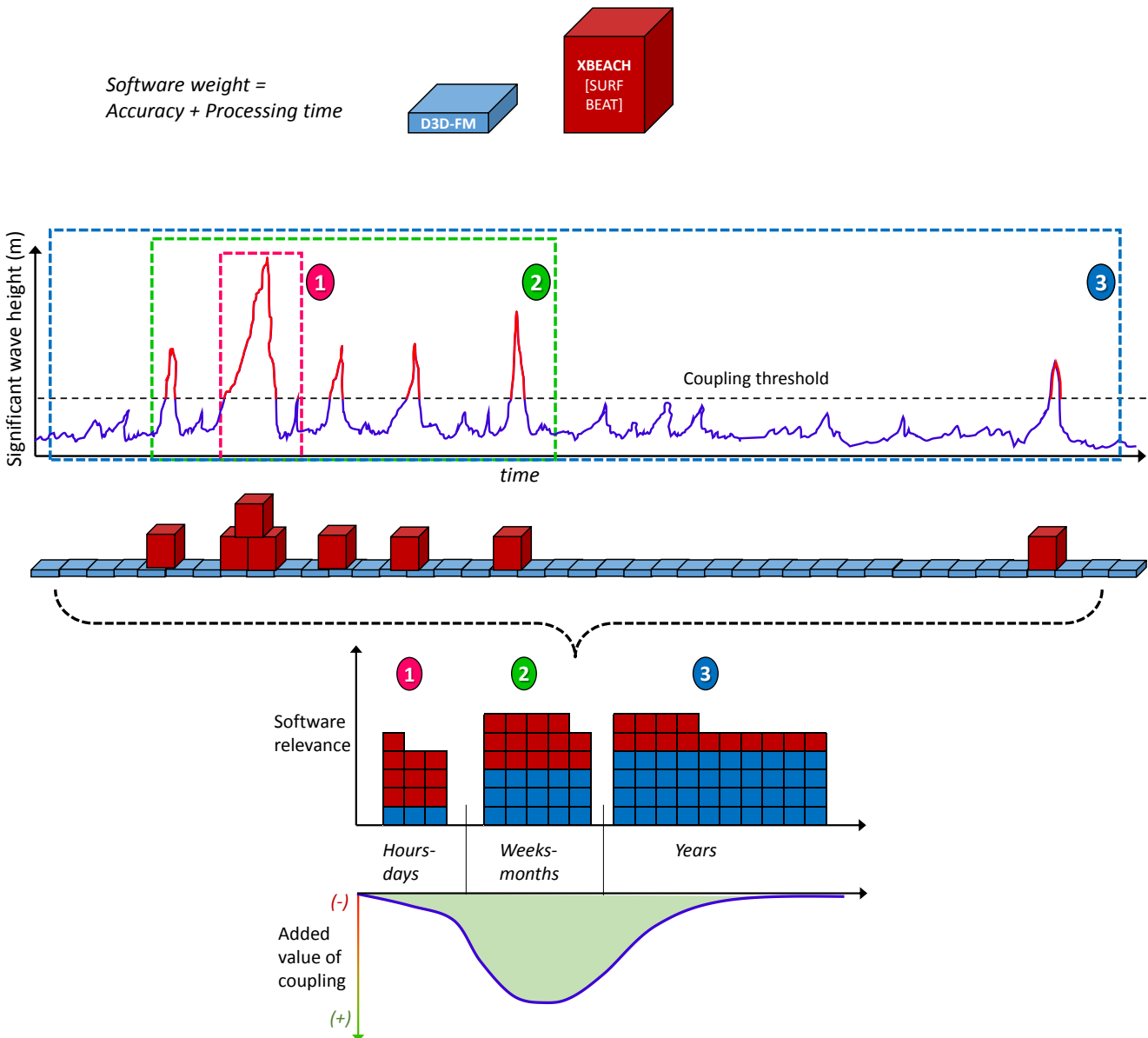
Figure 73: Summarized sketch of the added value of coupling. ① For short time scales XBeach alone is recommended; ② In an intermediate time scale both software seem to be relevant due to the morphological changes in the calmer periods and cumulative storms effects; ③ For longer time scales D3D alone gives the better average results.

5.4. Dry beach erosion and recovery balance

After analyzing the coupled model results, it was found that the dry beach recovery processes were not sufficient. To deal with this issue, two different paths were followed: the first had the goal of estimating the capabilities of a research version of D3D regarding beach accretion and; the second had the objective of assessing a research parameter in XBeach regarding the reduction of simulated beach erosion. Both analyses did not have the intention of achieving final morphological results but to provide some first tools which could be useful in the future towards obtaining a better morphological hindcast at Anmok beach or other locations.

Several authors have identified that the two most important processes regarding post-storm beach recovery are: the sand deposited by wave run-up in the foreshore, leading to a growth of a beach berm that acts as a sediment sink, and; the aeolian transport of this swash-deposited sediment farther into the backshore and dry beach or dunes (Thom & Hall, 1991; Morton et al., 1994; Brocchini & Baldock, 2008; Chardon-Maldonado et al., 2016). In an attempt to simulate this first process, a research version of D3D with swash zone sediment transport equations was assessed. The results obtained are promising in the sense that the deposition of sand near the shoreline was reasonably enhanced. In order to achieve these results the empirical coefficients present in the equations were amplified by several orders magnitude, deviating considerably from the values calibrated by the authors in experimental facilities (Larson et al., 2004; Larson & Wamsley, 2007). The high values obtained are in a practical sense seen as "modelling artifacts" that force the simulation to bring sediments onshore, but they could also compensate for unaccounted mechanisms such as: the interaction between short-wave run-up and long waves motion, which could lead to a constructive interference increasing the swash amplitude and flow velocities (Brocchini & Baldock, 2008), or; the fact that the energetics approach used in the present models is unable to accurately predict the swash zone dynamics. It has been found that a single swash event can transport in the order of $O(1/10)$ of the total sediment transport in the swash zone over an entire tidal cycle (Chardon-Maldonado et al., 2016). Bearing these limitations in mind, the results are encouraging, but they also confirm the lack of a mechanism (or process-based model) capable of transporting the swash-deposited sediment farther in the landward direction.

The second path that was followed comprised calibrating the XBeach model to simulate less supratidal beach erosion. This idea emerged after acknowledging the fact that the (modelled) dry beach erosion could not be counteracted with the present process-based models used in this thesis. To achieve this, a one month period with data from the year 2016 was used, and the calibration was focused on an experimental XBeach parameter (*bermslope*) that "forces" or tries to achieve a user-given slope in the foreshore. The result from this calibration raised great expectations since the dry beach erosion was severely reduced and an alternate sedimentation/erosion pattern at the shoreline was obtained, similar to what is depicted in the measurements. However when applying these settings back in the 2015 stormy season (medium-term simulation), software stability problems were encountered and the final results lost credibility. Despite these problems the final dry beach erosion was reduced suggesting that the use of this parameter is encouraging and should be further investigated in future releases of XBeach.

5.5. Computational performance

When developing the coupling methodologies, several parameters were looked upon in order to produce an effective coupling procedure, such as model stability and interpolation of variables. However one hypothesis that was a main thruster of this thesis project was that the inclusion of more model complexity (or additional physical phenomena) could be achieved without significantly increasing the processing time, by means of an activation of these complex models only when required (Deltares, 2016a).

To assess this hypothesis the processing times were measured, and the average results are summarized in Figure 74. The first thing to notice is that when moving from D3D to D3D-FM in Anmok beach simulations, the processing time increased by ~50%. This could have been reduced by a better construction of the grid. A major advantage of D3D-FM is that the grid can be built in such a way that

a large resolution is applied only where required (e.g. near the shoreline) while a smaller grid resolution could be set in the offshore region. This smart grid technique can severely reduce the processing time (Deltares, 2016b), although this analysis was kept out of the scope of work. When looking at the coupled D3D-FM model (GLM-EUL simulation), it is seen that the simulation time increases by ~140% with respect to the uncoupled simulations. This value could be further reduced, since at present time D3D-FM lacks the ability to execute large time-steps. This is possible in XBeach where by means of BMI the model time can be set manually, allowing the software to run only during the storms. If in a future release of D3D-FM a similar function is implemented, the additional processing time (with respect to the uncoupled simulation) is expected to be marginal. On the other hand the advantage of running both simulations in parallel is that the performance becomes independent of the significant wave height threshold chosen, as all time-steps need to be resolved for both instances. Therefore for any wave height threshold to be tested with the current methodology, the processing time would be known beforehand, and is around ~8 days.
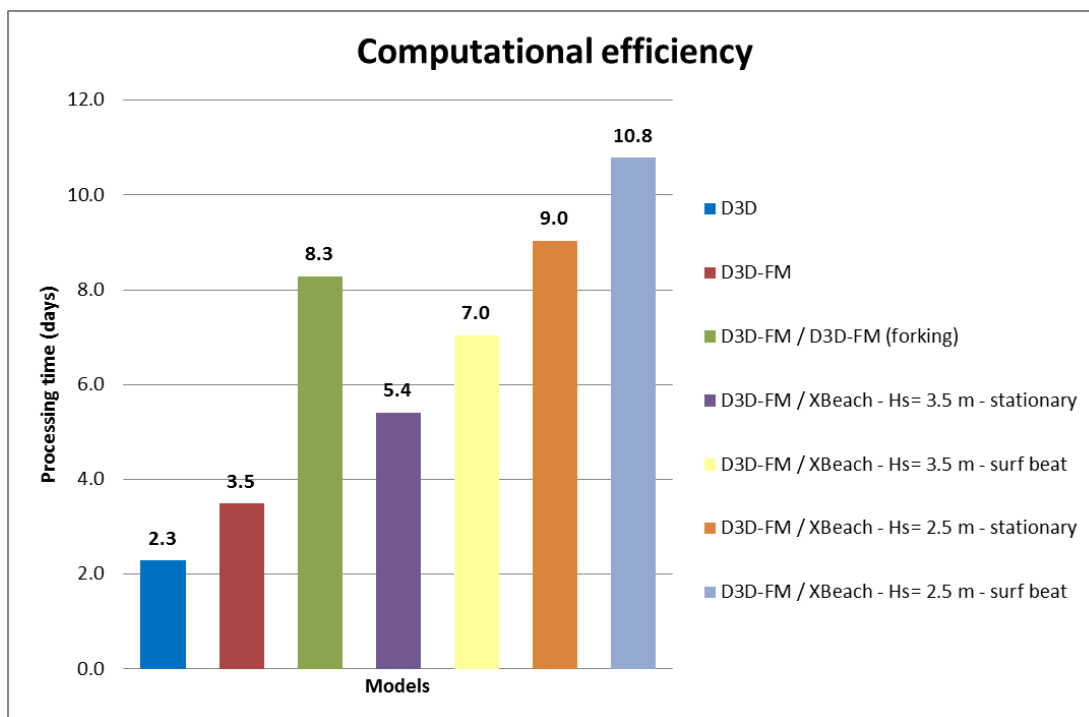
Figure 74: Computational performance for uncoupled and coupled models. Jun-Dec 2015 simulations.

Regarding the XBeach and D3D-FM coupled performance, a trend is observed where the lower the wave height threshold, the larger the time that XBeach runs, hence the greater the total processing time is. It can also be seen that the stationary simulation runs faster than the surf beat mode. The results show that the selection of a wave height threshold has the highest importance when it comes to computational expense. For instance the simulations with a 2.5 m threshold take approx. 50~60% larger processing times than the simulations with a 3.5 m threshold, both in stationary and surf beat modes. The XBeach stationary model efficiency could be improved by increasing the wave update interval from its default value of 1 min to 20 minutes as is done in D3D-FM. This is believed to significantly reduce the total computational time of the coupled stationary model.

Figure 75 shows a breakdown of the last 4 coupled-models shown in Figure 74, and it is plausible to say that the hypothesis from Deltares (2016a) is true and was achieved in this project. When moving from a 2.5 m to a 3.5 m threshold, the total running time of the (surf beat) coupled model decreases from 10.8 days to 7 days. This decrease is mainly due to XBeach, which is originally responsible for 62% of the computational resources (figure 75-d), but with the higher threshold lowers its demand to a 42% of the total time (figure 75-b). A similar behaviour is depicted for the stationary coupled models, where the computational demand due to XBeach decreased by approx. 50% (figures 75-c and 75-a). It is also seen that in general D3D-FM has roughly a constant processing time of about ~4 days in the present simulation.
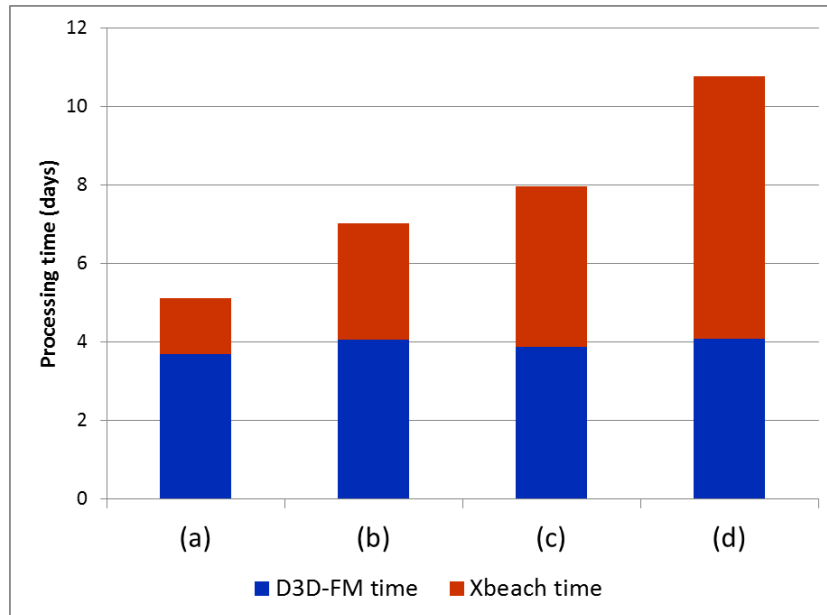
Figure 75: Breakdown of processing times as a percentage of total time for D3D-FM and XBeach coupled models: (a) Stationary model $H_s = 3.5\,m$; (b) Surf beat model $H_s = 3.5\,m$; (c) Stationary model $H_s = 2.5\,m$; (d) Surf beat model $H_s = 2.5\,m$

6. Conclusions and recommendations

6.1. Conclusions

In this thesis insight is obtained in the processes of integrating morphodynamic models with different physical mechanisms and an increasing level of complexity. This has been carried out by analyzing a morphological hindcast at Anmok beach, at the east coast of South Korea, first with a stand-alone D3D-FM model and later with coupled models of D3D-FM and XBeach.

The present chapter comprises the concluding remarks about this work by means of answering the research questions presented in Chapter 1. Finally, recommendations are given regarding future work.

6.1.1. Advantages and disadvantages of model coupling

What are the (dis)advantages of coupling different morphodynamic models regarding the beach evolution predictions at Anmok beach?

One of the biggest advantages of running a coupled simulation that was found in this work, is the possibility to include more complex phenomena in a medium-to-long term simulation with a reasonable increase in computational time. This allows for assessing the morphological effect of cumulative storms at Anmok beach. Despite the results being skewed towards beach erosion, the intra-seasonal shoreline predictions are believed to be better represented by the coupled model. In contrast, the uncoupled long-term simulations showed less morphological changes near the waterline. This is quite relevant if a worst case scenario is a primary decision tool within a project, either in critical beach width or soil stability of real estate located near the shore.

The use of a complex storm model for long periods of time is often (computationally) prohibitive to perform. In this thesis it has been shown that the coupling of D3D-FM with XBeach enables the optimization of computational resources. By including additional mechanisms only during storms instead of the whole stormy season, sensible results were achieved with an acceptable increase in processing time. This procedure also allowed identifying which mechanisms are not well represented by the current models.

A big advantage of coupling models from a practical point of view is the simplification in bookkeeping. In the case of the stormy season at Anmok beach, a coupled model was performed in which 1 input generated 1 output, without any intermediate steps. To construct the same model through an offline approach, a total of 13 models would have been required, which from a bookkeeping point of view is troublesome. Therefore, the developed coupling methodology is less prone to human error.

The major disadvantage found in this work is that the coupling of independently calibrated models does not necessarily provide better results than the ones obtained by each model separately. In the coupled models of Anmok beach, the dry beach erosion was severely over estimated. If a coupling procedure is chosen to be done, it is necessary to include all the relevant physical processes, in order to have a coherent morphodynamic balance.

6.1.2. Temporal activation of processes through model coupling

What is the morphological impact of including Eulerian mass transport or long (infragravity) waves only during storms at Anmok beach?

From the results obtained in this thesis, the largest impact seen is excessive dry beach erosion, and it can be concluded that the morphological predictions are not improved with the inclusion of more complex processes.

The coupled simulation which includes Eulerian (EUL) mass transport only during severe storms generates a result that in overall is better than the uncoupled simulation with Generalized Lagrangian Mean (GLM) mass transport, but is not as good as the uncoupled EUL simulation. The GLM-EUL coupled model predicts less shoreline erosion than the stand-alone EUL simulation, generating a

better resemblance with the field data, but the offshore accretion is under predicted, which deviates from the measurements.

The inclusion of infragravity waves produces dry beach erosion larger than measured; however the post-storm recovery mechanisms present in D3D (and D3D-FM) are not sufficient to restore the beach. An attempt to calibrate the storm model (XBeach) was undertaken by adjusting a parameter that reduces the supratidal beach erosion, and despite the promising results, the uncoupled D3D simulation still shows a better overall representation of the medium-to-long term morphology at Anmok beach.

6.1.3. Current development of D3D-FM

What are the (dis)advantages of applying D3D-FM over D3D in this particular project?

In this thesis the models previously developed in D3D were replicated in the new suite D3D-FM. This choice was made because the new software has the advantage of implementing the Basic Model Interface (BMI), which allows developing online and serial-online coupled simulations in a seamless manner, either with different instances of itself or with different software such as XBeach.

Among the disadvantages found in the use of D3D-FM, first is the fact that the processing times increased by roughly ~50 %, but this is before re-arranging the model grid in an efficient manner (applying high resolution only where required). This action is supposed to reduce the computational times. Another disadvantage is the fact that the wave module is still (in its last stage of) development, and some hydrodynamics were found to differ near the shoreline, indicating that at the moment the model is somewhat less sensitive to wave-driven currents with respect to D3D, at least in the present simulation of Anmok beach. Also, the morphology module is still in development, which led to model stability issues and made the simulations highly sensitive to certain model parameters. During the development of this thesis it was found that the Eulerian mass transport mode shows smaller morphological changes in D3D-FM with respect to its counterpart in D3D. However, the Eulerian mass transport option has been released only as research versions in both suites, and with such a complex model as the Anmok case it is not possibly to determine with certainty whether the former software is under predicting the offshore sediment transport, or if the latter model is making an over prediction.

6.1.4. Post-storm beach recovery

Can the beach recovery processes be enhanced by including specialized swash zone sediment transport formulations in D3D?

The results from the coupled models indicate that a post-storm recovery mechanism is missing which is capable of accreting to beach after severe storm erosion. An attempt was made to simulate these mechanisms by running a research version of D3D with specialized sediment transport equations in the swash zone, and the outcome of this procedure is promising. The accretion of the shoreline and lower dry beach was reasonably enhanced, especially when considering all the limitations involved in modelling the morphodynamics of the swash zone with an energetics approach. However, from these results two important remarks must be mentioned: 1) The fairly good results must be handled with care, since an "*overshooting*" of the empirical coefficients from the equations was required, reaching final values that differ in 3 or more orders of magnitude with respect to experimentally calibrated values, and; 2) The models are able to deposit sediment at the lower backshore at best. Hence there is still the need of a mechanism/process capable of transporting the sediments farther upslope into the dry beach and/or dunes. From literature, a plausible candidate is believed to be an aeolian process-based model. Also the implementation of the swash zone module should be revised, since it was expected from the large coefficients to wet the beach at higher elevations.

6.1.5. Concluding remarks regarding the added value of coupling models

Some concluding remarks regarding model coupling are presented next, and it is believed that the insight obtained in this work and expressed in the following statements will be useful in future works or as a part of guidelines for coupling models and their added value:

- There is no single answer for the question "*When should a model be coupled?*", as this will depend in a case-by-case basis. Running a coupled simulation might improve the overall results, but it also means an increase in the time and effort required to set-up the models since a calibration of each simulation is required.
- One important advantage of coupling different morphodynamic models is that more physics/processes can be added if they are required or if they are known to play fundamental roles. An online coupling of models is paramount if the feedback between the models is expected to play an essential role in their morphodynamic response. The coupling of models allows investigating the inclusion and exclusion of these different mechanisms, regarding the impact they have in the morphological development of the study site.

6.2. Recommendations

From the development of this thesis, the following recommendations for future research are proposed:

Include all the relevant processes that shape the coastline

It is recommended to add additional mechanisms that enhance the post-storm recovery of the beach. At the moment there is not any process based model that accurately represents post-storm recovery processes. One alternative could be to implement the D3D-swash zone transport module in D3D-FM and couple this with XBeach and another additional model. The idea would be that D3D-FM (with swash zone equations) brings sediment into the shore, and the additional model (possible aeolian sediment transport) could bring the sediment into the supratidal (dry) beach, so XBeach can erode it later during severe storms. A triple calibration could become troublesome but results have the potential to be much more realistic both in the long-term and during the intra-seasonal variations. To achieve this, the coupling procedure should be extended (modified) to include additional software with online coupling capabilities (preferably BMI). It is also recommended to analyze the implementation of the D3D-swash zone transport module and its ability to wet the beach (and bring sediments) at higher elevations. It is expected that a better parameterization of the swash zone can increase the accretion the intertidal and supratidal areas.

Study the Eulerian mass transport software implementation

It is recommended to analyze the differences in Eulerian mass transport in detail (in D3D and D3D-FM), comparing the respective implementation in each source code. One unknown that could not be answered in this thesis is whether the Eulerian implementation in D3D is over predicting the morphological changes or the implementation in D3D-FM is delivering an under prediction. A set of simple 1D cross-shore models could be used assess and find this answer. Further research in this topic is suggested.

Calibrate the coupled models simultaneously

One hypothesis drawn in this thesis that happens to be in line with previous attempts in model-coupling, is not try to achieve "*perfect*" independent calibrations (in the medium-to-long term) and then couple them, but try to achieve a simultaneous calibration where one model represents better the storms and the other the calmer periods. This simultaneous calibration will probably take longer, but the results could severely improve, since the feedback between models is not a process known beforehand. This is still to be proven and it is an interesting line of future work.

Analyze different wave height thresholds

It is recommended to perform a thorough significant wave height threshold analysis. In this work due to the mild changes of the Eulerian mass transport in D3D-FM (with respect to the GLM simulation), only one wave threshold was assessed, however it is recommended for future works to analyze what significant wave height value/conditions generate the best morphodynamic results when following the already developed coupling procedure. The hypothesis at this point is that a better morphological result could be achieved by having model settings representative of calm (or recovery) periods and

different settings during storms. It is believed that this could lead to better outcomes, following the idea and results obtained by Pender & Karunarathna (2013) in a different location.

Current practice on model coupling

For current practice, the recommendation on whether to run coupled or uncoupled models is dependent on the phenomena and time scale that are being analyzed. If beach or dune erosion is analyzed in the time scale of a single storm, the post-storm recovery mechanisms are not believed to be important, and it is recommended to develop a single uncoupled storm model such as XBeach. If a long-term morphological study is developed, to assess effects such as sea level rise or reduction in sediment supply of a coastal cell, then an uncoupled long-term model such as D3D (or D3D-FM) is recommended. In this case the erosion due to storms is expected to be compensated by the post-storm recovery mechanisms and averaged out in the long run. An exception is when storms change the regime of beach, for instance in the case of a breach of barrier islands during severe storms. In that particular case a coupled approach is recommended in order to include the modelling of the breach. Finally, in the medium-term both the calm and storm conditions are expected to have a significant impact in beach morphology. In this time scale, based on the current software limitations, an uncoupled approach is recommended to predict the average behaviour of the coast, and a coupled simulation is recommended when the worst case scenario regarding beach erosion or coastline retreat is required.

References

Baart, F., Den Bieman, J., Van Koningsveld, M., Parteli, E., Plant, N., & Roelvink, J. (2012). An integrated coastal model for aeolian and hydrodynamic sediment transport. *Geophysical Research Abstracts.*

Battjes, J. A. (1974). *Computation of set-up, longshore currents, run-up and overtopping due to wind-generated waves.* PhD Thesis, Delft University of Technology, Delft.

Bosboom, J., & Stive, M. (2013). *Lecture notes Coastal Dynamics I.* Delft: Delft University of Technology. VSSD. ISBN: 978-90-656-286-0.

Brocchini, M., & Baldock, T. E. (2008). Recent advances in modeling swash zone dynamics: Influence of surf-swash interaction on nearshore hydrodynamics and morphodynamics. *Reviews of Geophysics, 46*(3).

Callaghan, D., Nielsen, P., Short, A., & Ranasinghe, R. (2008). Statistical simulation of wave climate and extreme beach erosion. *Coastal Engineering*(55), 375-390.

Chardón-Maldonado, P., Pintado-Patiño, J., & Puleo, J. (2016). Advances in swash-zone research: Small-scale hydrodynamic and sediment transport processes. *Coastal Engineering*(115), 8-25.

Deltares. (2014). *Delft3D-FLOW. Simulation of multi-dimensional hydrodynamic flows and transport phenomena, including sediments. User Manual.* Technical Report. Version: 3.15.34158., Delft.

Deltares. (2015a). *D-Waves. Simulation of short-crested waves with SWAN. User Manual. Version 2016. Rev. 41915.* Technical Report, Delft.

Deltares. (2015b). *Xbeach user manual.* Retrieved December 12, 2016, from Xbeach documentation: http://xbeach.readthedocs.io/en/latest/user_manual.html

Deltares. (2016a). *CoMIDAS - East Coast Case. Numerical model study of Anmok Beach.* Technical Report, Delft.

Deltares. (2016b). *D-Flow Flexible Mesh Technical Reference Manual - DRAFT . Version: 1.1.0. Revision: 48665.* Technical Report, Delft.

Deltares. (2016c). *D-Flow Flexible Mesh User Manual - DRAFT. Version: 1.2.1. Revision: 48668.* Technical Report, Delft.

den Bieman, J. (2012). *Simulating Barrier Island Evolution. Coupling Process-Based Models.* MSc Thesis, Delft University of Technology.

Gallagher, B. (1971). Generation of surfbeat by non-linear wave interactions. *J. Fluid Mech., 49*, 1-20.

Hillen, R., de Ruig, J., Roelse, P., & Hallie, F. (1991). *De basiskustlijn: Een technisch/morfologische uitwerking (in Dutch).* Rijkswaterstaat, DGW.

Holthuijsen, L. H. (2010). *Waves in oceanic and coastal waters.* Cambridge University Press.

Hoonhout, B. (2015). *XbeachMI.* Retrieved January 6, 2017, from XbeachMI documentation: http://xbeachmi.readthedocs.io/en/latest/

Hughes, S. (2004). Estimation of wave run-up on smooth, impermeable slopes using the wave momentum flux parameter. *Coastal Engineering*(51), 1085-1104.

Kernkamp, H., van Dam, A., Stelling, G., & de Goede, E. (2011). Efficient scheme for the shallow water equations on unstructured gris with application to the Continental Shelf. *Ocean Dynamics*(61), 1175-118.

Koudstaal, K. R. (2016). *Modeling the contribution of infragravity and incident band swash on East coast South-Korean beaches.* MSc Thesis, Delft University of Technology, Delft.

Larson, M., & Wamsley, T. (2007). A formula for longshore sediment transport in the swash. *Sixth International Symposium on Coastal Engineering and Science of Coastal Sediment Process.* New Orleans, Lousiana.

Larson, M., Kubota, S., & Erikson, L. (2004). Swash-zone sediment transport and foreshore evolution: field experiments and mathematical modeling. *Marine Geology*(212), 61-79.

Lesser, G., Roelvink, J., van Kester, J., & Stelling, G. (2004). Development and validation of a three-dimensional morphological model. *Coastal Engineering, 51*, 883-915.

Longuet-Higgins, M., & Stewart, R. (1962). Radiation stress and mass transport in surface gravity waves with application to "surf beats". *J. Fluid Mech., 29*, 481-504.

Longuet-Higgins, M., & Stewart, R. (1964). Radiation stress in water waves: a physical discussion with applications. *Deep-Sea Research, II*, 529-562.

Mangor, K. (2008). *Definitions of coastal terms.* Retrieved December 12, 2016, from Coastal Wiki: http://www.coastalwiki.org/wiki/Definitions_of_coastal_terms

Morton, R., Paine, J., & Gibeaut, J. (1994). Stages and durations of post-storm beach recovery, southeastern Texas coast, USA. *Journal of Coastal Research*, 884-908.

Munk, W. (1949). Surf beats. *Eos Trans. AGU, 30*, 849-854.

Nederhoff, C. (2014). *Modeling the effects of hard structures on dune erosion and overwash. Hindcasting the impact of Hurricane Sandy on New Jersey with XBeach.* MSc Thesis, Delft University of Technology.

Peckham, S., Hutton, E., & Norris, B. (2013). A component-based approach to integrated modeling in the geosciences: The design of CSDMS. *Computers & Geosciences, 53*, 3-13.

Pekkeriet, T. (2011). *Morphodynamics of mega-nourishment. Integrated model approach for the design and management of mega-nourishment.* MSc Thesis, Delft University of Technology, Delft.

Pender, D., & Karunarathna, H. (2013). A statistical-process based approach for modelling beach profile variability. *Coastal Engineering*(81), 19-29.

Reniers, A., van Dongeren, A., Battjes, J., & Thornton, E. (2002). Linear modeling of infragravity waves during Delilah. *Journal of Geophysical Research: Oceans, 107*(C10), 1-1–1-18.

Roelvink, D., Stelling, G., Hoonhout, B., Risandi, J., Jacobs, W., & Merli, D. (2012). Development and field validation of a 2DH curvilinear stom impact model. *Proceedings of the 33rd International Conference on Coastal Engineering.* Santander.

Roelvink, J. (1993). *Surf beat and its effect on cross-shore profiles.* PhD Thesis, Delft University of Technology, Delft.

Roelvink, J., & Stive, M. (1989). Bar generating cross-shore flow mechanisms. *J. Geophys. Res, 94*, 4785–4800.

Roelvink, J., Reniers, A., van Dongeren, A., van Thiel de Vries, J., Lescinski, J., & McCall, R. (2010). *XBeach Model Description and Manual. Technical report.* Unesco-IHE, Deltares and Delft University of Technology, Delft.

Roelvink, J., Reniers, A., van Dongeren, A., van Thiel de Vries, J., McCall, R., & Lescinski, R. (2009). Modelling storm impacts on beaches, dunes and barrier islands. *Coastal Engineering, 56*, 1133-1152.

Sallenger, A. (2000). Storm impact scale for barrier islands. *Journal of Coastal Research, 16*(3), 890-895.

Smits, B. (2016). *Morphodynamic optimisation study of the design of semi-permeable dams for rehabilitation of a mangrove-mud coast.* MSc. Thesis, Delft University of Technology.

Stengs, B. (2013). *Implementation of wave effects in the unstructured Delft3D suite.* MSc Thesis, Delft University of Technology.

Stive, Marcel J.F., de Schipper, Matthieu A., Luijendijk, Arjen P., Aarninkhof, Stefan G.J., van Gelder-Maas, Carola, van Thiel de Vries, Jaap S.M., de Vries, Sierd, Henriquez, Martijn, Marx, Sarah; Ranasinghe, Roshanka. (2013). A new alternative to saving our beaches from sea-level rise: The sand engine. *Journal of Coastal Research, 29*(5), 1001-1008.

Sutherland, J., Peet, A., & Soulsby, R. (2004). Evaluating the performance of morphological models. *Coastal Engineering, 51*, 917-939.

The SWAN team. (2016, 09 22). *Scientific and technical documentation*. Retrieved March 06, 2017, from SWAN. Simulating WAves Nearshore: http://swanmodel.sourceforge.net/

Thom, B. G., & Hall, W. (1991). Behaviour of beach profiles during accretion and erosion dominated periods. *Earth Surface Processes and Landforms, 16*(2), 113-127.

Ton, A. (2017). *Process based modelling of hydro- and morphodynamics around submerged breakwaters.* MSc Thesis, Delft University of Technology, Delft.

USACE. (1984). *Shore protection manual.* Coastal engineering Research Center, Department of the Army, Waterways Experiment Station.

USACE. (2008). *Coastal Engineering Manual (CEM), volume 1100.*

van Dongeren, A.; Battjes, J.; Janssen, T.; van Noorloos, J.; Steenhauer, K.; Steenbergen, G.; Reniers, A. J. H. M. (2007). Shoaling and shoreline dissipation of low-frequency waves. *Journal of Geophysical Research: Oceans, 112*(C2).

van Koningsveld, M., & Mulder, J. (2004). Sustainable coastal policy developments in the Netherlands. A systematic approach revealed. *Journal of Coastal Research*, 375-385.

van Santen, R., Steetzel, H., van Thiel de Vries, J., & van Dongeren, A. (2012). Modelling storm impact on complex coastlines westkapelle, The Netherlands. *Proceedings of the 33rd International Conference on Coastal Engineering.* Santander.

van Son, S. (2009). *Monitoring and modeling nearshore morphodynamic behaviour on storm time scales.* Msc Thesis, Delft University of Technology, Delft.

van Thiel de Vries, J. S. (2008). Analysis of dune erosion processes in large-scale flume experiments. *Coastal Engineering, 55*(12), 1028-1040.

van Thiel de Vries, J. S. (2009). *Dune erosion during storm surges.* PhD Thesis, Delft University of Technology, Delft.

van Thiel de Vries, J. v. (2011). The effect of the longshore dimension on dune erosion. *Coastal Engineering Proceedings, 1*(32).

van Zanten, S. (2016). *Towards engineering the ecosystem services of a mega-nourishment. A forecast of the ecosystem service dynamics of the Sand Motor.* MSc Thesis, Delft University of Technology.

Velhorst, R. (2017). *Towards a coupled morphodynamic model of the nearshore zone and the beach at the Sand Engine. Combining waves, tide, morphodynamics and aeolian sediment transport into a process-based model.* MSc Thesis, Delft University of Technology.

Walstra, D., Roelvink, J., & Groeneweg, J. (2001). Calculation of wave-driven currents in a 3D mean flow model. *Proc. 27th Int. Conf. Coastal Eng*, (pp. 1050-1063). Sydney, Australia.

MODELS PARAMETERS

In this appendix the different model parameters (as input in the configuration files) are presented. Only the values that differ from the *default model value* are presented.

Table A-10: D3D-FM Flow parameters

Parameter	Value	Parameter	Value	Parameter	Value
Layertype	1	UnifFrictCoef	65	Sedimentmodelnr	4
BedlevType	1	Rhomean	1025 kg/m^3	TransportVelocity	1 eul (0 glm)
AngLat	37.77	Doodsonstart	55.565	DtUser	10 s
Conveyance2D	-1	Doodsonstop	375.575	DtMax	10 s
Turbulencemodel	1	Wavemodelnr	3	DtInit	0.6 s
Epshu	0.01	Wind velocity	0 m/s	MorStt	14400 s
TransportTimestepping	1	Gammax	0.8	MorFac	3
MorUpd	True	SusW	0.02	BedW	0.05
HMaxTH	1.5	camax	0.05	updinf	True
Cref	1600 kg/m^3	CDryB	1600 kg/m^3	RhoSol	2650 kg/m^3
SedDia D50	5e-4 m	Chezy coeff.	65 m$^{0.5}$/s	Chezy coeff. at port and SBW	35 m$^{0.5}$/s

Table A-11: D3D-FM Wave parameters

Parameter	Value	Parameter	Value	Parameter	Value
DirConvention	Nautical	WindGrowth	False	MaxIter	30
WaterDensity	1025	WhiteCapping	Westhuysen	SpectrumSpec	from file
GenModePhys	3	Quadruplets	False	StartDir	1
Breaking	true	Refraction	true	EndDir	361
BreakAlpha	1.0	FreqShift	true	FreqMin	0.02
BreakGamma	0.73	WaveForces	dissipation 3d	FreqMax	0.49
Triads	false	UseHotFile	true	NFreq	48
Diffraction	False	FlowBedLevel	2		
TriadsBeta	2.2	FlowWaterLevel	2		
BedFriction	jonswap	FlowVelocity	0		
BedFricCoef	0.038	FlowWind	0		

Table A-12: D3D Flow parameters

Parameter	Value	Parameter	Value	Parameter	Value
Latitude	37.77	BedW	0.05	Cref	1600 kg/m^3
Number of layers	1	SusW	0.05	Viscosity at boundaries	100 m^2/s
Bathimetry at	Cell corners	Wind	False	Chezy coeff.	65 m$^{0.5}$/s
Thin dams for port	yes	Lateral boundaries	Neumann	Chezy coeff. at port and SBW	35 m$^{0.5}$/s
Timestep	0.1 min	Offshore boundary	Water level	Offshore reflection α	100
MorStt	240 min	Gammax	0.55	D50 m	5e-4 m
MorFac	3	CDryB	1600 kg/m^3	RhoSol	2650 kg/m^3
updinf	False				

Table A-13: D3D Wave parameters

Parameter	Value	Parameter	Value	Parameter	Value
DirConvention	Nautical	WindGrowth	False	MaxIter	30
WaterDensity	1025	WhiteCapping	Westhuysen	SpectrumSpec	from file
GenModePhys	3	Quadruplets	False	StartDir	1
Breaking	true	Refraction	true	EndDir	361
BreakAlpha	1.0	FreqShift	true	FreqMin	0.02
BreakGamma	0.73	WaveForces	dissipation 3d	FreqMax	0.49
Triads	false	UseHotFile	true	NFreq	48
Diffraction	False	FlowBedLevel	2		
TriadsBeta	2.2	FlowWaterLevel	2		
BedFriction	jonswap	FlowVelocity	0		
BedFricCoef	0.038	FlowWind	0		

Table A-14: XBeach surf beat model parameters

Parameter	Value	Parameter	Value	Parameter	Value
D50	5E-4	dtheta	10	morfac	3
D90	7.5E-4	alfa	-134.6	morfacopt	1
Scheme	warmbeam	xori	493339.3068	facAs	0.25
front	Abs_2d	yori	4182183.0	facSk	0.1
left	Neumann	vardx	1	instat	Swan
right	Neumann	posdwn	-1	break	Roelvink_daly
back	Wall	nx	214	wavint	300
lwave	1	ny	234	defuse	1
Single_dir	1	struct	1	gamma	0.55
Dtheta_S	10	sedtrans	1	gamma2	0.3
thetanaut	1	morphology	1	wavint	300

Table A-15: XBeach stationary model parameters

Parameter	Value	Parameter	Value	Parameter	Value
D50	5E-4	xori	493339.3068	facAs	0.25
D90	7.5E-4	yori	4182183.0	facSk	0.1
Scheme	warmbeam	vardx	1	instat	Stat_table
front	Abs_1d	posdwn	-1	break	Baldock
left	Neumann	nx	214	defuse	1
right	Neumann	ny	234	morfacopt	1
back	Wall	struct	1	morfac	3
lwave	0	sedtrans	1	alfa	-134.6
thetanaut	1	morphology	1	dtheta	10
gamma	0.78	wavint	60		

In this chapter the results from the hydrodynamic validation are presented. Figures B-76 and B-77 show the comparison of wave spectra between the measurements, D3D and D3D-FM models in buoys W1, S2 and V3. It can be seen that for periods of low wave energy ($H_s < 1\,m$) both models show the same result in wave energy for the all the buoys. However during an event of higher wave energy ($H_s \sim 2\,m$), indicated in Figure B-77 by the vertical dashed line in the time series, a difference in predicted wave spectra is observed behind the breakwater (buoy V3). The energy spectrum peak in this location is usually showing a frequency shift between the different models during these high wave events. Figure B-78 shows the total (integrated) spectral energy in buoys S2 and V3, where it can be seen that despite some differences the total energy in V3 is similar between both models. The energy in buoys S1, S2 and W1 is the same for both models.
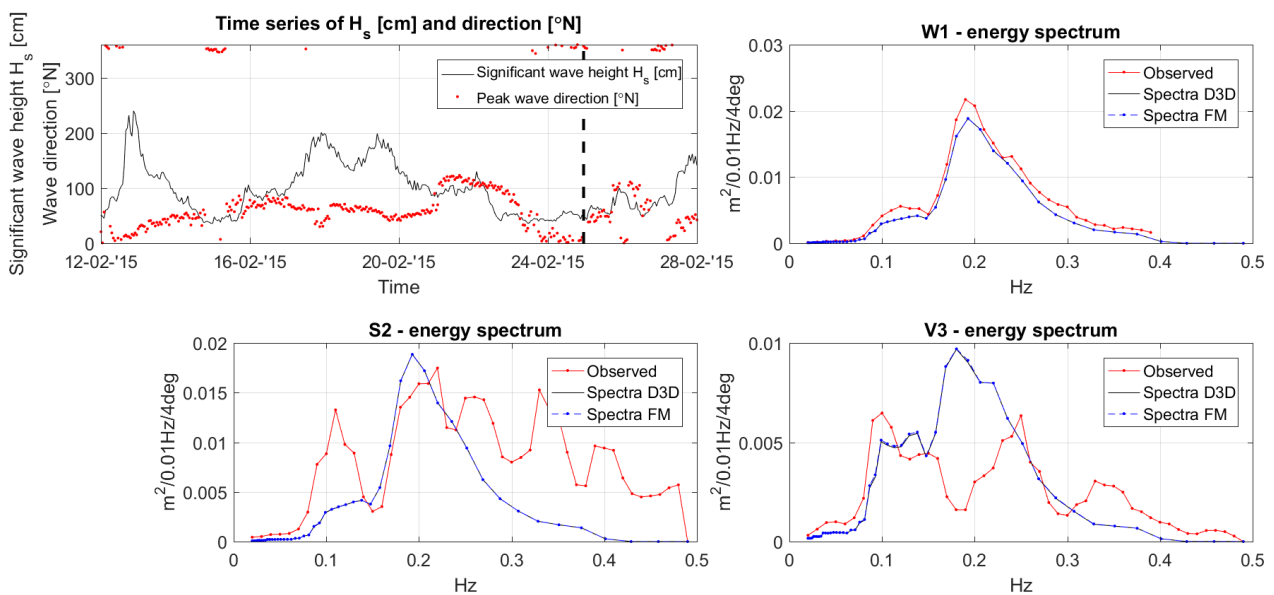
Figure B-76: Measured and modelled wave spectra comparison, 25-02-2015
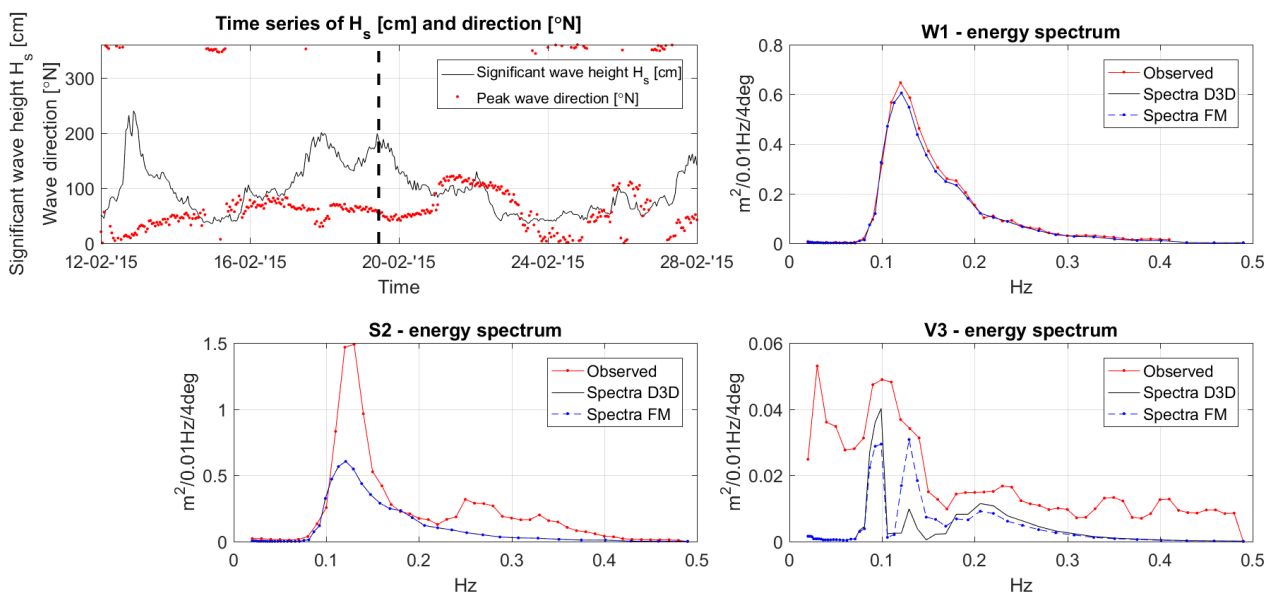
Figure B-77: Measured and modelled wave spectra comparison, 19-02-2015

73
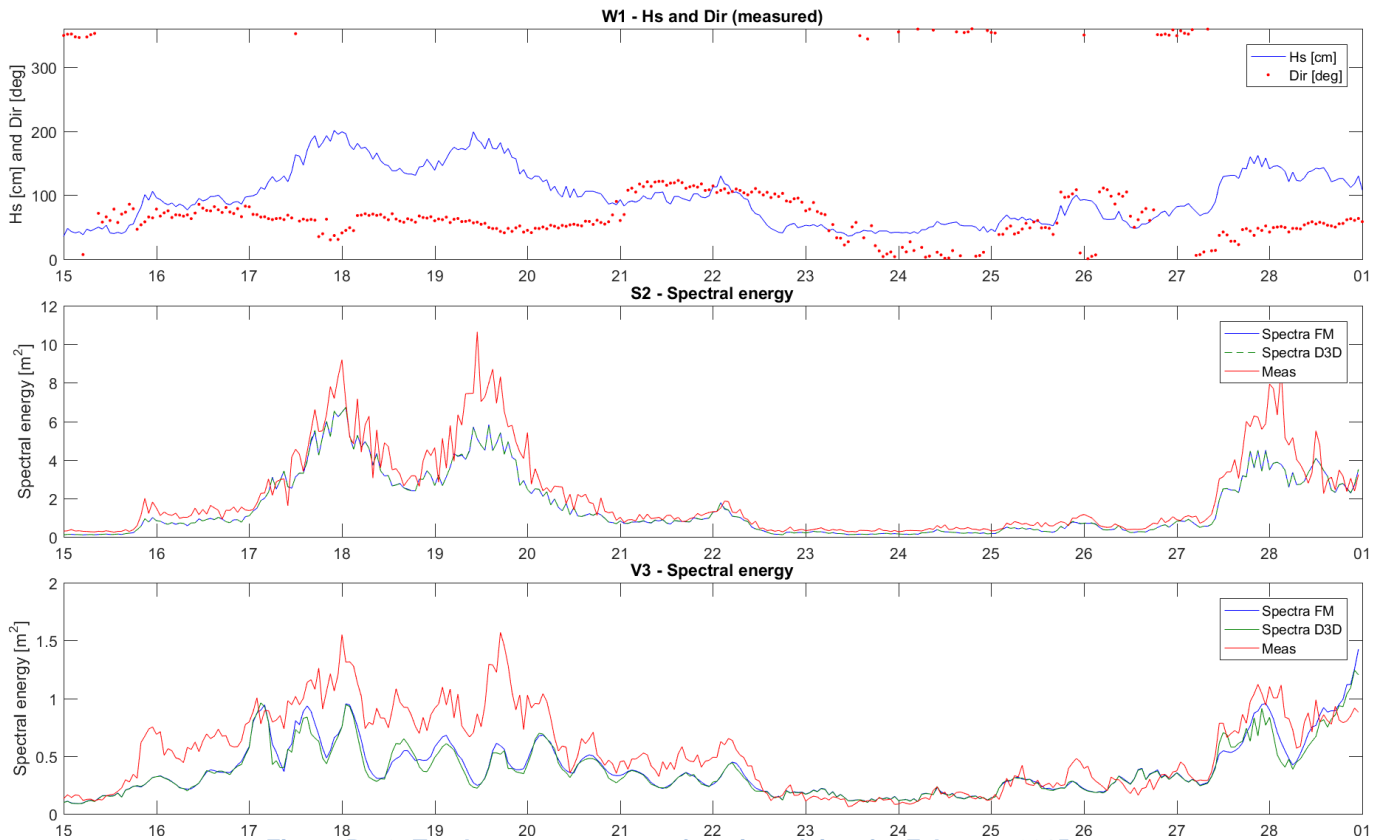
Figure B-78: Total wave energy as a function of time for February-2015

The comparison between modelled and measured water depths is shown in figures B-90, B-91 and B-81 for buoys W1, S2 and V3. Here it is depicted that both models predict a similar water depth for the different locations, with the largest difference located behind the SBW, of approx. ~0.4 m. This was already noticed by Deltares (2016a) and Ton (2017), where it was discussed that this difference is due to issues with the measured bathymetry and/or uncertainties in the instrument sensor reference level. However, the trend and periodicity of the measurements is in agreement with both models, and when this difference or *offset* is corrected from the measurement as a constant value (0.4 m) the results show a good agreement (figures B-80b and B-81b). Overall the differences between both models do not exceed ± 5 cm which is considered acceptable.
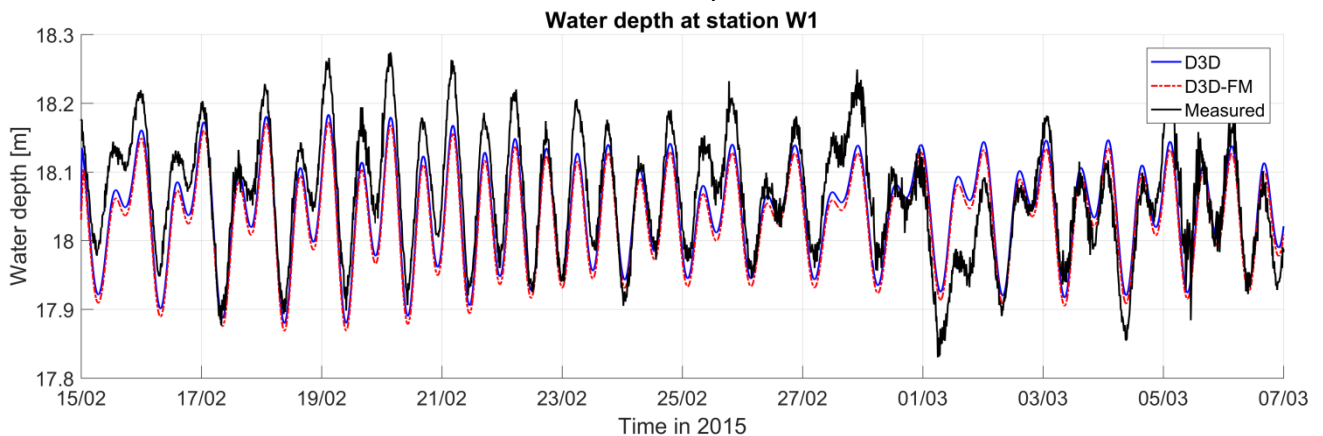
Figure B-79: Measured and modelled water depth.
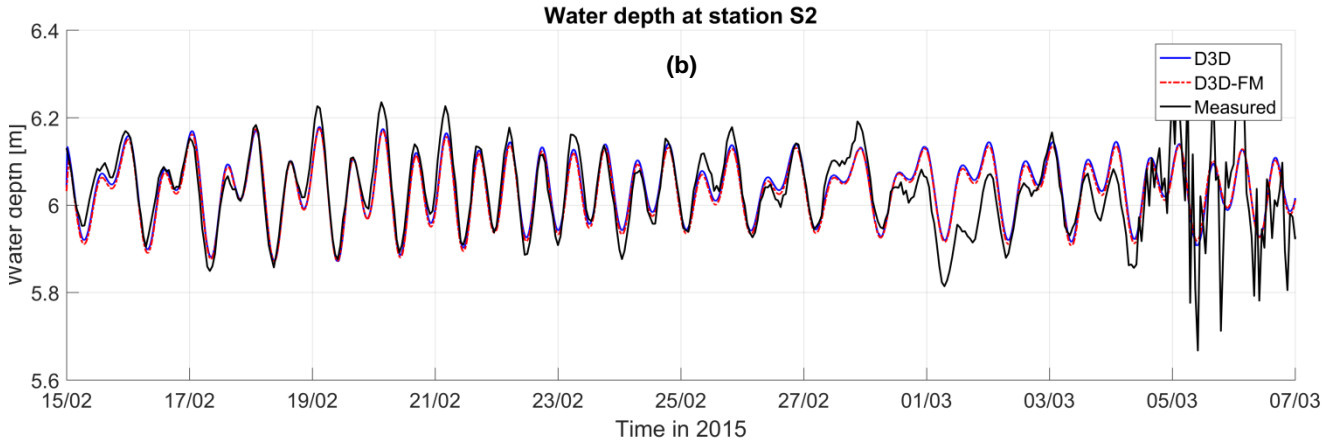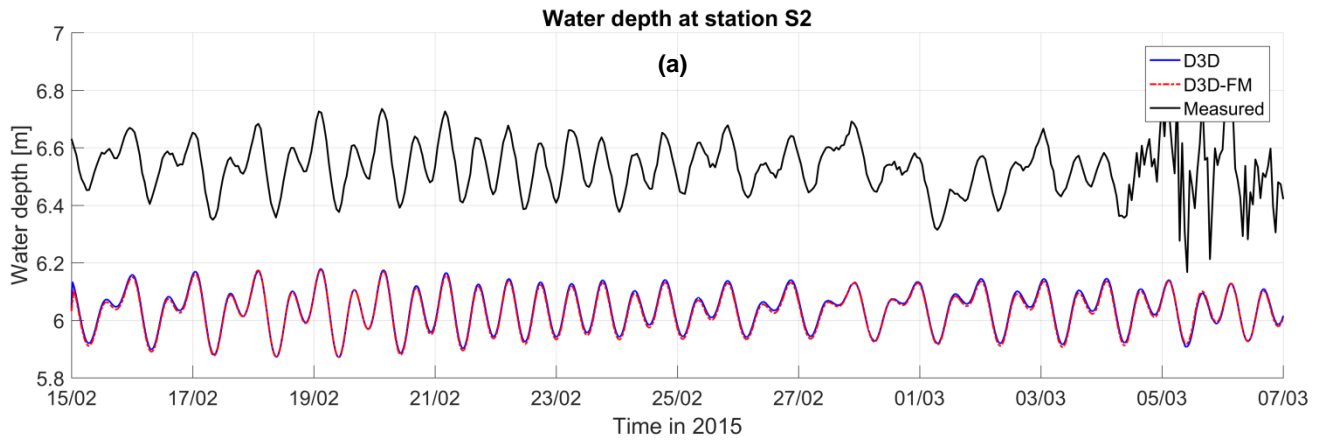
Figure B-80: Measured and modelled water depth. (a): Raw data; (b): Corrected data by 0.4 m offset.
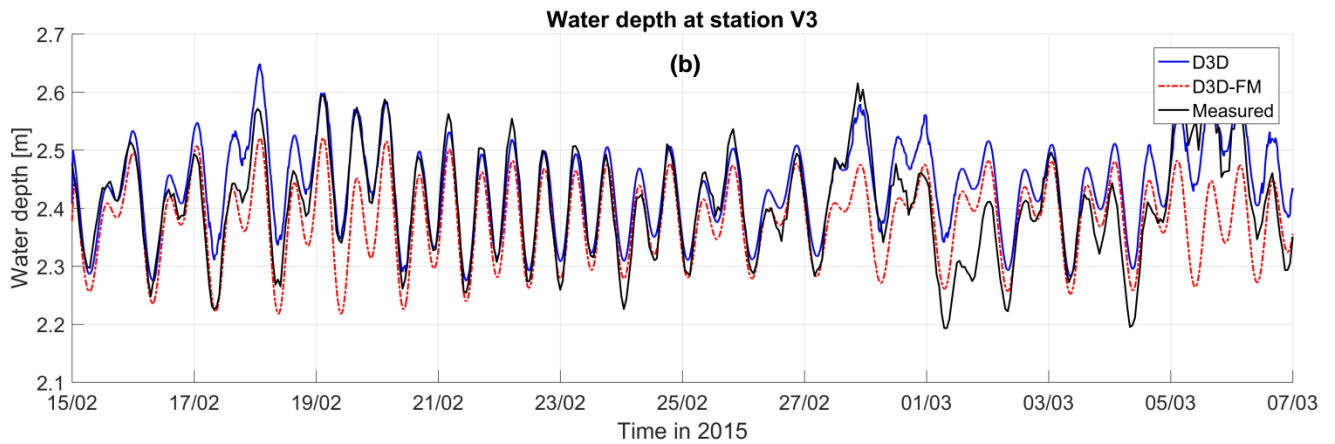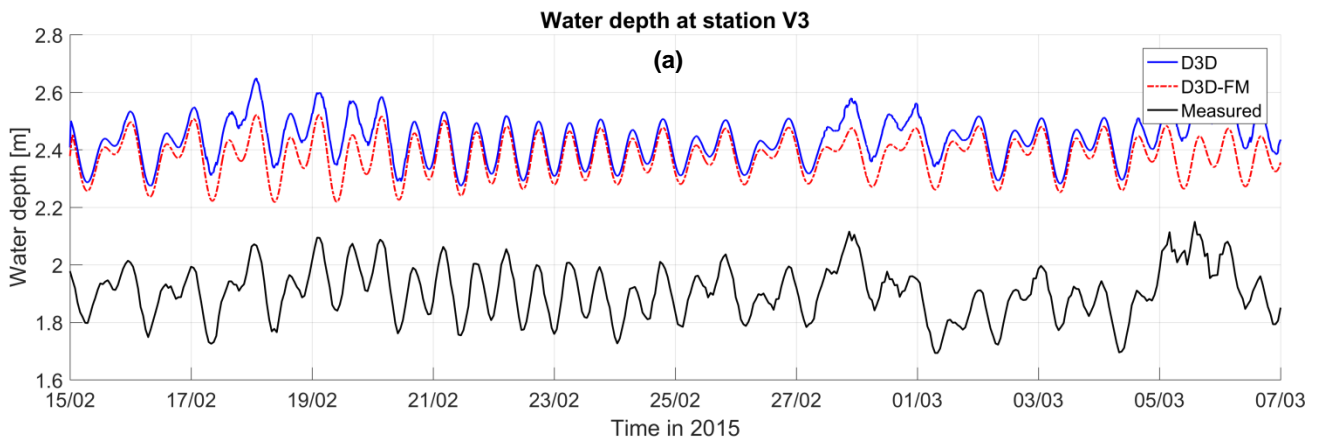
Figure B-81: Measured and modelled water depth. (a): Raw data; (b): Corrected data by 0.4 m offset.

With respect to current velocities an unexpected behaviour was found. Figures B-82 and B-83 show the mean flow direction in W1 and S2. It can be seen that farther offshore (W1), the flow is mostly tide-dominated, whereas in the nearshore (S2), a relevant variation in flow direction is observed, both for measurements and D3D model. This is not seen all the time in the D3D-FM simulation. The latter model seems to be somewhat less sensitive to wave-generated currents at some moments, or at least this is the case for the present simulation. This can be confirmed when looking at a velocity field plot for two different times, as shown in Figure B-84.
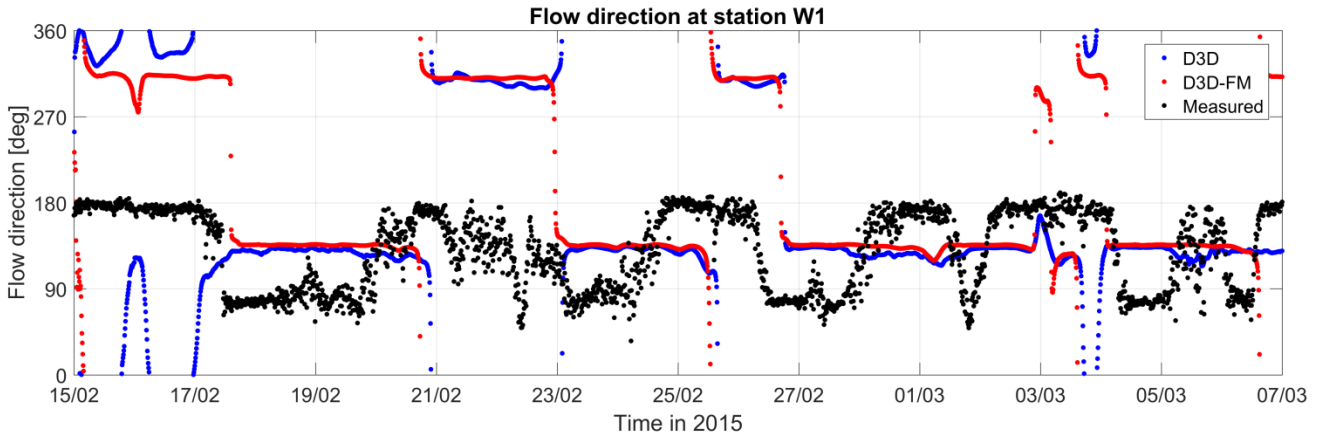
Figure B-82: Measured and modelled flow direction
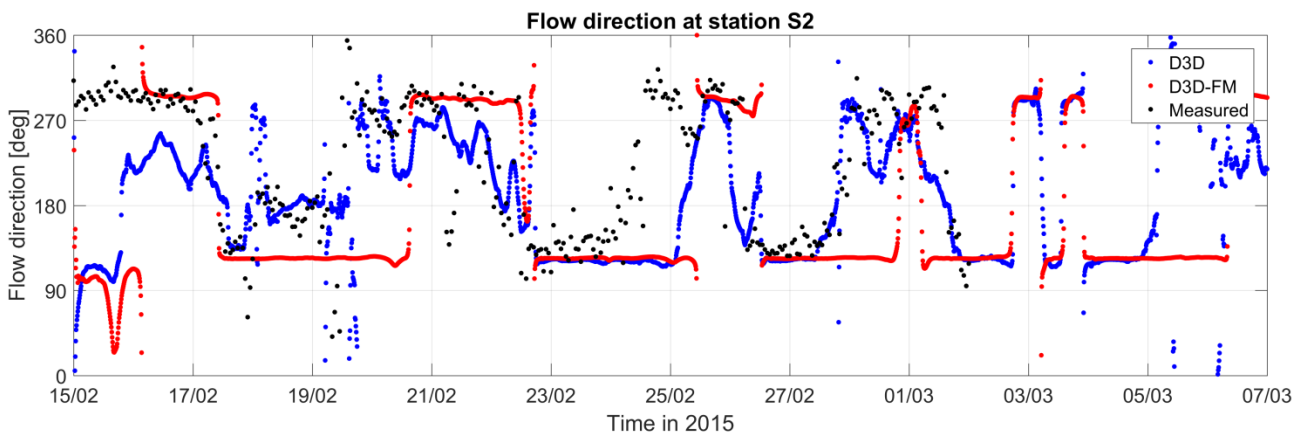
Figure B-83: Measured and modelled flow direction
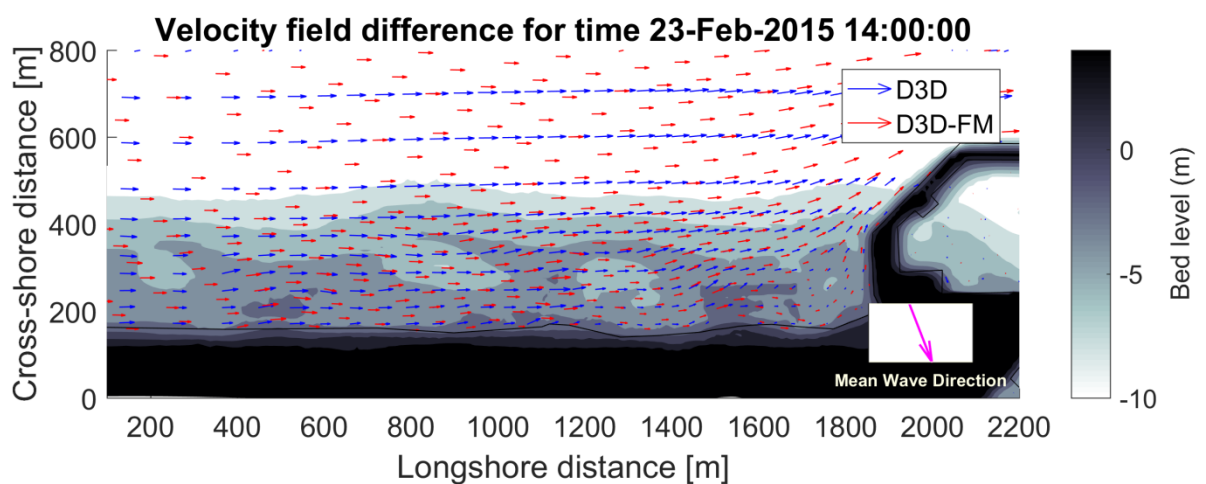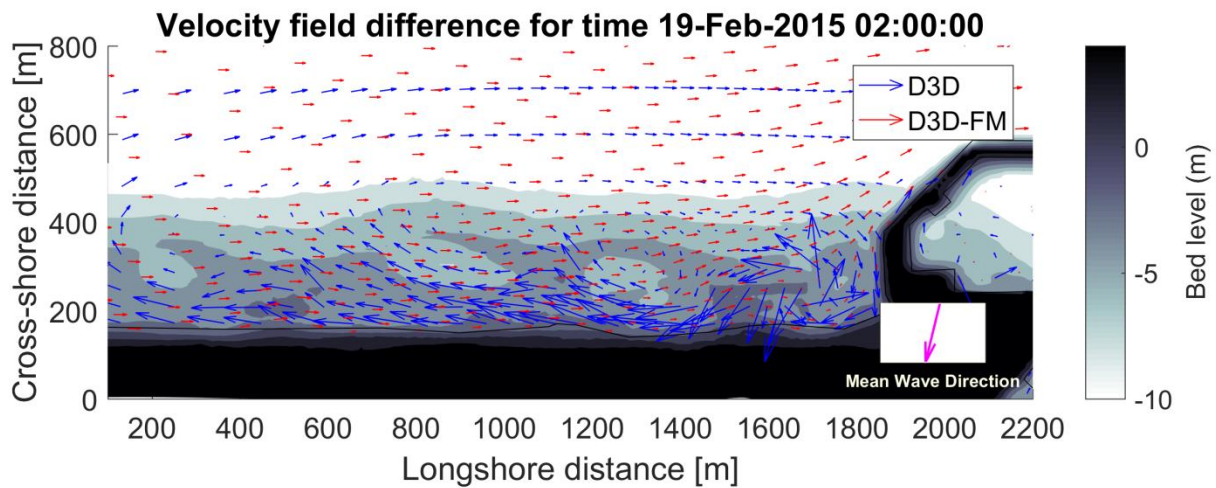
Figure B-84: Velocity field comparison between D3D and D3D-FM. Arrows represent the mean flow velocity in each model. *Top*: Wave driven current direction opposing tide direction. *Bottom*: Wave driven current direction following tide direction.

The differences in velocity magnitude between both models are shown in figures B-85 and B-86. It can be seen that most of the time the differences between models are small, in the order of 5 cm/s, which is in the order of 10% of the maximum velocities. At the offshore buoy both models follow the same trend, while in the nearshore (S2) the changes in velocity magnitude in the D3D model are somewhat larger and more frequent than in the D3D-FM model.
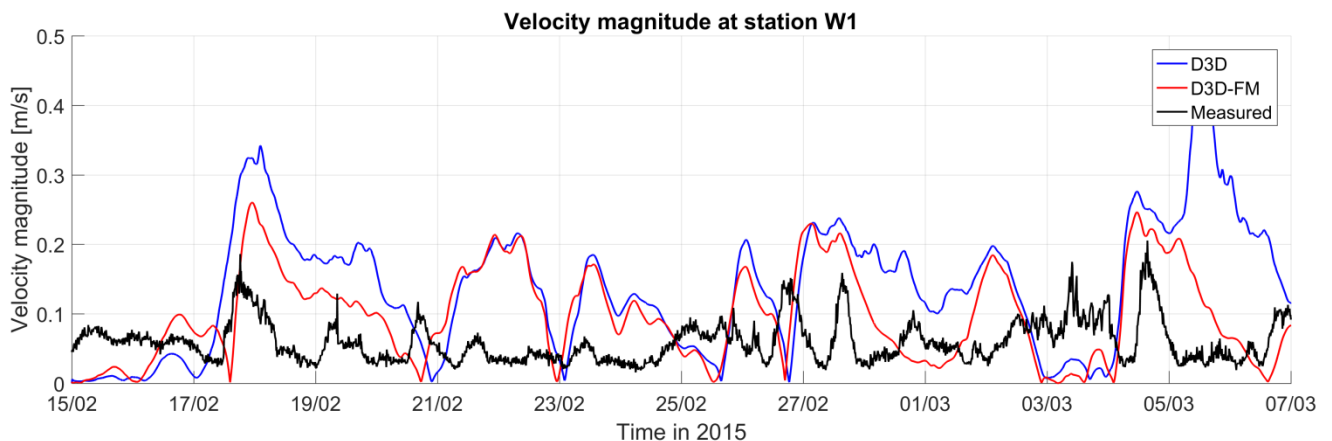
Figure B-85: Measured and modelled flow magnitude
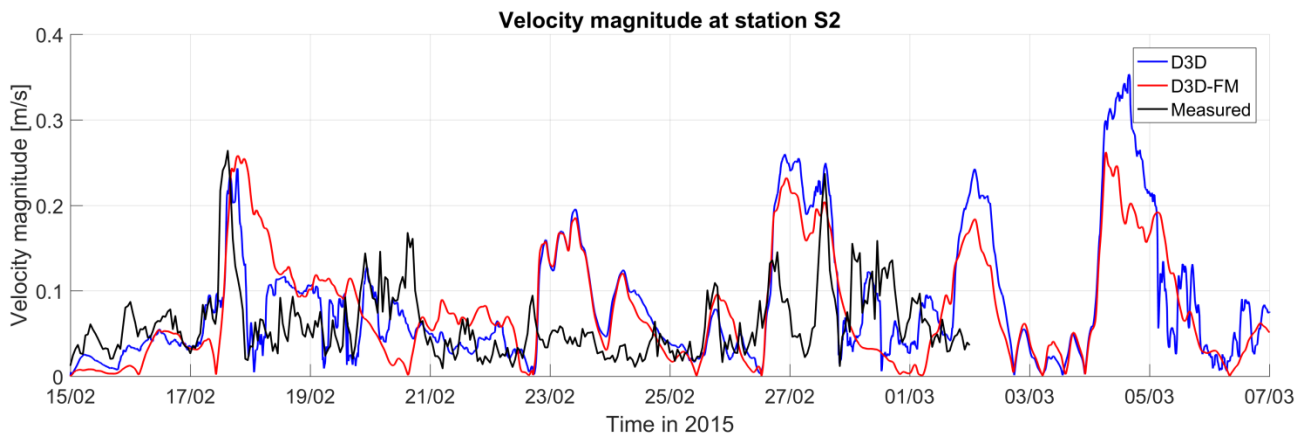
Figure B-86: Measured and modelled flow direction
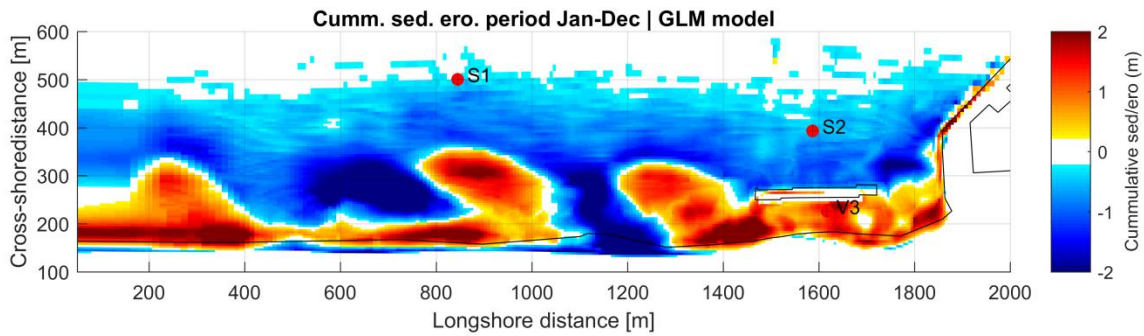
Figure C-87: Modelled cumulative sedimentation/erosion patterns. Delft3D GLM model.
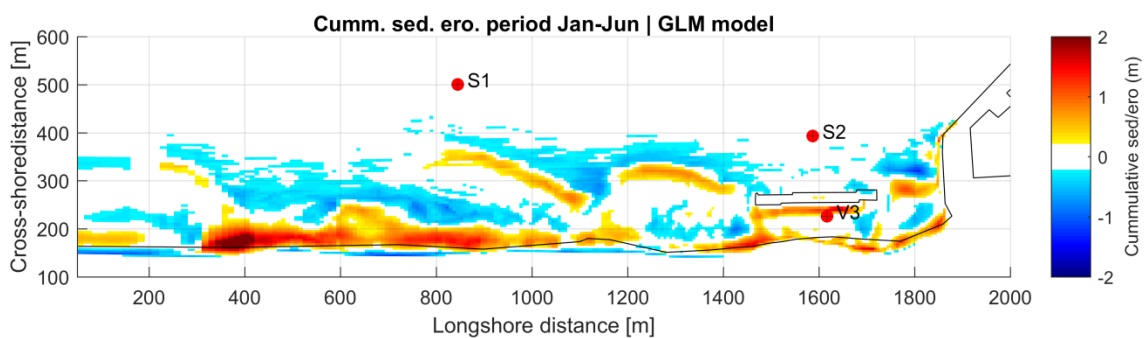
Figure C-88: Modelled cumulative sedimentation/erosion patterns. Delft3D GLM model.
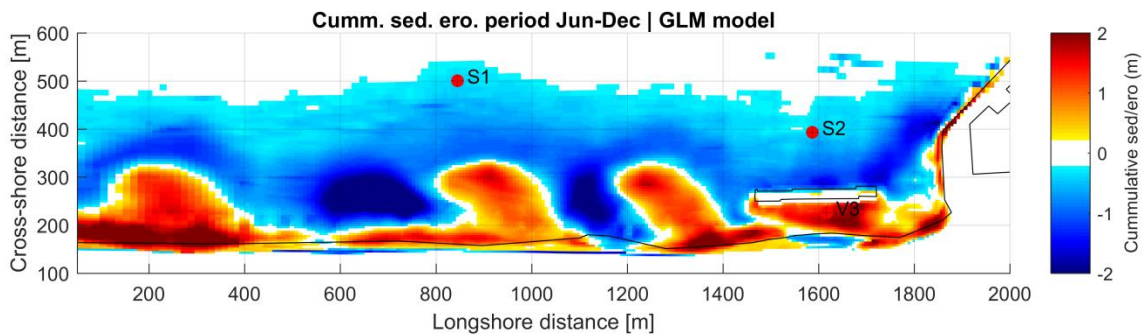
Figure C-89: Modelled cumulative sedimentation/erosion patterns. Delft3D GLM model.
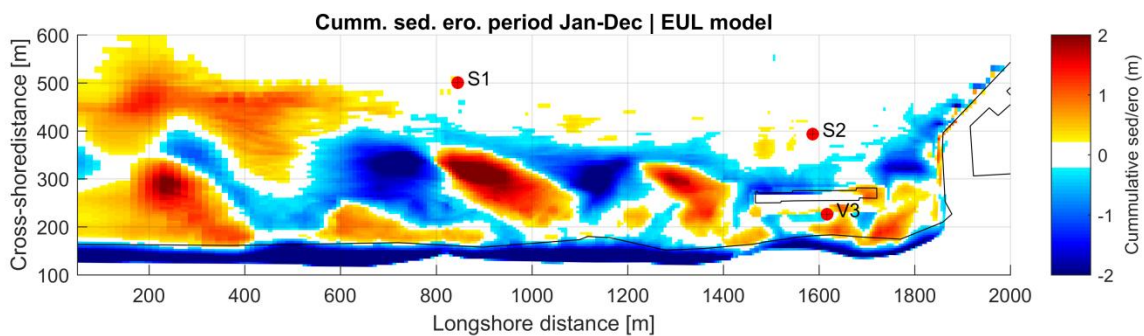
Figure C-90: Modelled cumulative sedimentation/erosion patterns. Delft3D EUL model.
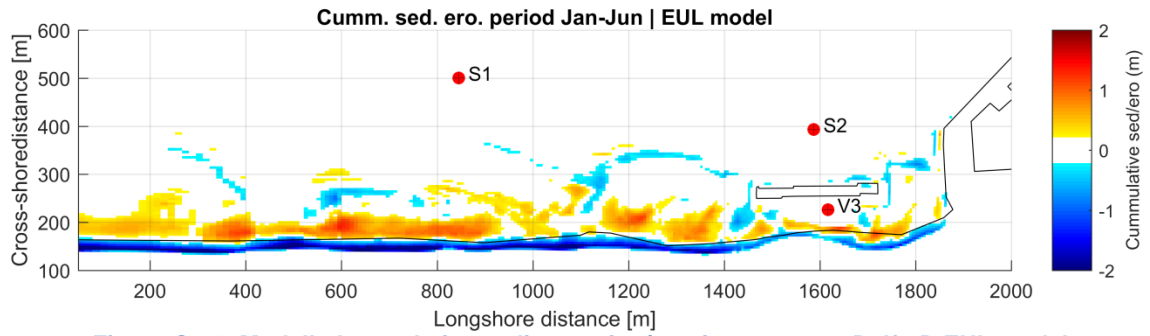
Figure C-91: Modelled cumulative sedimentation/erosion patterns. Delft3D EUL model.
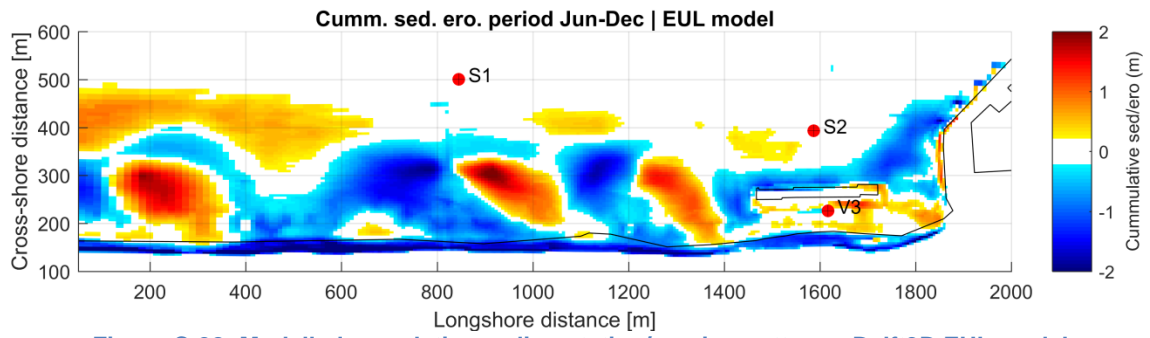
Figure C-92: Modelled cumulative sedimentation/erosion patterns. Delft3D EUL model.

ADDITIONAL MORPHODYNAMIC COUPLED MODEL RESULTS
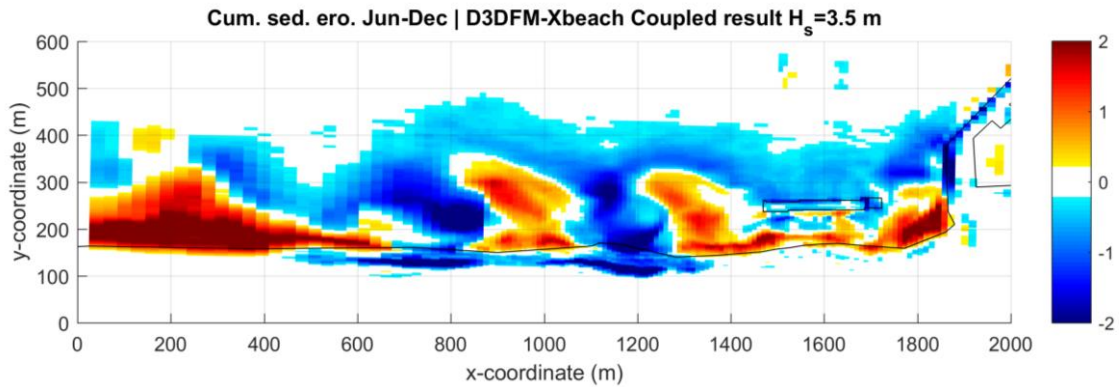
Figure D-93: Modelled cumulative sedimentation/erosion patterns. D3D-FM & XBeach (stationary) coupled model.
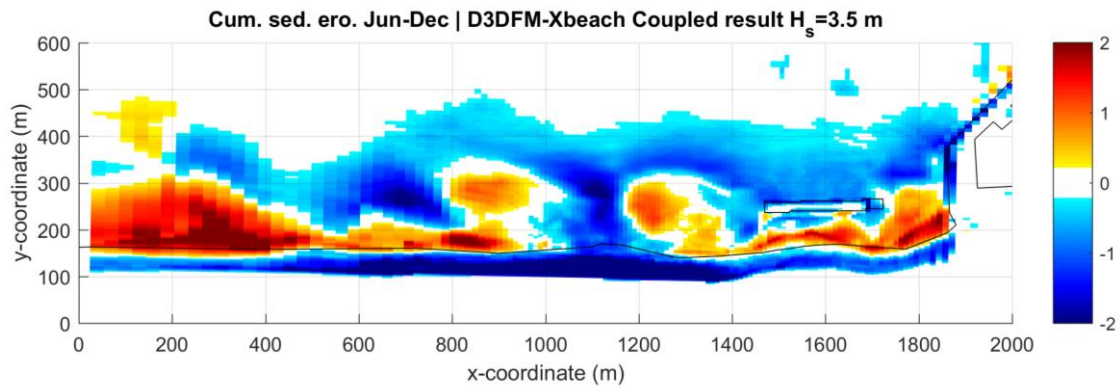
Figure D-94: Modelled cumulative sedimentation/erosion patterns. D3D-FM & XBeach (surf beat) coupled model.
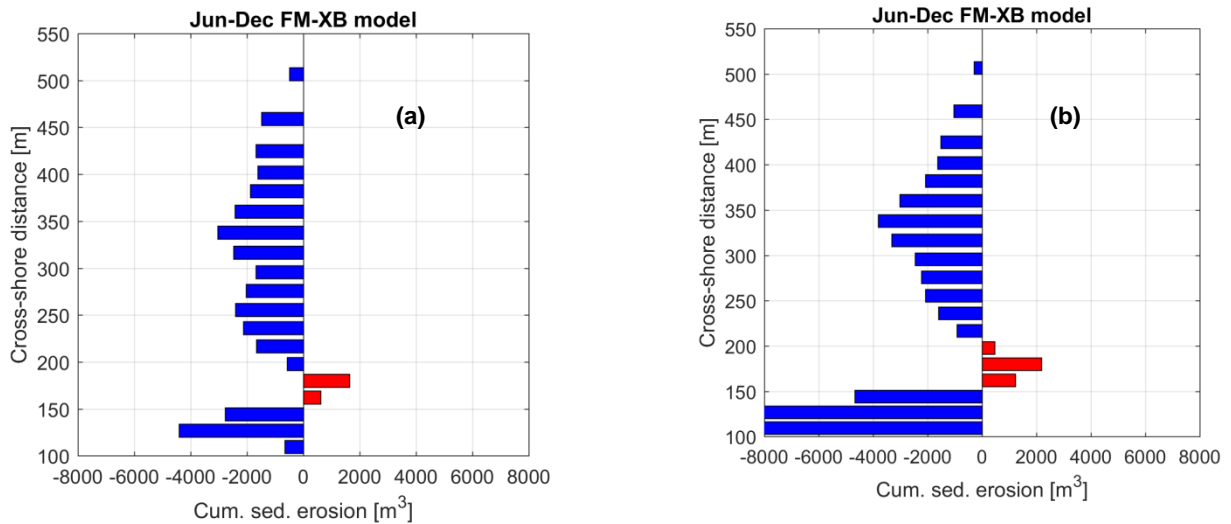
Figure D-95: Cross-shore sedimentation/erosion bars for June-December. D3D-FM & XBeach coupled model.
H_s **threshold = 3.5 m. (a) XBeach in stationary mode; (b) XBeach in surf beat mode**
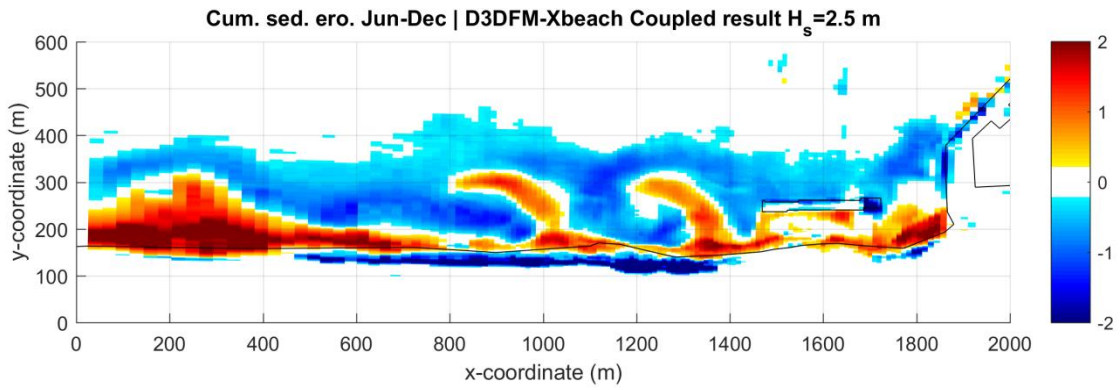
Figure D-96: Modelled cumulative sedimentation/erosion patterns. D3D-FM & XBeach (stationary) coupled model.
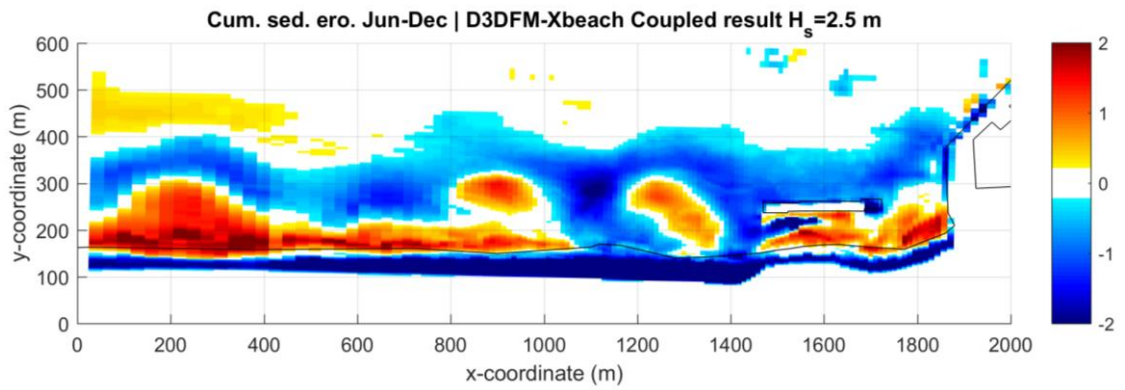
Figure D-97: Modelled cumulative sedimentation/erosion patterns. D3D-FM & XBeach (surf beat) coupled model.
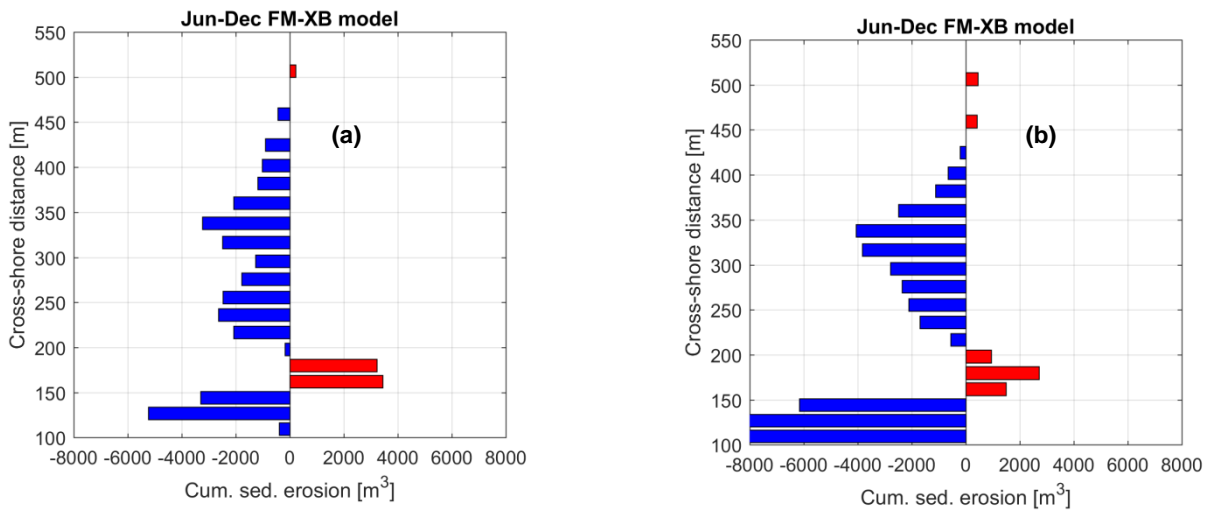
Figure D-98: Cross-shore sedimentation/erosion bars for June-December. D3D-FM & XBeach coupled model.
H_s **threshold = 2.5 m. (a) XBeach in stationary mode; (b) XBeach in surf beat mode**
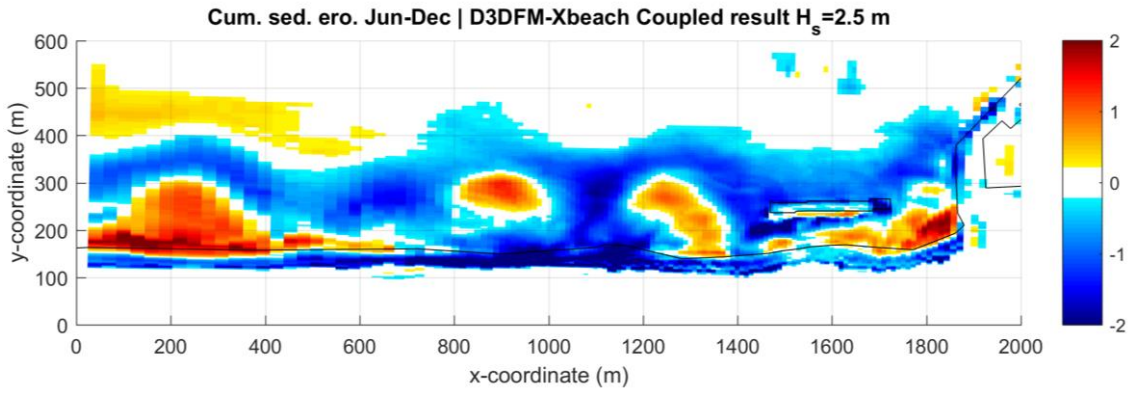
Figure D-99: Modelled cumulative sedimentation/erosion patterns. D3D-FM & XBeach (surf beat) coupled model. Avalanching algorithm turned off
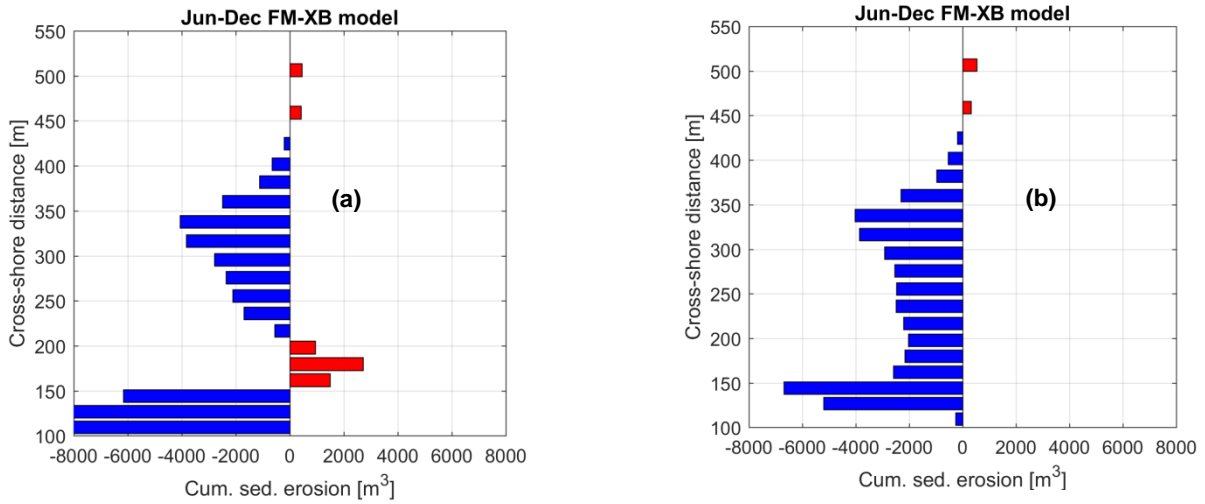
Figure D-100: Cross-shore sedimentation/erosion bars for June-December. D3D-FM & XBeach (surf beat) coupled model. H_s threshold = 2.5 m. (a) Avalanching on; (b) Avalanching off.
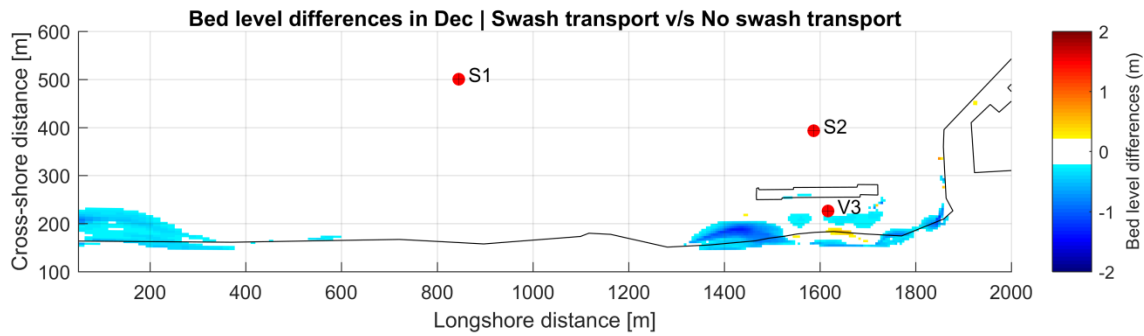
Figure E-101: Bed level difference between model 01 and no-swash (base case) D3D simulation at the end of the stormy season. Blue indicates lower bed level, red indicates higher bed level.
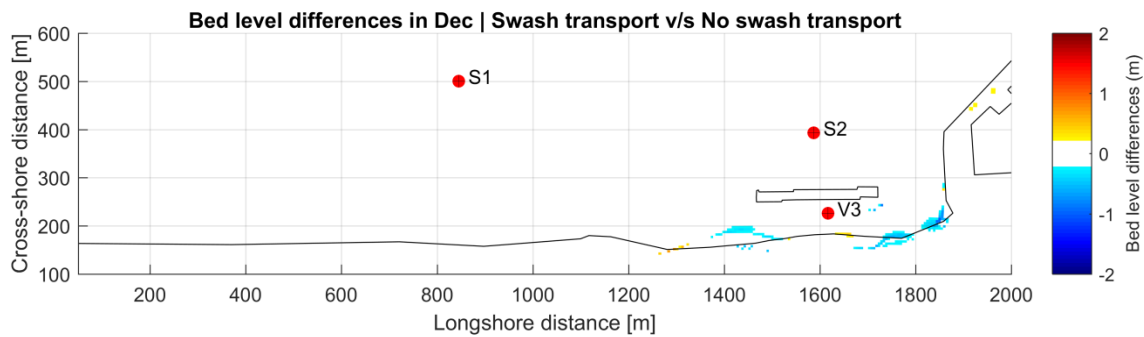
Figure E-102: Bed level difference between model 02 and no-swash (base case) D3D simulation at the end of the stormy season. Blue indicates lower bed level, red indicates higher bed level.
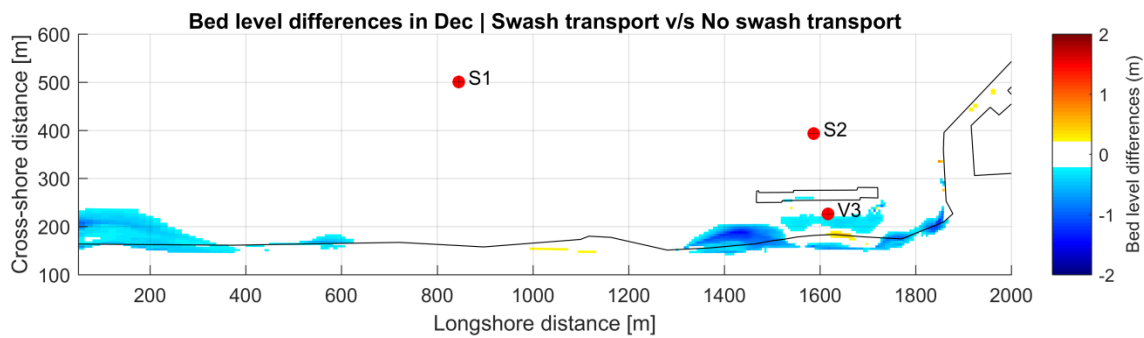
Figure E-103: Bed level difference between model 03 and no-swash (base case) D3D simulation at the end of the stormy season. Blue indicates lower bed level, red indicates higher bed level.
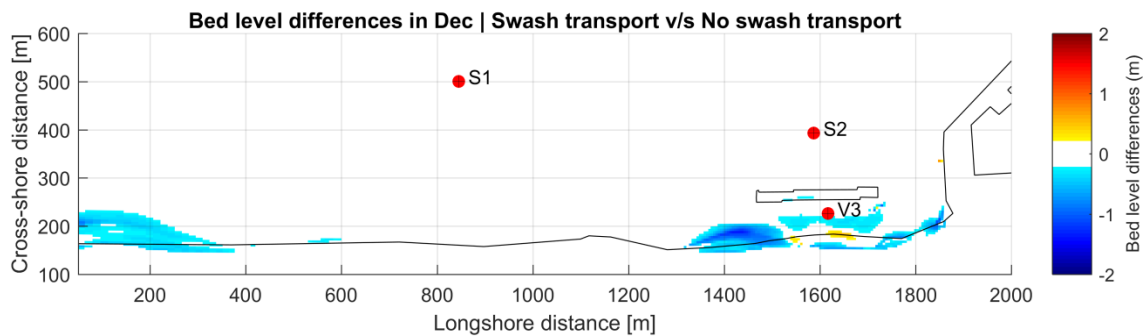
Figure E-104: Bed level difference between model 04 and no-swash (base case) D3D simulation at the end of the stormy season. Blue indicates lower bed level, red indicates higher bed level.
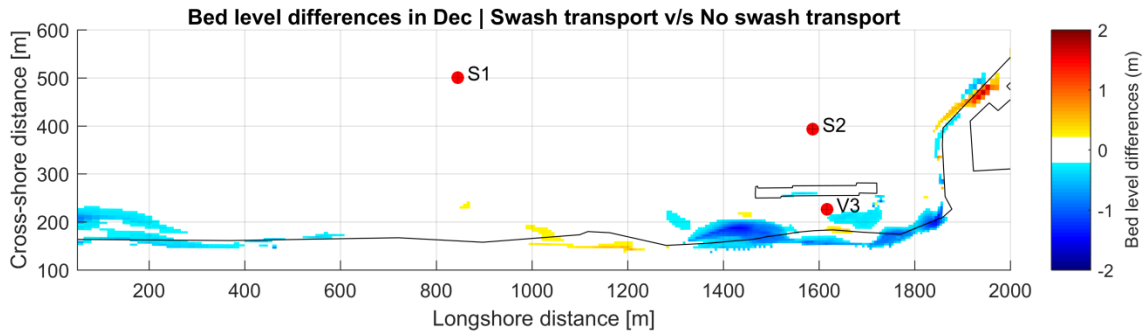
Figure E-105: Bed level difference between model 05 and no-swash (base case) D3D simulation at the end of the stormy season. Blue indicates lower bed level, red indicates higher bed level.
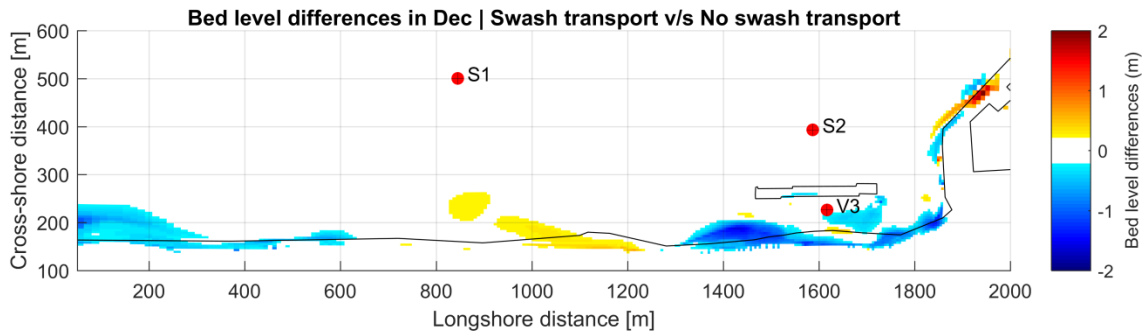
Figure E-106: Bed level difference between model 06 and no-swash (base case) D3D simulation at the end of the stormy season. Blue indicates lower bed level, red indicates higher bed level.
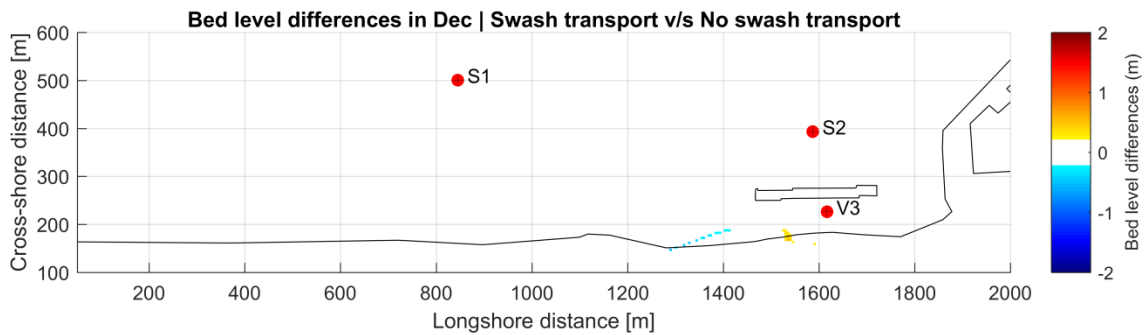
Figure E-107: Bed level difference between model 07 and no-swash (base case) D3D simulation at the end of the stormy season. Blue indicates lower bed level, red indicates higher bed level.
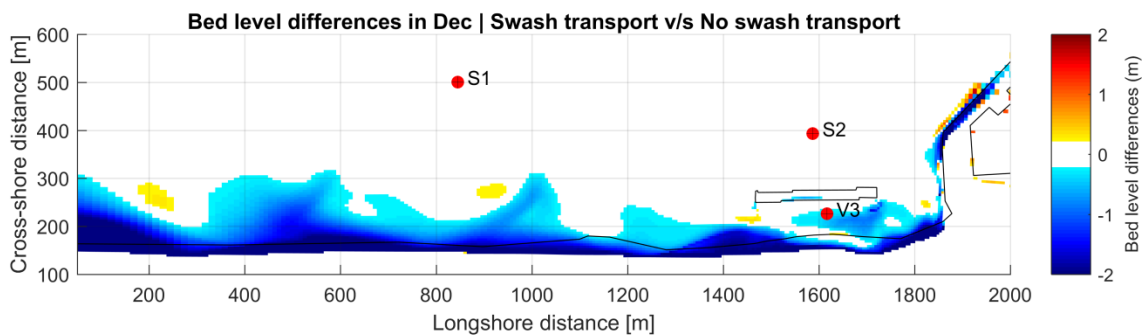
Figure E-108: Bed level difference between model 08 and no-swash (base case) D3D simulation at the end of the stormy season. Blue indicates lower bed level, red indicates higher bed level.
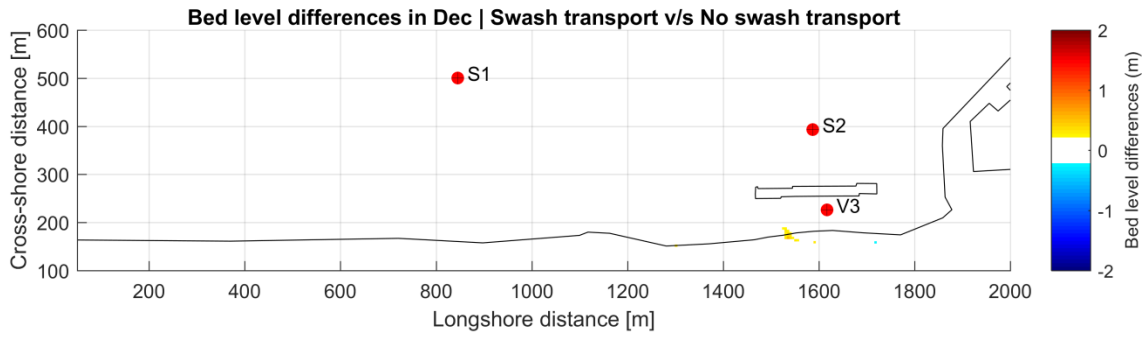
Figure E-109: Bed level difference between model 09 and no-swash (base case) D3D simulation at the end of the stormy season. Blue indicates lower bed level, red indicates higher bed level.
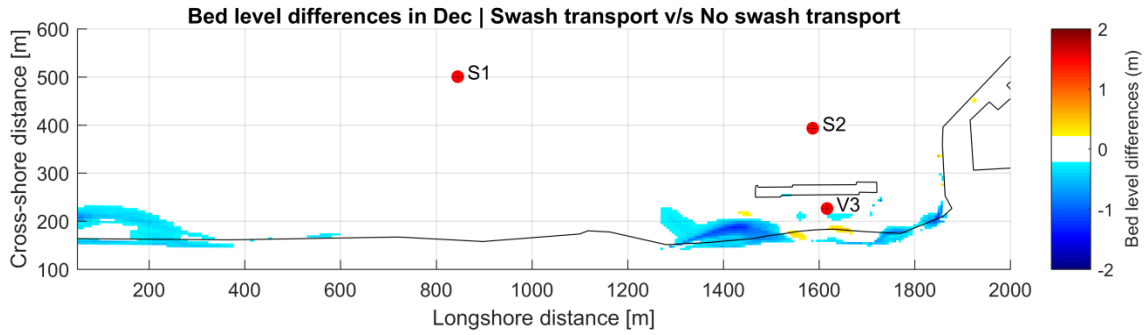
Figure E-110: Bed level difference between model 10 and no-swash (base case) D3D simulation at the end of the stormy season. Blue indicates lower bed level, red indicates higher bed level.
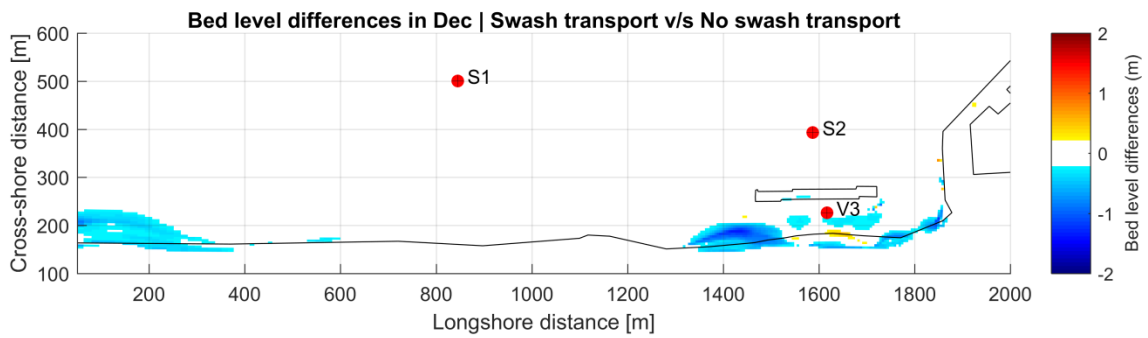
Figure E-111: Bed level difference between model 11 and no-swash (base case) D3D simulation at the end of the stormy season. Blue indicates lower bed level, red indicates higher bed level.
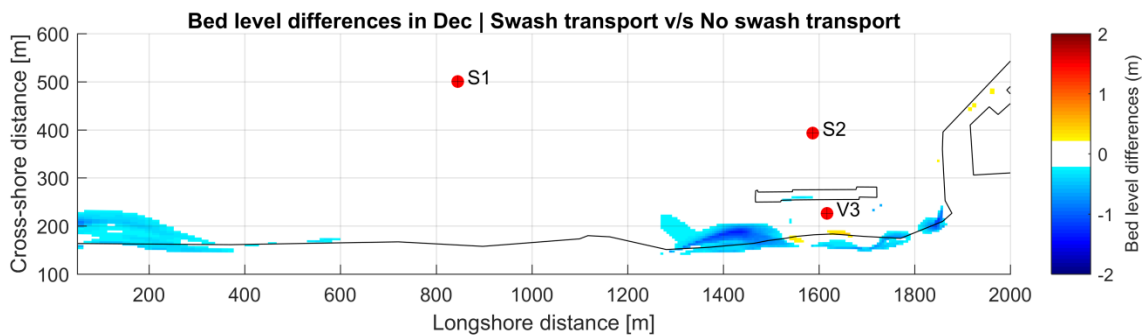
Figure E-112: Bed level difference between model 12 and no-swash (base case) D3D simulation at the end of the stormy season. Blue indicates lower bed level, red indicates higher bed level.
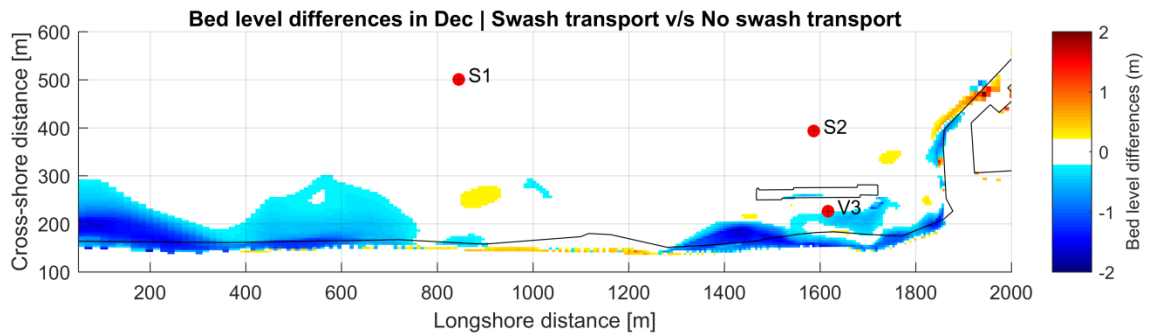
Figure E-113: Bed level difference between model 13 and no-swash (base case) D3D simulation at the end of the stormy season. Blue indicates lower bed level, red indicates higher bed level.
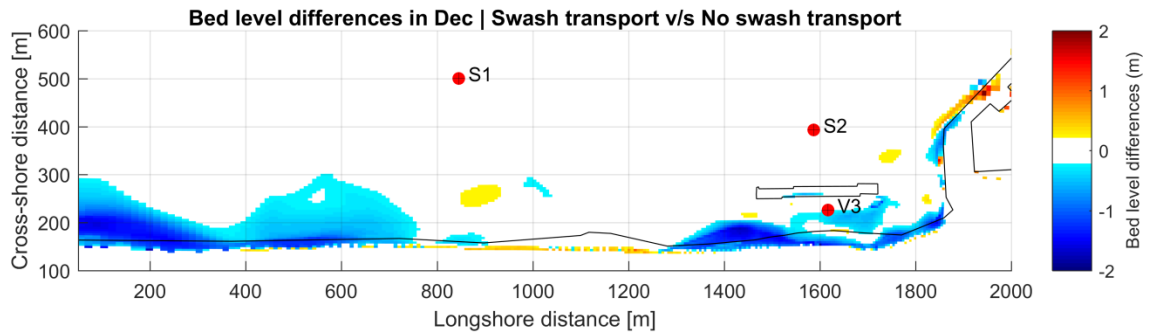
Figure E-114: Bed level difference between model 14 and no-swash (base case) D3D simulation at the end of the stormy season. Blue indicates lower bed level, red indicates higher bed level.
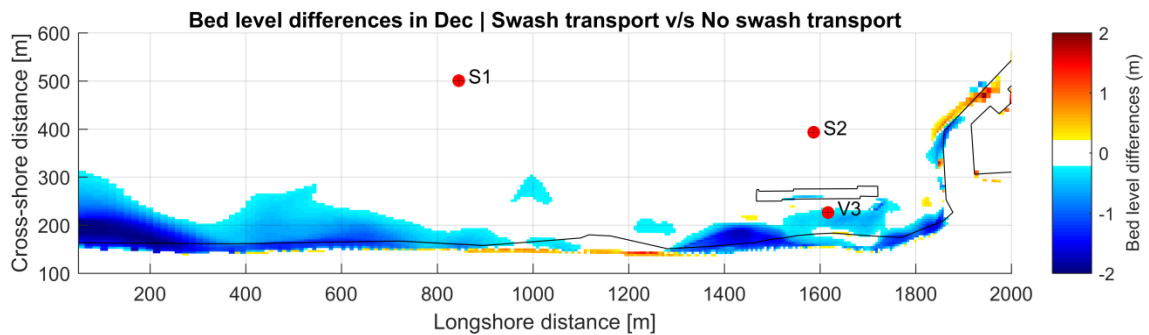
Figure E-115: Bed level difference between model 15 and no-swash (base case) D3D simulation at the end of the stormy season. Blue indicates lower bed level, red indicates higher bed level.
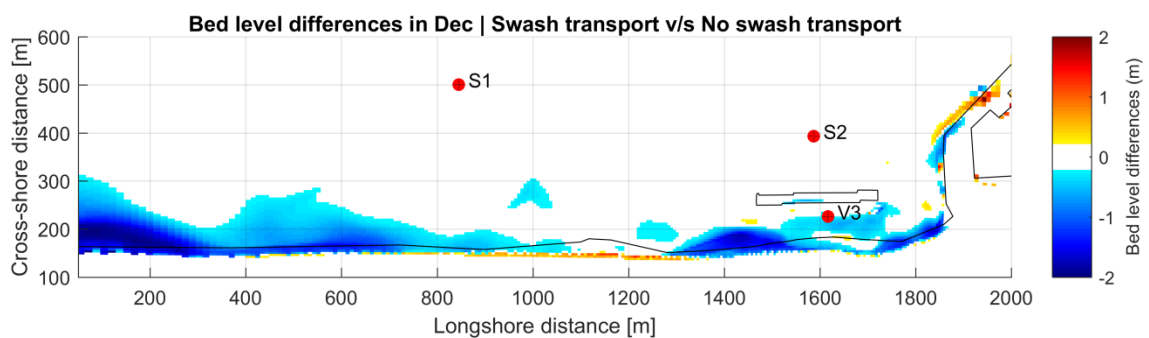
Figure E-116: Bed level difference between model 16 and no-swash (base case) D3D simulation at the end of the stormy season. Blue indicates lower bed level, red indicates higher bed level.
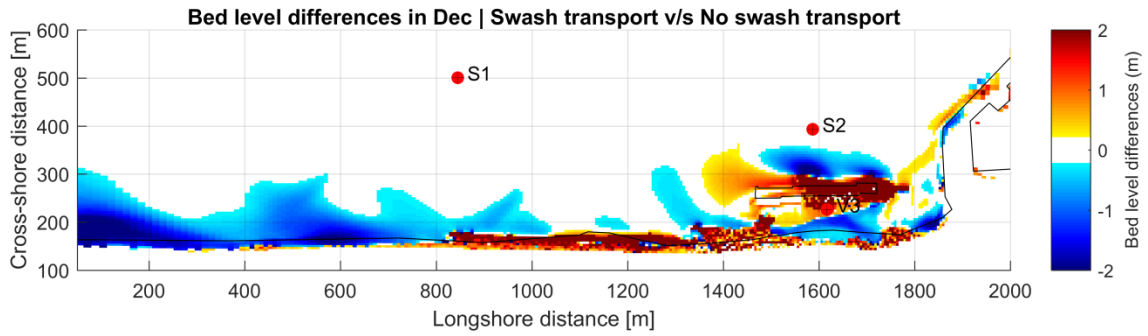
Figure E-117: Bed level difference between model 17 and no-swash (base case) D3D simulation at the end of the stormy season. Blue indicates lower bed level, red indicates higher bed level.
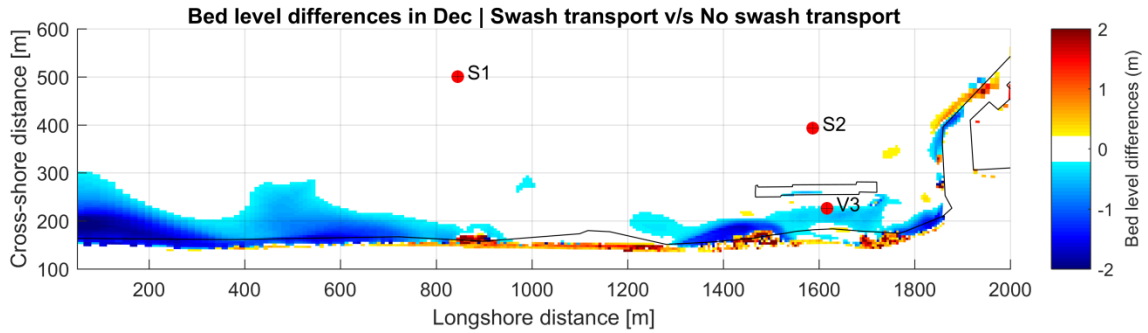
Figure E-118: Bed level difference between model 18 and no-swash (base case) D3D simulation at the end of the stormy season. Blue indicates lower bed level, red indicates higher bed level.
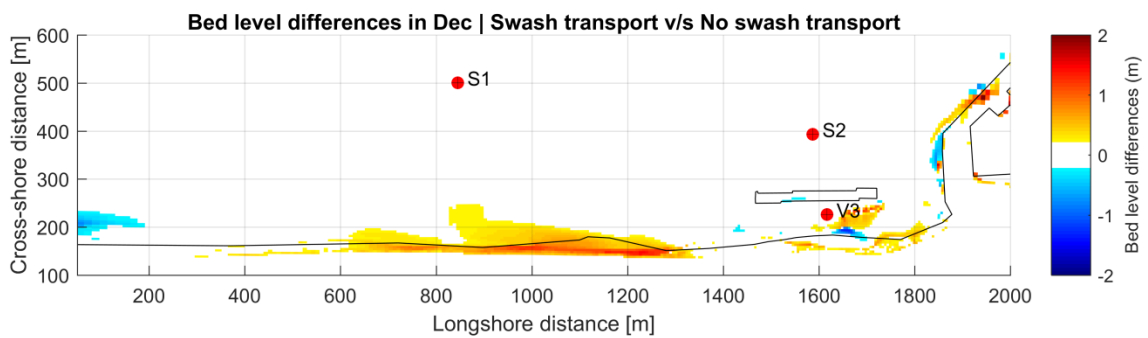
Figure E-119: Bed level difference between model 19 and no-swash (base case) D3D simulation at the end of the stormy season. Blue indicates lower bed level, red indicates higher bed level.
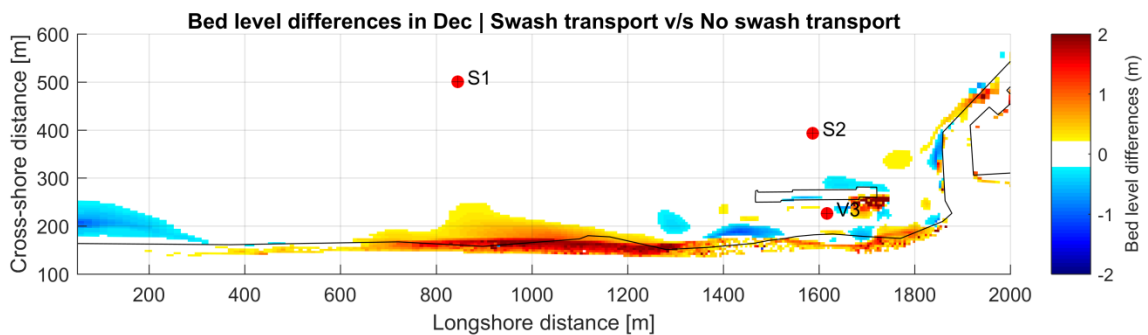
Figure E-120: Bed level difference between model 20 and no-swash (base case) D3D simulation at the end of the stormy season. Blue indicates lower bed level, red indicates higher bed level.

88
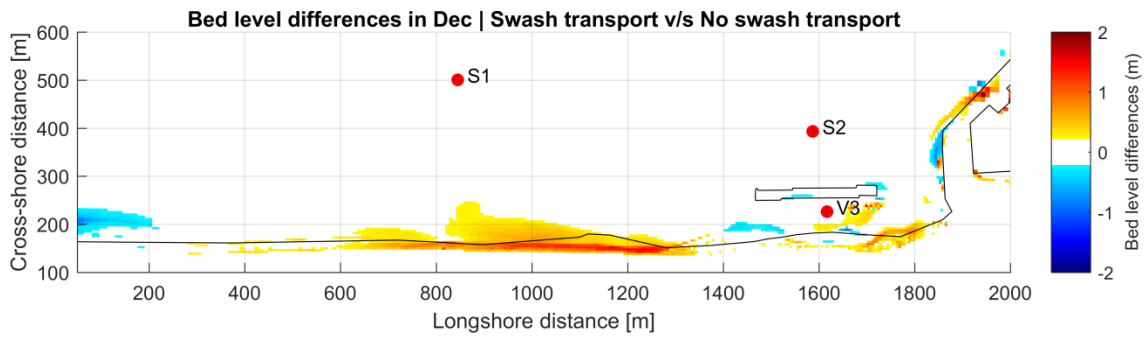
Figure E-121: Bed level difference between model 21 and no-swash (base case) D3D simulation at the end of the stormy season. Blue indicates lower bed level, red indicates higher bed level.
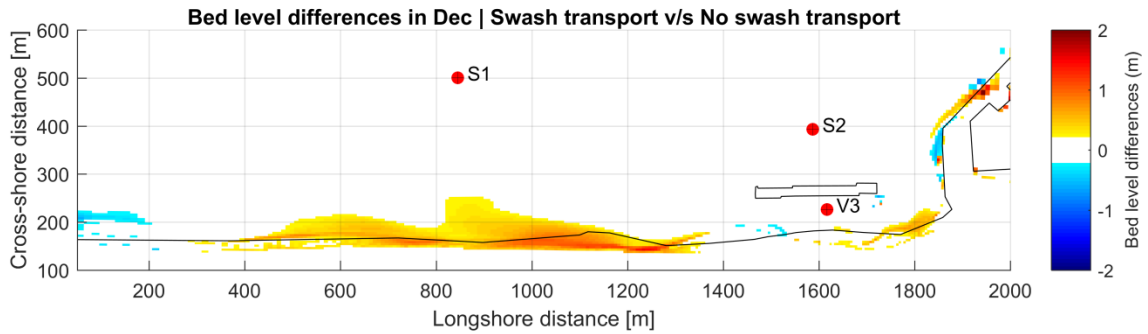
Figure E-122: Bed level difference between model 22 and no-swash (base case) D3D simulation at the end of the stormy season. Blue indicates lower bed level, red indicates higher bed level.
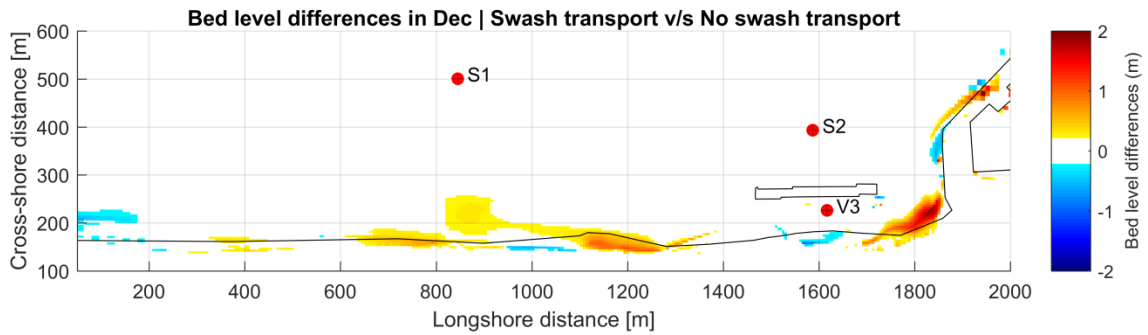
Figure E-123: Bed level difference between model 23 and no-swash (base case) D3D simulation at the end of the stormy season. Blue indicates lower bed level, red indicates higher bed level.
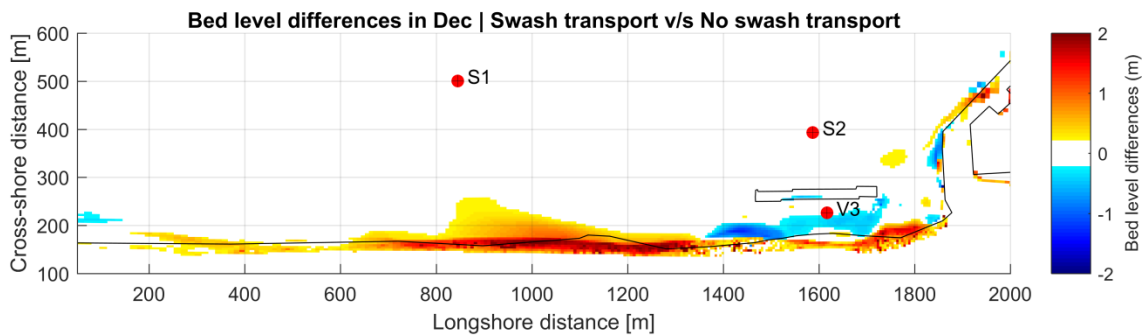
Figure E-124: Bed level difference between model 24 and no-swash (base case) D3D simulation at the end of the stormy season. Blue indicates lower bed level, red indicates higher bed level.
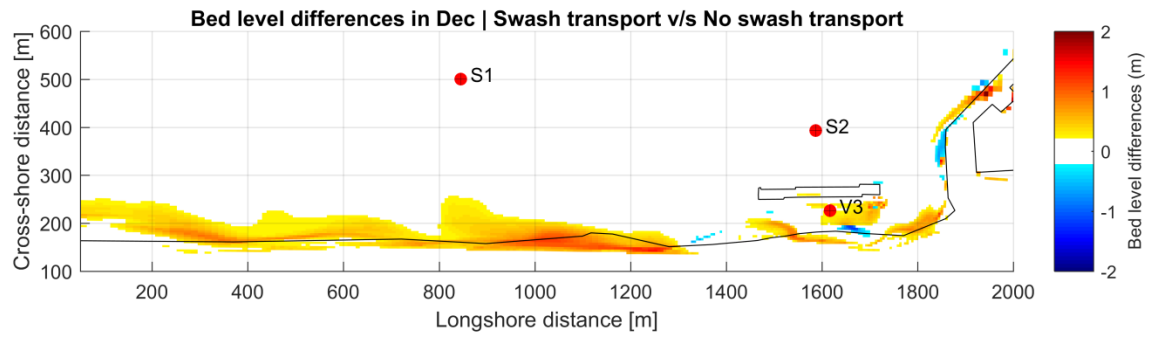
Figure E-125: Bed level difference between model 25 and no-swash (base case) D3D simulation at the end of the stormy season. Blue indicates lower bed level, red indicates higher bed level.

ALONGSHORE UNIFORM COAST MORPHOLOGICAL TEST CASE

In this appendix a simple 2D alongshore uniform coast model was set-up in both Delft3D (version 6.02.08.000000) and Delft3D-FM (version 1.1.192.50908), and a 1 day simulation with a morphological acceleration factor of 3.0 was ran first with a GLM mass transport and later with an Eulerian one. Lateral Neumann boundary conditions were applied on the sides, and a Jonswap spectrum was applied at the offshore boundary (being the only external forcing). The initial bathymetry and model grid are shown in Figure F-126, and the full model settings are shown in tables F-16 and F-17 (settings not shown are understood to be default settings).
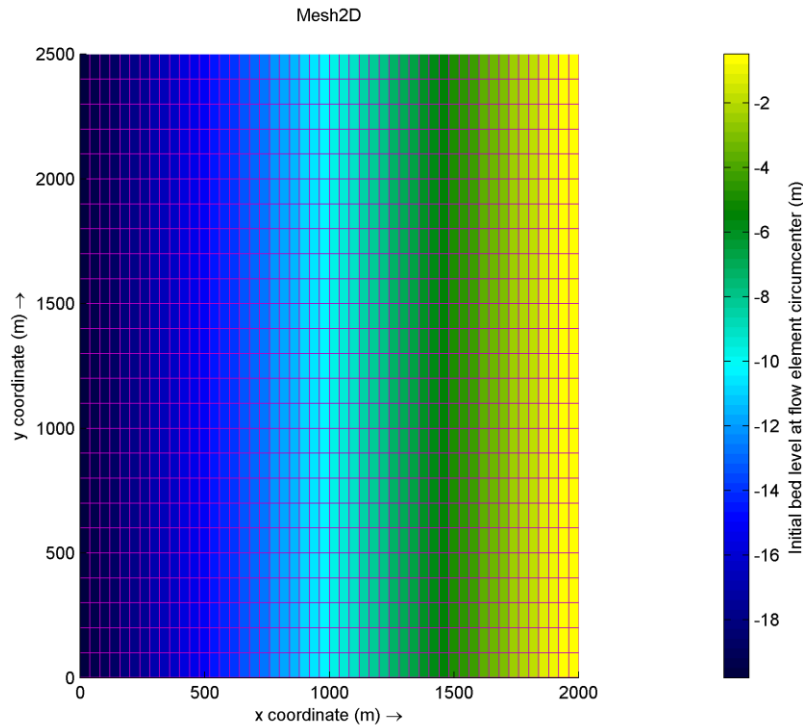
Figure F-126: Initial bathymetry and model grid for 2D alongshore uniform mass transport test case.

Table F-16: D3D (& D3D-FM) Flow parameters

Parameter	Value	Parameter	Value	Parameter	Value
Layertype	1	UnifFrictCoef	65	Sedimentmodelnr	4
BedlevType	1	Rhomean	1025 kg/m^3	RhoSol	2650 kg/m^3
AngLat	37.77	Chezy coeff.	65 m$^{0.5}$/s	DtUser	6 s
Conveyance2D	-1	SedDia D$_{50}$	5e-4 m	DtMax	6 s
Turbulencemodel	1	Wavemodelnr	3	DtInit	1 s
Eulerisoglm	True(EUL), False (GLM	Wind velocity	0 m/s	MorStt	60 min
Cref	1600 kg/m^3	Gammax	0.5	MorFac	3
MorUpd	True	SusW	0.05	BedW	0.05
HMaxTH	1.5	camax	0.05	updinf	True
CDryB	1600 kg/m^3	IniSedThick	10 m		

Parameter	Value	Parameter	Value	Parameter	Value
DirConvention	Nautical	WhiteCapping	Komen	EndDir	0
WaterDensity	1025	Quadruplets	True	FreqMin	0.05
GenModePhys	3	Refraction	True	FreqMax	1.0
Breaking	true	FreqShift	True	NFreq	24
BreakAlpha	1.0	WaveForces	radiation stresses <2013	spectrumspec	parametric
BreakGamma	0.73	UseHotFile	true	spshapetype	jonswap
Triads	false	FlowBedLevel	0	periodtype	peak
Diffraction	False	FlowWaterLevel	0	dirspreadtype	power
TriadsBeta	2.2	FlowVelocity	0	peakenhancefac	3.3
BedFriction	jonswap	FlowWind	0	gaussspread	9.99e-03
BedFricCoef	0.067	MaxIter	15	waveheight	2.81
WindGrowth	True	StartDir	0	period	7.0

The relative morphological changes between the different mass transport simulations (GLM & EUL) were estimated for both software, and are depicted in Figure F-127. What is seen in these figures is that for the exact same settings, the differences between Lagrangian and Eulerian mass transport is stronger in D3D depicting larger bed level differences at the end of the simulation, in the order of $\pm 0.05\ m$, whereas in D3D-FM the changes are ~5 times smaller in the order of ± 0.01 m. To confirm this, the thickness of the sediment layer at the end of each simulation was plotted (shown in Figure F-128), which is similar to analyze the cumulative sedimentation/erosion yet avoiding any post-processing manipulation or error, as this variable is a direct output in both software. What can be recognized is that the GLM results have a similar behaviour in both suites, yet the Eulerian model shows milder changes in D3D-FM. The pattern of nearshore accretion / offshore erosion seen in the GLM D3D simulation is inverted when changing to the EUL model, however this inversion is not fully replicated in D3D-FM, where less offshore erosion is seen indeed (probably due to an offshore mass transport and further sedimentation), yet it is not enough to invert the pattern.
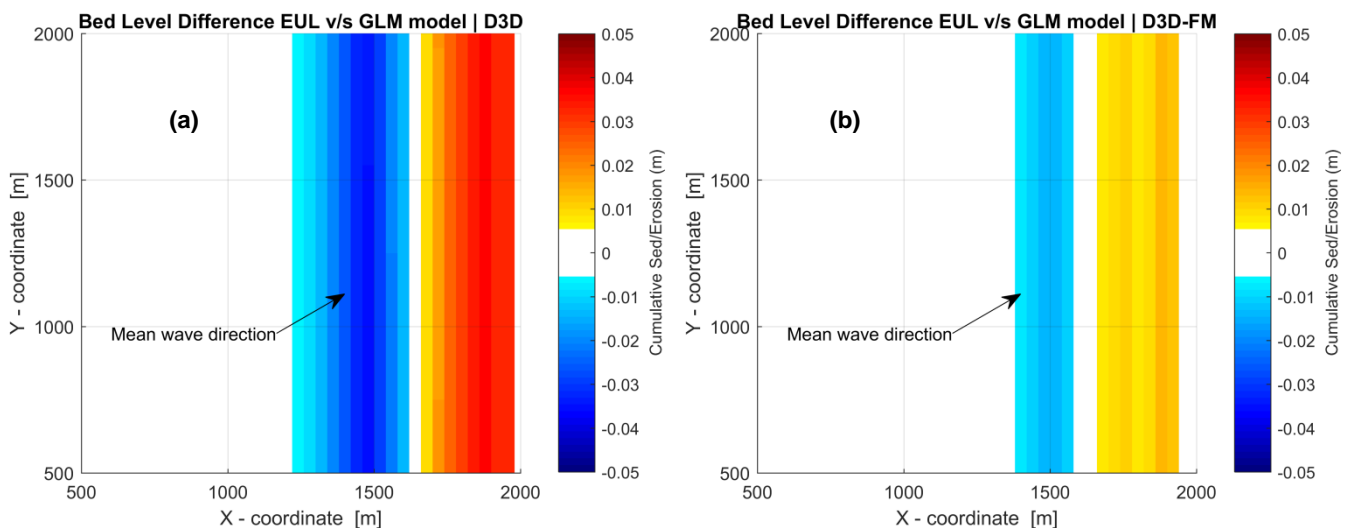
Figure F-127: Bed level difference between Eulerian and GLM simulations after 3 (morphological) days with a 2.8 m offshore significant wave height forcing. (a) Delft3D results; (b) Delft3D-FM results.
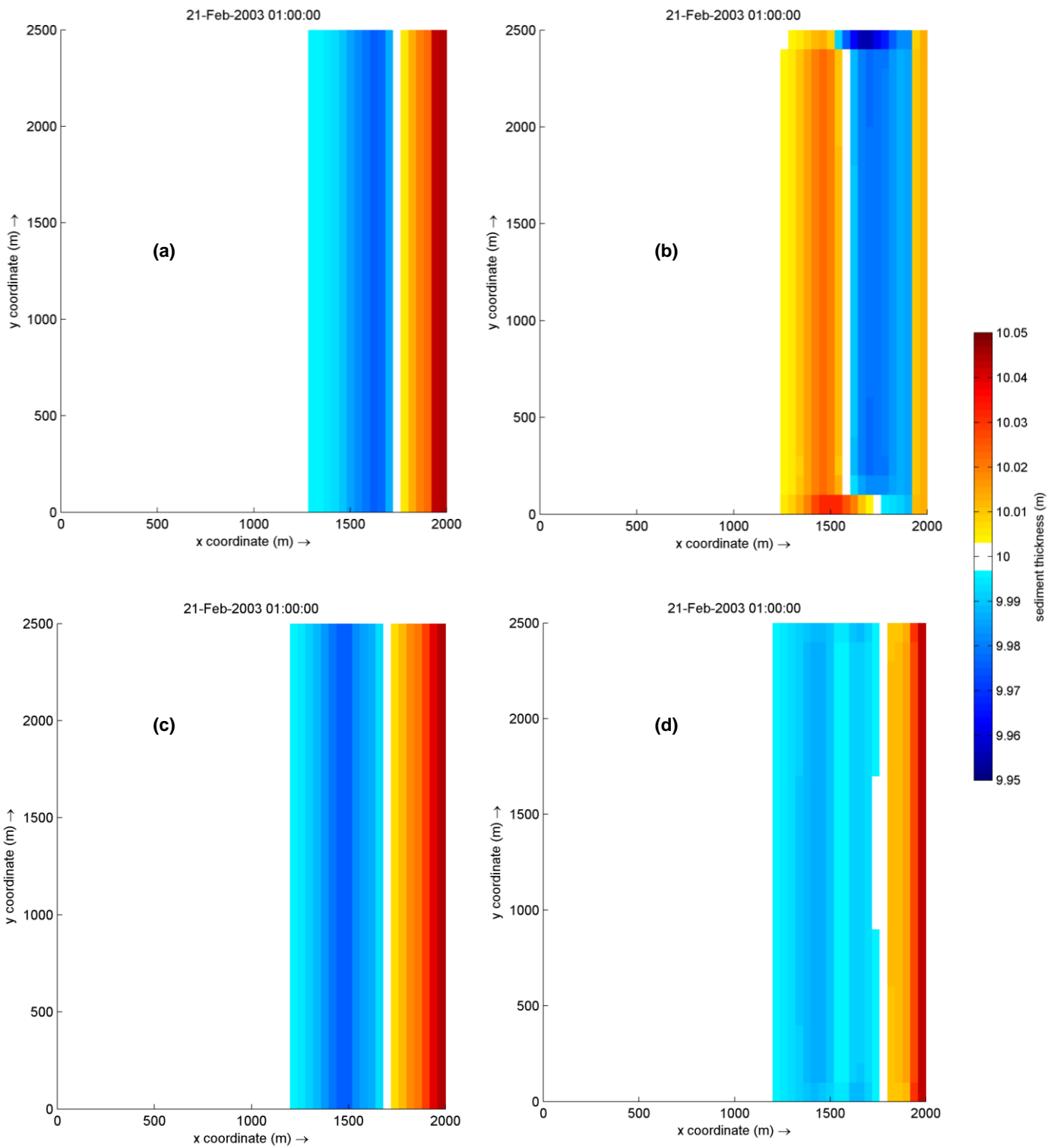
Figure F-128: Sediment thickness after 3 (morphological) days with a 2.8 m offshore significant wave height forcing, starting from a uniform thickness of 10 m. (a) Delft3D GLM results; (b) Delft3D EUL results; (c) Delft3D-FM GLM results; (d) Delft3D-FM EUL results.

93

AUGUST-SEPTEMBER 2016 STORM CALIBRATION RESULTS
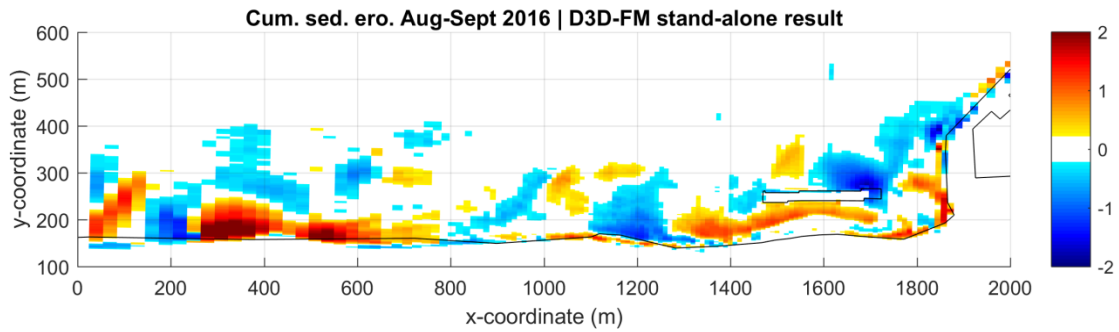
Figure G-129: Modelled cumulative sedimentation/erosion patterns. D3D-FM stand-alone model
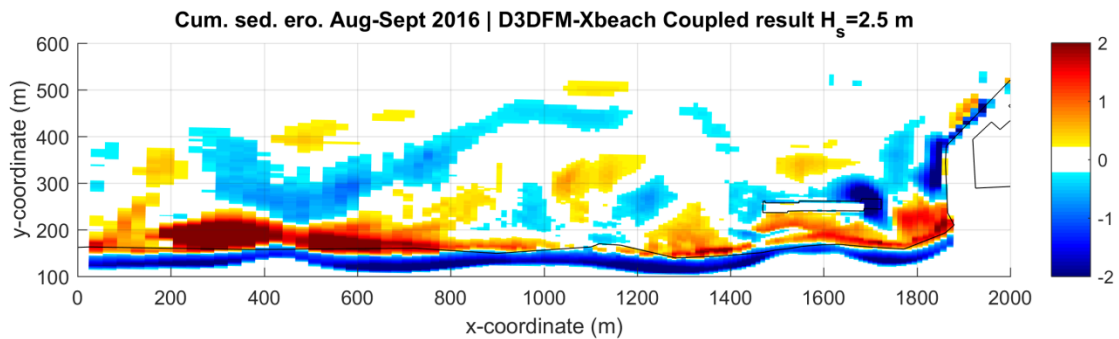
Figure G-130: Modelled cumulative sedimentation/erosion patterns. D3D-FM & XBeach coupled model. XBeach with default settings
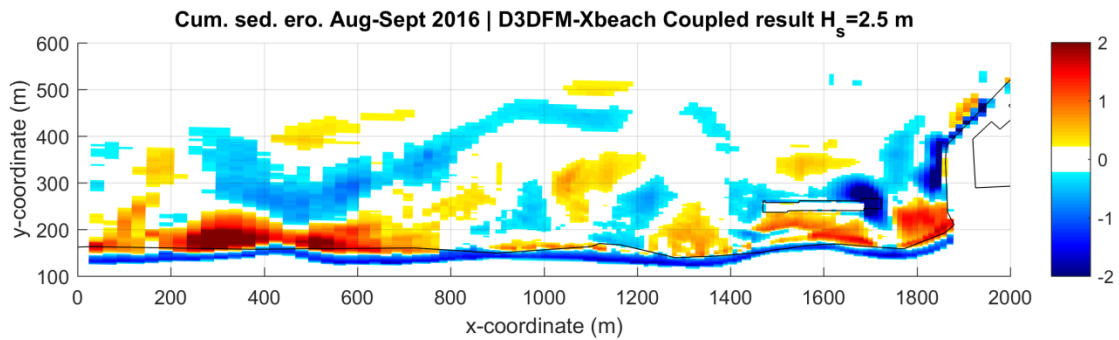
Figure G-131: Modelled cumulative sedimentation/erosion patterns. D3D-FM & XBeach coupled model. XBeach *avalanching* = off
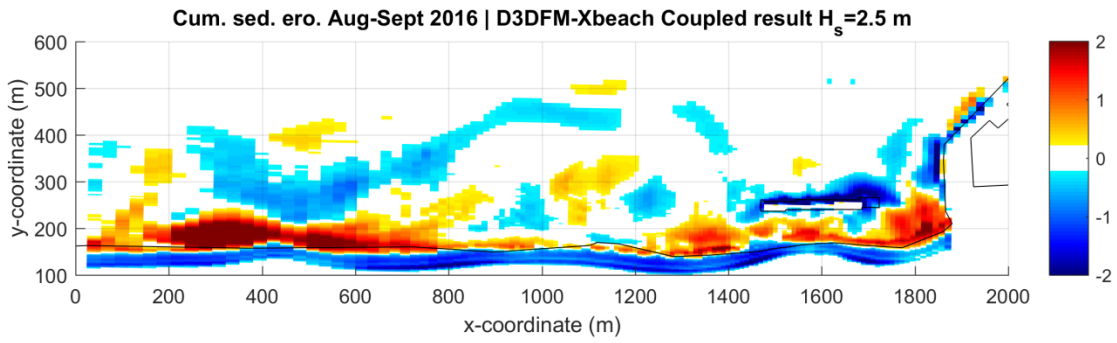
Figure G-132: Modelled cumulative sedimentation/erosion patterns. D3D-FM & XBeach coupled model. XBeach *bermslope* = 0.1
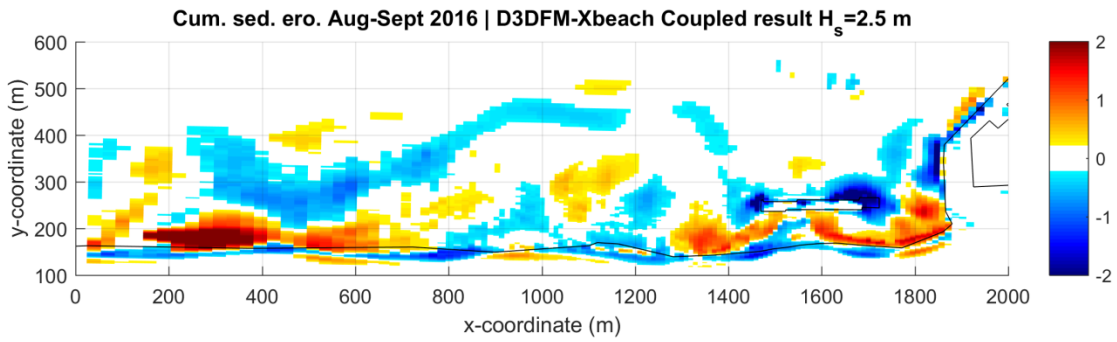
Figure G-133: Modelled cumulative sedimentation/erosion patterns. D3D-FM & XBeach coupled model. XBeach *bermslope* = 0.3
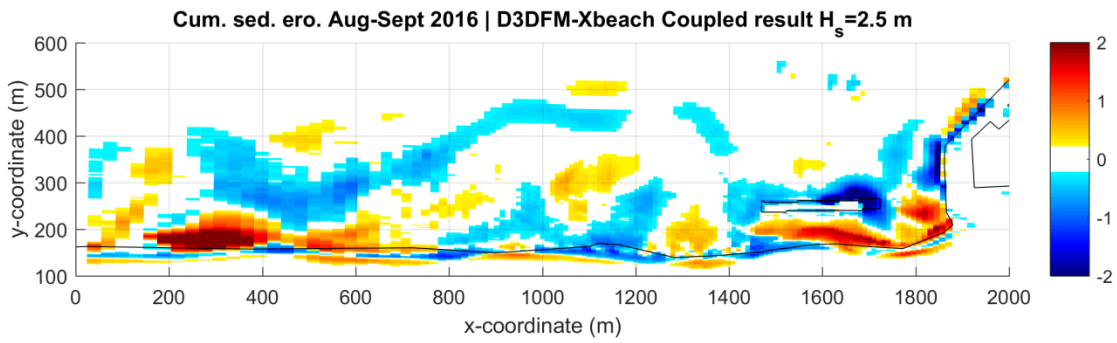
Figure G-134: Modelled cumulative sedimentation/erosion patterns. D3D-FM & XBeach coupled model. XBeach *bermslope* = 0.5

MOMENTARY COASTLINE METHOD ADAPTATION

In this chapter the results of an adaptation from the momentary coastline method (van Koningsveld & Mulder, 2004) are presented. The momentary coastline or *MKL* approach is a way to objectively define the coastline position as a function of the volume of sand (per unit length) in the near shore zone. The volume (or area) at any cross-shore profile is defined between two boundaries: The landward boundary located at the dune foot, and the seaward boundary located at the intersection of the lower plane and the land surface, as depicted in Figure H-135.

The advantages of defining the coastline with this method are that it is objective, as the swash motions end up being averaged, and; when defining the coastline from model outputs the uncertainty related to the poor performance of process based models in the shallow water parts is reduced, and a more stable coastline position is obtained when compared to for instance the 0 m contour, which can have large (unreliable) variations. The disadvantages of applying the MKL approach in the present project are that this method was developed for the coasts of the Netherlands, and its applicability to the South Korean coast is not direct and has not been validated. First of all, the definition of the MKL required the location of the *Dune foot*, whereas at Anmok beach there are no dunes. Also the method requires the height between Dune foot and mean low water level, and due to the large tidal variations in the Dutch coast this height is in the order of $O(3\,m)$ (van Zanten, 2016), whereas at Anmok beach there is a micro-tidal regime, hence the mean low water level is in the order of $O(-0.2\,m)$ and the distance to the (non-existent) dune foot is believed to be much lower.

Bearing these limitations in mind, the applicability of this methodology to the east coast of South Korea is questionable, and a thorough analysis on the extrapolation and validation of this methodology outside the Dutch coast is recommended, however it falls outside the scope of work and main objective of this thesis. Thus for simplicity an adaptation of the MKL method for Anmok beach is attempted by testing two different scenarios: Defining the value of H as 1.0 and 2.0 meters respectively. This means locating the equivalent "Dune foot" 1 or 2 m above the mean low water level. Also for simplicity and based on the micro-tidal regime, the mean low water level is just taken as mean sea level for these analyses.

H = Height between dune foot and mean low water [m]
A = Momentary Coastline Zone [m^2]
B = A / 2H = Momentary Coastline position [m]
C = Distance dune foot to reference [m]
X$_{MCL}$ = B + C = Momentary Coastline position + Distance dune foot to reference [m]
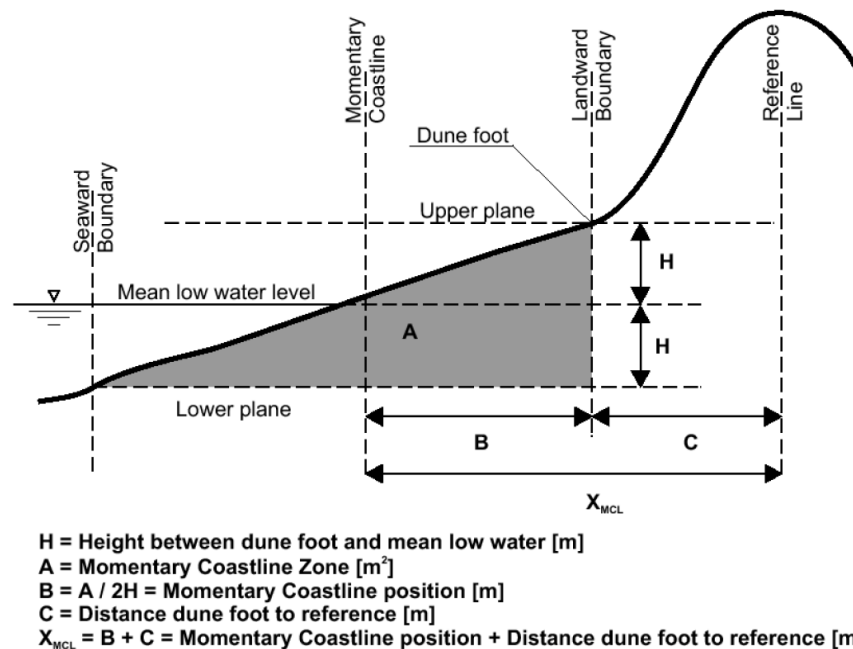
Figure H-135: Calculation of momentary coastline (MKL). Figure from (Hillen et al., 1991) as cited in (van Koningsveld & Mulder, 2004)

Following the aforementioned procedure, the adapted or modified MKL was estimated at every cross-shore profile for both values of H respectively. The MKL was obtained from the measurements at the beginning and end of the stormy season, as well as from the uncoupled D3D-FM model and coupled D3D-FM and XBeach with a significant wave height threshold of $H_{S\ threshold} = 2.5\ m$. Results are depicted in figures H-136 and H-137. What can be identified is that when choosing a lower water-to-dune height ($H = 1\ m$), the coastline looks in general smoother, and there is a better alignment between the measured coastline and the bed level variations (plotted in the background). However the coastline right after the first storm event has some irregularities, which are smoothed out by the end of the simulation. When choosing a larger water-to-dune height ($H = 2\ m$) there are less irregularities after the first storm event, since they are "averaged" when choosing a larger volume for the MKL estimation, but at the same time the overall results are less smooth, especially the ones obtained from the measurements. The general trends however are the same and when excluding the *smoothness* of the coastlines from the analysis, the coastline position of both values are approximately the same, indicating that this parameter is not too sensitive to the results. Therefore the MKL obtained with a value of $H = 1\ m$ (Figure H-136) is chosen as a representative coastline based on the slightly better shoreline representation of the measurements.
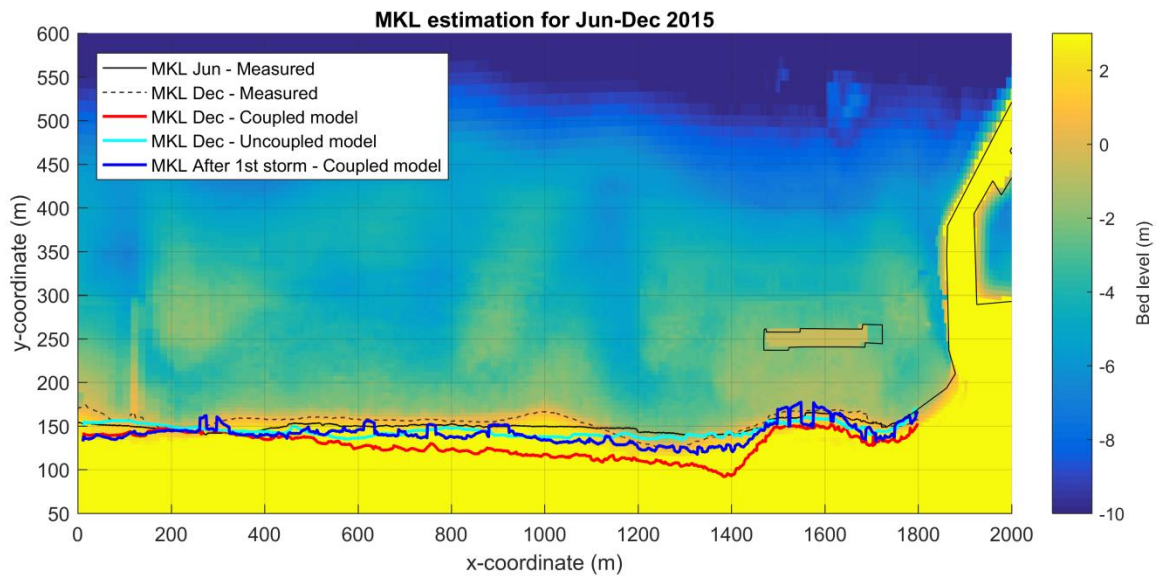
Figure H-136: Momentary coastline (MKL) methodology modification at Anmok beach for measurements and models. The coupled model refers to the D3D-FM & XBeach (surf beat) simulation with a $H_s\ threshold$ = 2.5 m. The bed level at the background is the measured bathymetry from December 2015. Water-to-dune height $H = 1\ m$
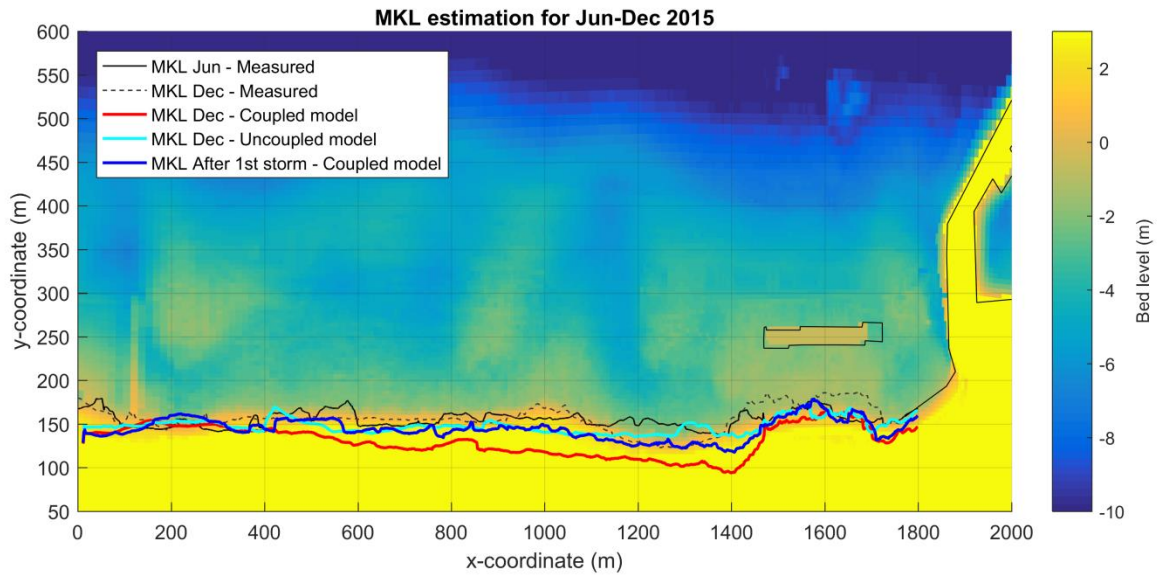
Figure H-137: Momentary coastline (MKL) methodology modification at Anmok beach for measurements and models. The coupled model refers to the D3D-FM & XBeach (surf beat) simulation with a $H_s\ threshold$ = 2.5 m. The bed level at the background is the measured bathymetry from December 2015. Water-to-dune height $H = 2\ m$